universität wien

DISSERTATION / DOCTORAL THESIS

Titel der Dissertation /Title of the Doctoral Thesis

„Short Filament Approximation

to Lamellipodium Dynamics“

verfasst von / submitted by

Gervy Marie Angeles

angestrebter akademischer Grad / in partial fulfilment of the requirements for the degree of

Doktorin der Naturwissenschaften (Dr. rer. nat.)

Wien, 2023/ Vienna 2023

Studienkennzahl lt. Studienblatt / degree programme code as it appears on the student record sheet:	UA 796 605 405
Dissertationsgebiet lt. Studienblatt / field of study as it appears on the student record sheet:	Mathematik
Betreut von / Supervisor:	Univ.-Prof. Dr. Christian Schmeiser

Acknowledgments

First and foremost, I am greatly indebted to my supervisor *Christian Schmeiser*, who had always supported and guided me even before I started my doctoral studies in Vienna. Despite his busy schedule, he has never failed to squeeze in time for consultations. His expertise, enthusiasm and stamina in mathematics have proved to be contagious and have motivated me to continue in academia. I will definitely miss our mathematically enlightening meetings – which come with (free) coffee in his bright office and a great view of Donaukanal!

During my studies, I have met mathematicians in different career stages – PhD students, professors and prominent mathematicians from all over the world – thanks to the *Vienna School of Mathematics* (VSM) and the *Doctoral Program Dissipation and Dispersion in Nonlinear PDEs* (DK). The talks and seminars, training sessions, colloquiums, and summer and winter schools have all been helpful in every aspect of my student life. The *Department of Mathematics and Computer Science* (DMCS) of the *University of the Philippines – Baguio* (UPB), especially *Sir Jic* and *Ma'am Precy*, continued to support me even after I left the Philippines. Online interactions with my former department have alleviated my homesickness.

I thank the friends I made in Vienna for making my stay worth the while: *Katya*, my dormmate, for the many days and nights of conversations, walks in parks, drinks, sweets and music! *Juny*, for bringing with her everything I miss from the Philippines (e.g. Filipino cuisine). *Steffen*, for always lending a helping hand in the office. *Ira*, for the unending conversations, whenever we see each other in the office. *Mina, Steffi, Ania*, for coffee and dinner times.

My warm gratitude belongs to one of my closest friends, *Reymart*. We have been in close proximity (in the Philippines and in Austria) for more than a decade, sharing (almost) the same academic (and professional) journey from being an undergraduate to a postgraduate student. Among others, the camaraderie, food, drinks, and trips around Europe that we have are treasures that I will keep forever.

While in Vienna, I found my best friend and my home away from home, *John Sebastian*. The long hours we spent talking over the phone kept us close while we were physically apart. I am ultimately grateful for the times we are right next to each other: in between mathematics, music and silly games. Thank you for your love and understanding, much so that you read and commented on my thesis. More adventures to come!

Finally, my family, *Gerwin*, *Maria Victoria*, and *Genniel*, deserve recognition for being a consistent support system wherever I go and a source of inspiration in whatever I do.

This project has been supported by the *OeAD-GmbH – Agency for Education and Internationalisation* in the framework of the *Ernst Mach Grant ASEA-UNINET* financed by *Bundesministerium für Bildung, Wissenschaft und Forschung* (BMBWF). Special mention goes to my OeAD regional advisor, Ms Karin Kietreiber, who has helped and assisted me in the administrative aspects of living in Vienna.

Abstract

In contact with flat surfaces, several biological cells develop a thin membrane protrusion called the *lamellipodium*. Employing a dense *actin filament* meshwork along with other accessory proteins, the lamellipodium drives the crawling motility of the cell. Cell crawling by lamellipodium dynamics has become the subject of a series of papers under the framework of the *Filament Based Lamellipodium Model* (FBLM), a two-dimensional continuum model systematically derived from a microscopic description of two interacting families of locally parallel actin filaments.

In contrast to previous works, we have assumed that the width of the lamellipodium around the cell periphery is *small* relative to the cell circumference. This regime has enabled us to perform short filament approximations to the FBLM, resulting in mathematically simpler and computationally less expensive models. Further, simplifying assumptions that are not too restrictive and concentrate on the mechanical parts rather than the biochemical ingredients of the model have been applied.

First, we derive a rigid filament version of the FBLM that accounts for filament-to-substrate adhesions and the twisting of cross-links. With a vanishing lamellipodium width, this FBLM version has produced a circular-shaped cell in equilibrium, consistent with the numerical findings of available literature. Second, we analyze the FBLM with pressure, where instabilities with respect to non-symmetric perturbations emerge. This issue has been resolved by introducing the tension energy of the center-of-mass curve. Consequently, the competing effects of pressure and tension have generated a pitchfork bifurcation away from the trivial, stationary, steady state when the ratio between the stiffness parameters exceeds a critical value. The nontrivial steady state, on the other hand produces a nonvanishing velocity that allows translocation of the lamellipodial strip. Finally, we study a model for filament density derived from the FBLM with pressure. We have investigated special solutions to this system by numerical implementation of a semi-implicit conservative scheme.

Zusammensfassung

Im Kontakt mit flachen Oberflächen entwickeln einige Arten biologischer Zellen eine dünne Membranausstülpung, das *Lamellipodium*. Das Lamellipodium treibt die kriechende Zellmotilität an unter Verwendung eines dichten Netzwerks von *Aktinfilamenten* und anderer Proteine. Zellkriechen durch die Dynamik des Lamellipodiums wurde in einer Reihe von Publikationen durch das *Filament Based Lamellipodium Model* (FBLM) beschrieben, einem zweidimensionalen Kontinuumsmodell, systematisch hergeleitet aus einer mikroskopischen Beschreibung zweier interagierender Familien lokal paralleler Aktinfilamente.

Im Gegensatz zu früheren Arbeiten wird hier angenommen, dass die Breite des Lamellipodiums *klein* ist im Vergleich zum Umfang der Zelle. In diesem Regime wird eine Approximation des FBLM für kurze Filamente hergeleitet, was zu mathematisch einfacheren Modellen führt, die auch billiger numerisch zu lösen sind. Weitere vereinfachende aber nicht zu restriktive Annahmen wurden gemacht, die die mechanischen (aber nicht die biochemischen) Aspekte des Modells betreffen.

Zunächst wurde eine Version des FBLM für steife Filamente hergeleitet unter Berücksichtigung von Adhäsion zum Substrat und Rotationssteifigkeit von Filamentverbindungen. Das asymptotische Modell für kleine Lamellipodiumsbreite produziert ein kreisförmiges Equilibrium konsistent mit numerischen Resultaten für das volle FBLM. Weiters wurde ein FBLM mit Druck analysiert, wo sich Instabilitäten unter nicht-symmetrischen Störungen zeigen. Diese können durch einen zusätzlichen Spannungsterm regularisiert werden. Die einander entgegenwirkenden Effekte von Druck und Spannung erzeugen eine Heugabelverzweigung, wenn ein Steifigkeitsparameter einen kritischen Wert erreicht. Die Verzweigung erzeugt einen nichttrivialen Zustand mit nichtverschwindender Geschwindigkeit. Schließlich wird noch ein einfaches Modell für die Filamentdichte untersucht, das aus einem FBLM mit Druck entsteht. Spezielle Lösungen werden numerisch mit Hilfe eines semi-impliziten Verfahrens berechnet.

Contents

List of Figures

Chapter I

Introduction

Over the past few decades, a significant amount of attention has been dedicated to the study of cell migration and the underlying dynamics of the cytoskeleton. This is motivated by the fact that different processes in living organisms, such as morphogenesis, wound healing, tumor metastasis, and immune response, are steered by the movement of cells [Alb+02; AE07]. An important motility organelle of several cell types is the *lamellipodium* (see Figure I.1). First identified by Abercrombie [Abe80], lamellipodia are quasi-two-dimensional, thin layers of cytoplasm which contain a meshwork of actin filaments, mostly lying in a plane parallel to flat adhesive substrates. Lamellipodia are dynamic cell protrusions, relying on actin polymerization that drives the plasma membrane outward. The actin filament network then depolymerizes at the rear of the protrusion in a treadmilling mode. In the presence of adhesive contact with a substrate, this process drives the crawling motility of the cell [Abe80; Alb+02; Ara16; CPV10; Lod+08].

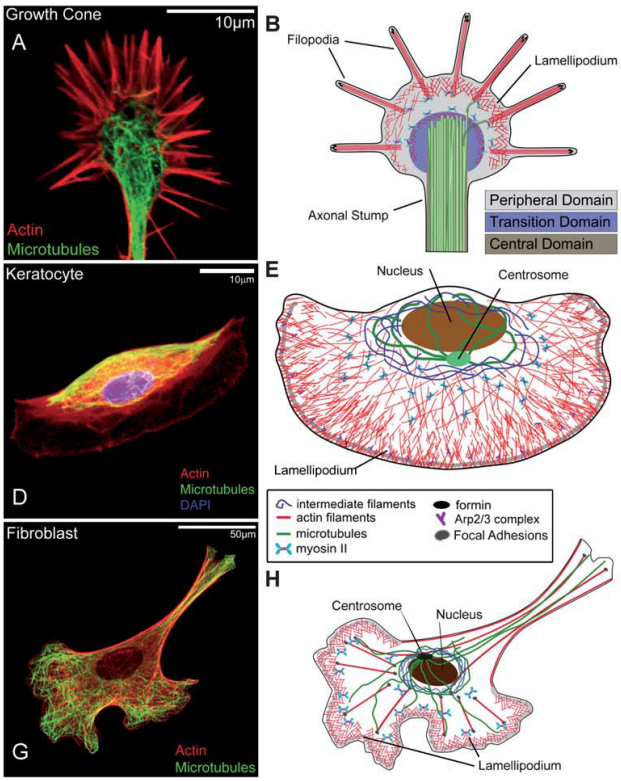

Figure I.1: Lamellipodium of different cell types. Left column: Fluorescent images of NG108 growth cone, keratocyte and SVT2 fibroblast. Right column: Illustrations of growth cone, keratocyte and fibroblast.

Image reproduced / adapted with permission from Soft Matter [Kno+11].

Actin dynamics is a very complex process influenced and regulated by a large number of cytoskeletal proteins. Although several biochemical and mechanical aspects are already well-established, the picture is still far from complete. Mathematical modeling of subprocesses started roughly 30 years ago [Mog09], followed by the formulation of models for the whole lamellipodium system. These efforts have continued until today and can be categorized into two groups [OS10b]. The first group models the mechanisms of the actin network as a continuum. Examples of continuum models include a two-phase formulation for cytoplasm dynamics [AD99], a one-dimensional (1D) viscoelastic model [GO04], a 1D system for the actin distribution [MMB01], and a two-dimensional (2D) elastic multiscale description of motile cells [RJM05]. These models typically rely on assumptions on the rheological properties of the network built into off-the-shelf continuum models. The second group, on the other hand, makes conjectures about the microscopic structure of actin filament networks (see for example [Lac+07; MB01; Mar+06; MO96; Pol07; STB07]).

In the past ten years, a group around C. Schmeiser (involving his former PhD students and PostDocs) has tried to integrate the two approaches in the *Filament Based Lamellipodium Model* (FBLM). The FBLM is a two-dimensional, two-phase, anisotropic continuum model, systematically derived from a microscopic description based on individual actin filaments. From a mechanical point of view, it incorporates elastic contributions from filament bending, viscous contributions from dynamic cross-linking and cell-to-substrate adhesion, and active contributions from actin-myosin interactions. On the other hand, it contains detailed accounts of biochemical processes such as filament branching, capping, polymerization, and depolymerization. The analysis, extensions, and numerical simulations of the FBLM have continually been sustained (see e.g. [HMS17; MS17; Man+15; Sfa+18]).

The FBLM is a new type of continuum model, meaning that existing analytical results of continuum mechanics are not applicable and hardly any analytical results are available, with the exception of a local-in-time existence theorem for the rotationally symmetric lamellipodium [OS10a]. From a modeling point of view, the FBLM is seen as a model for cell fragments without any cell organelle aside from the lamellipodium and the cell membrane. A mechanically more realistic model of cell motility would require a description of the mechanics of the passive parts of a cell (e.g. nucleus) and its coupling to the FBLM. In [Sfa+18] cell-cell interaction has been introduced to the model and groups of several cells have been numerically simulated. This shows the potential of the model to describe cell monolayers. However, by the complexity of the model for individual cells, the numerical cost of simulating larger cell ensembles is prohibitive. The issues raised in this paragraph serve as motivation for our work.

Filament movement in the FBLM results from a quasi-stationary balance of forces acting on the lamellipodium. Positions and deformations of filaments are assumed to minimize a potential energy functional alongside dominating friction effects and biologically motivated constraints. The model derivation based on individual accounts of filaments makes the FBLM highly flexible in the sense of ease in inclusion and (or) removal of contributions and (or) constraints. In this thesis, we incorporate the assumption that the lamellipodial width around the outer parts of the cell is *small* compared to the cell circumference. This assumption makes the filaments short and, consequently, rigid. The length of the filaments can therefore be treated as a *small parameter*, and techniques from asymptotic analysis and perturbation theory help us develop mathematically simpler and computationally less expensive models. Below, we briefly discuss each proposed model.

Zero-width limit for lamellipodium. A reparametrization of the full FBLM allows us to fix the varying coordinate domain of the original model and introduce the filament length as a small parameter

into our equations. Solutions of the formal limiting system turn out to be straight lines, which has led to the derivation of FBLM with rigid filaments. This situation puts us into the other extreme case of what was considered in [HMS17], where the limit of large bending stiffness produced stiff actin filaments.

Instead of inserting the straight filament ansatz into the reparametrized FBLM, we have decided to systematically derive the rigid filament version of the FBLM from the formulation of a Lagrangian that includes only a minimal number of contributions. This strategy has enabled us to discuss each effect in detail and study model problems. We have reproduced the degenerate cases of a dissolving lamellipodium (where filaments are all parallel) and its collapse into a dense ring (where filaments of different directions are anti-parallel), consistent with the numerical results in [OSS08].

With simplifying, but not too restrictive assumptions, we pass to the vanishing width limit for the lamellipodium. The asymptotic model for small lamellipodium width is a coupled interaction between the evolution of the cell boundary and the solutions of differential equations along this curve. Searching for equilibria (i.e. when the cell shape is fixed), we are able to produce the desired circular-shaped cell. This outcome agrees with the numerical results of previous works for the rotationally symmetric lamellipodium in [OSS08], and the stationary cross-link dominated equilibrium in [HMS17].

Lamellipodial strip with pressure. A different scaling of parameters modifies the leading order problem of the FBLM as the filament length vanishes. Solutions to this reduced FBLM account for filament bending, in contrast to the rigid filament ansatz discussed above. With the conjecture of convergence to straight lines (inspired by the result in [Oel11]), we study equilibrium states which lead us back to rigid filaments. However, we focus on the pressure term included in the FBLM version of [Man+15] to stabilize the system.

In our analysis, we found that the pressure term causes instabilities with respect to non-symmetric perturbations, which has already been observed in the supplementary material of [Man+15] but was not further investigated. Pressure instabilities can be regularized by an additional stress term, which in our case is a tension energy for the center-of-mass curve. The opposing effects of pressure and tension create a pitchfork bifurcation when a stiffness parameter reaches a critical value. The bifurcation produces a non-trivial state with non-vanishing velocity for the lamellipodium strip.

Filament density models. A simple model for the *filament density* has been investigated, which arises from an FBLM with pressure. A transformation to Eulerian coordinates has enabled us to discuss special solutions and their physical interpretations. Guided by system sturcture, a semi-implicit conservative scheme has been proposed and implemented to solve a specific numerical example.

The thesis is organized as follows: In the next chapter, we collect the notations and preliminary concepts that are used throughout the manuscript. For completeness, the full FBLM is presented in Chapter III. Approximations of the FBLM with rigid and short filaments are found in Chapter IV, where the potential energy only includes contributions necessary to produce nontrivial dynamics. Discussions regarding the pressure term in the FBLM are collected in Chapter V. To supplement the results of the latter, a model for the evolution of filament density is investigated in Chapter VI. A summary of our study and topics for future work are collected in the final chapter.

Chapter II

Preliminaries

Contents

This short chapter collects the notations and preliminary concepts that are helpful to motivate the discussions in the thesis.

II.1 Notations

The set of all real numbers is denoted by $\mathbb{R}$.

Vectors and operations. All vectors and vector-valued functions are indicated by a bold font, such as $\mathbf{F}$, $\boldsymbol{\omega}$, and $\mathbf{z}$. The *orthogonal complement* of a vector $\mathbf{z} = (z_1, z_2)^\top \in \mathbb{R}^2$ is defined by

$$\mathbf{z}^\perp := (-z_2, z_1)^\top,$$

where $\top$ denotes matrix transposition. The *scalar product* of two vectors $\mathbf{z} = (z_1, z_2)^\top$ and $\mathbf{y} = (y_1, y_2)^\top$ is the value

$$\mathbf{z} \cdot \mathbf{y} = \mathbf{z}^\top \mathbf{y} = z_1 y_1 + z_2 y_2,$$

while their *tensor product* is the matrix

$$\mathbf{z} \otimes \mathbf{y} = \mathbf{z}\mathbf{y}^\top = \begin{bmatrix} z_1 y_1 & z_1 y_2 \\ z_2 y_1 & z_2 y_2 \end{bmatrix}.$$

Orthogonal projection and vector decomposition. A nonzero unit vector $\boldsymbol{\omega} \in \mathbb{R}^2$ and its orthogonal complement $\boldsymbol{\omega}^\perp$ constitute an orthonormal basis for the vector space $\mathbb{R}^2$. Indeed, with the *orthogonal projection to the unit vector* $\boldsymbol{\omega}$ defined by

$$\Pi_\omega := \boldsymbol{\omega} \otimes \boldsymbol{\omega},$$

a vector $\mathbf{z} \in \mathbb{R}^2$ can be decomposed as

$$\mathbf{z} = \Pi_{\boldsymbol{\omega}}\mathbf{z} + \Pi_{\boldsymbol{\omega}^\perp}\mathbf{z}. \tag{II.1.1}$$

The unit vector $\boldsymbol{\omega}$ can written in the form $\boldsymbol{\omega}(\varphi) = (\cos\varphi, \sin\varphi)^\top$ with its direction angle φ. With this, the decomposition in (II.1.1) is just the Fourier expansion of $\mathbf{z}$.

Big O symbol. Consider $\varepsilon_0 > 0$ and a Banach space $\mathscr{B}$ equipped with norm $\|\cdot\|$. Suppose $y_\varepsilon \in \mathscr{B}$ and $g_\varepsilon > 0$ for $0 < \varepsilon \leq \varepsilon_0$. We say that y_ε is of order g_ε as ε approaches zero, denoted by

$$y_\varepsilon = O(g_\varepsilon) \quad \text{as} \quad \varepsilon \to 0,$$

if and only if there exists a constant $C > 0$ such that

$$\|y_\varepsilon\| \leq C g_\varepsilon \quad \text{for} \quad 0 < \varepsilon \leq \varepsilon_0.$$

Fréchet and Gâteaux derivatives. Suppose $\mathscr{B}$ is a Banach space with normed dual $\mathscr{B}^*$ and duality pairing $\langle\cdot,\cdot\rangle : \mathscr{B} \times \mathscr{B}^* \to \mathbb{R}$. A functional $\mathcal{F} \in \mathscr{B}$ is *Fréchet-differentiable at a point* $\mathbf{u} \in \mathscr{B}$ if there exists a bounded linear map $\delta\mathcal{F}(\mathbf{u}) \in \mathscr{B}^*$, called the *differential of* $\mathcal{F}$ *at* $\mathbf{u}$, such that

$$\frac{|\mathcal{F}[\mathbf{u}+\mathbf{v}] - \mathcal{F}[\mathbf{u}] - \delta\mathcal{F}[\mathbf{u}]\mathbf{v}|}{\|\mathbf{v}\|_{\mathscr{B}}} \longrightarrow 0 \quad \text{as} \quad \|\mathbf{v}\|_{\mathscr{B}} \to 0. \tag{II.1.2}$$

If $\mathcal{F}$ is a Fréchet differentiable functional, then the *Gâteaux-derivative of* $\mathcal{F}$ *at* $\mathbf{u}$ *in the direction* $\boldsymbol{\delta}\mathbf{u}$ is given by

$$\frac{\mathrm{d}}{\mathrm{d}\varepsilon}\mathcal{F}[\mathbf{u} + \varepsilon\boldsymbol{\delta}\mathbf{u}]\Big|_{\varepsilon=0} = \langle \boldsymbol{\delta}\mathbf{u}, \delta\mathcal{F}[\mathbf{u}]\rangle =: \delta\mathcal{F}[\mathbf{u}]\boldsymbol{\delta}\mathbf{u}. \tag{II.1.3}$$

For such $\mathcal{F}$, a point $\mathbf{u} \in \mathscr{B}$ is said to be *critical* if $\delta\mathcal{F}(\mathbf{u}) = 0$.

Oftentimes, we use the notation $\mathcal{F}(t)[\mathbf{u}, \varphi]$ to emphasize that $\mathcal{F}$ is a functional that depends on t with a vector argument $\mathbf{u}$ and scalar φ. Assuming that both the partial Fréchet derivatives exist and are continuous at $(\mathbf{u}, \varphi)$, then

$$\delta\mathcal{F}(t)[\mathbf{u}, \varphi](\boldsymbol{\delta}\mathbf{u}, \delta\varphi) = \partial_{\mathbf{u}}\mathcal{F}[\mathbf{u}, \varphi]\boldsymbol{\delta}\mathbf{u} + \partial_\varphi\mathcal{F}[\mathbf{u}, \varphi]\delta\varphi,$$

with the notations

$$\partial_{\mathbf{u}}\mathcal{F}[\mathbf{u}, \varphi]\boldsymbol{\delta}\mathbf{u} := \frac{\mathrm{d}}{\mathrm{d}\varepsilon}\mathcal{F}[\mathbf{u} + \varepsilon\boldsymbol{\delta}\mathbf{u}, \varphi]\Big|_{\varepsilon=0} \quad \text{and} \quad \partial_\varphi\mathcal{F}[\mathbf{u}, \varphi]\delta\varphi := \frac{\mathrm{d}}{\mathrm{d}\varepsilon}\mathcal{F}[\mathbf{u}, \varphi + \varepsilon\delta\varphi]\Big|_{\varepsilon=0}. \tag{II.1.4}$$

II.2 Variational considerations

Suppose $\Omega \subset \mathbb{R}^n$ and $L^2(\Omega)$ denote the usual class of Lebesgue (square-) integrable functions from Ω to $\mathbb{R}$. For a functional $\mathcal{F}$ defined on some dense subspace of $L^2(\Omega)$, we define the linear functional $\mathcal{G}_{\mathbf{u}}$ by

$$\mathcal{G}_{\mathbf{u}}(\mathbf{v}) = \lim_{\varepsilon\to 0} \frac{\mathcal{F}[\mathbf{u} + \varepsilon\mathbf{v}] - \mathcal{F}[\mathbf{u}]}{\varepsilon}.$$

Initially, $\mathcal{G}_{\mathbf{u}}$ is defined for smooth functions $\mathbf{v}$ such that $(\mathbf{u} + \varepsilon\mathbf{v})$ lies in the domain of $\mathcal{F}$, and is then extended to have a domain as large as possible. Let us therefore assume that $\mathcal{G}_{\mathbf{u}}$ can be extended to a bounded linear functional on $L^2(\Omega)$, and thus be defined on the whole space (e.g. when $\mathcal{F}$ is reasonably well-behaved and $\mathbf{u}$ is smooth enough). Then by the *Riesz Representation theorem* [Kre91], there exists an element $\mathbf{w}_{\mathbf{u}} \in L^2(\Omega)$ such that

$$\mathcal{G}_{\mathbf{u}}(\mathbf{v}) = \langle \mathbf{v}, \mathbf{w}_{\mathbf{u}} \rangle$$

with the usual L^2-inner product $\langle \mathbf{v}, \mathbf{w} \rangle = \int_\Omega \mathbf{v}\mathbf{w}^* \, \mathrm{d}x$, where $*$ denotes complex conjugation.

Variational derivative. The *variational derivative* of $\mathcal{F}$ at $\mathbf{u}$ is defined to be $\mathbf{w}_{\mathbf{u}}$ (which is the Riesz representation of the Fréchet derivative, c.f. (II.1.2)). For any $\mathbf{v} \in L^2(\Omega)$ with $\|\mathbf{v}\| = 1$,

$$\langle \mathbf{v}, \mathbf{w}_{\mathbf{u}} \rangle$$

defines the *directional derivative* of $\mathcal{F}$ at $\mathbf{u}$ in the $\mathbf{v}$-direction (c.f. Gâteaux-derivative (II.1.3)).

In analogy with the finite-dimensional vector space $\mathbb{R}^n$, if $\mathcal{F} : \mathbb{R}^n \to \mathbb{R}$, then $\mathbf{w}_{\mathbf{u}}$ may be defined as above and is the *gradient* of $\mathcal{F}$ at $\mathbf{u}$, denoted by $\nabla\mathcal{F}$. This motivates the notation $\nabla\mathcal{F}$ for the variational derivative $\mathbf{w}_{\mathbf{u}}$.

Potential energy and gradient flow. Now, suppose that $\mathbf{u} \in L^2(\Omega)$ denotes the state of some mechanical system, and let $\mathcal{E} : L^2(\Omega) \to \mathbb{R}$ be a *potential energy functional* of the form

$$\mathcal{E}[\mathbf{u}] = \int_\Omega \mathcal{F}[\mathbf{u}, \nabla\mathbf{u}, \mathbf{x}] \, \mathrm{d}\mathbf{x}.$$

If $\mathbf{u}$ satisfies some boundary conditions, these would be incorporated implicitly into the definition of the domain of $\mathcal{E}$. Here, let us further assume that $\mathbf{u}$ satisfies a *no-flux boundary condition* $\nabla\mathbf{u} \cdot \boldsymbol{\nu} = 0$ on the boundary $\partial\Omega$, where $\boldsymbol{\nu}$ is a unit normal vector with respect to $\partial\Omega$ (Dirichlet or other conditions can also be incorporated).

The requirement $\mathcal{E} < \infty$ imposes a natural integrability (smoothness) condition upon $\mathbf{u}$, so we will assume that the domain of $\mathcal{E}$ is dense in $L^2(\Omega)$. The abstract ordinary differential equation (ODE)

$$\mathbf{u}_t = -\nabla\mathcal{E}[\mathbf{u}] \tag{II.2.1}$$

is called the *gradient flow* for the energy $\mathcal{E}$, where the state $\mathbf{u}$ evolves through time in a way to decrease $\mathcal{E}$ continually. This differential equation can be solved by the implicit Euler method

$$\frac{\mathbf{u}_h(t) - \mathbf{u}_h(t-h)}{h} = -\nabla\mathcal{E}[\mathbf{u}_h(t)],$$

which has the *variational formulation*

$$\mathbf{u}_h(t) = \operatorname{argmin}_{\mathbf{v} \in L^2(\Omega)} \left(\frac{\|\mathbf{v} - \mathbf{u}_h(t-h)\|^2}{2h} + \mathcal{E}[\mathbf{v}] \right). \tag{II.2.2}$$

The gradient flow is a useful method to find minima of $\mathcal{E}$: Equation (II.2.1) implies

$$\frac{\mathrm{d}\mathcal{E}[\mathbf{u}]}{\mathrm{d}t} = \langle \nabla\mathcal{E}[\mathbf{u}], \mathbf{u}_t \rangle = -\|\nabla\mathcal{E}[\mathbf{u}]\|^2.$$

On the other hand, the gradient flow can also serve as a model where forces are derived from a potential energy and from friction effects. Below we discuss some examples.

Example (Dirichlet principle). Consider the Dirichlet energy

$$\mathcal{E}[\mathbf{u}] = \int_\Omega \left(\frac{\|\nabla \mathbf{u}\|^2}{2} + \mathcal{H}[\mathbf{u}] \right) \mathrm{d}\mathbf{x}, \tag{II.2.3}$$

where $\mathcal{H}$ is possibly a nonlinear function of $\mathbf{u}$. We would like to find $\mathbf{u}$ that continually decreases $\mathcal{E}$ and satisfies a no-flux boundary condition, so that the domain is given by

$$\mathcal{D}(\mathcal{E}) := \left\{ \mathbf{u} \in L^2(\Omega) : \nabla \mathbf{u} \cdot \boldsymbol{\nu} = 0 \text{ on } \partial\Omega \right\}.$$

This problem can be written as the abstract ODE (II.2.1) with energy (II.2.3). The variational derivative of $\mathcal{E}$ at $\mathbf{u}$ is computed through the expansion

$$\mathcal{E}[\mathbf{u} + \varepsilon \mathbf{v}] - \mathcal{E}[\mathbf{u}] = \varepsilon \int_\Omega \left(\nabla \mathbf{u} \cdot \nabla \mathbf{v} + \frac{\mathrm{d}\mathcal{H}}{\mathrm{d}\mathbf{u}} \mathbf{v} \right) \mathrm{d}\mathbf{x} + O(\varepsilon^2).$$

Integration by parts yields

$$\mathcal{G}_{\mathbf{u}}(\mathbf{v}) = \int_\Omega \left(\nabla \mathbf{u} \cdot \nabla \mathbf{v} + \frac{\mathrm{d}\mathcal{H}}{\mathrm{d}\mathbf{u}} \mathbf{v} \right) \mathrm{d}x = \int_\Omega \left(-\Delta \mathbf{u} + \frac{\mathrm{d}\mathcal{H}}{\mathrm{d}\mathbf{u}} \right) \mathbf{v} \, \mathrm{d}\mathbf{x} + \int_{\partial\Omega} \mathbf{v} \nabla \mathbf{u} \cdot \boldsymbol{\nu} \, \mathrm{d}A,$$

where $\mathrm{d}A$ is an area element. The last term is annihilated by the boundary conditions (note that $\mathbf{v}$ also satisfies a no-flux boundary condition). Therefore,

$$\mathcal{G}_{\mathbf{u}}(\mathbf{v}) = \int_\Omega \left(-\Delta \mathbf{u} + \frac{\mathrm{d}\mathcal{H}}{\mathrm{d}\mathbf{u}} \right) \mathbf{v} \, \mathrm{d}\mathbf{x} = \langle \mathbf{v}, \nabla \mathcal{E}[\mathbf{u}] \rangle .$$

Initially, we require $\nabla \mathbf{v}$ to be in $L^2(\Omega)$ for $\mathcal{G}_{\mathbf{u}}$ to exist, however, after integration by parts, we only need $\mathbf{v} \in L^2(\Omega)$. The price to be paid is the extra smoothness that must be assumed for $\mathbf{u}$, i.e. $\Delta \mathbf{u} \in L^2(\Omega)$. The evolution of $\mathbf{u}$ follows a gradient flow for $\mathcal{E}$:

$$\mathbf{u}_t = \Delta \mathbf{u} + \frac{\mathrm{d}\mathcal{H}}{\mathrm{d}\mathbf{u}}(\mathbf{u}).$$

This is a semilinear parabolic equation, which we derived here from a minimization of the Dirichlet energy through the variational form (II.2.2).

Constraints and Lagrange multiplier method. For more general systems, we may have a constraint of the form

$$\int_\Omega g_1(\mathbf{u}, \nabla \mathbf{u}, \mathbf{x}) \, \mathrm{d}\mathbf{x} = 0.$$

The energy $\mathcal{E}$ is then augmented to become the Lagrangian functional

$$\mathcal{L}[\mathbf{u}] = \int_\Omega \left(\mathcal{F}[\mathbf{u}, \nabla \mathbf{u}, \mathbf{x}] + \lambda g_1(\mathbf{u}, \nabla \mathbf{u}, \mathbf{x}) \right) \mathrm{d}\mathbf{x},$$

with a Lagrange multiplier λ independent of $\mathbf{x}$. As a result, we obtain an evolution equation involving λ, which may be a function of time and assumes values in a way to maintain the constraint. If on the

other hand we have a constraint of the form $g_2(\mathbf{u}, \nabla\mathbf{u}, \mathbf{x}) = 0$ for $\mathbf{x} \in \Omega$, then the multiplier λ is allowed to depend on $\mathbf{x}$ in the augmented energy.

To illustrate, suppose $\mathbf{u} = (u, v) : \mathbb{R}^2 \to \mathbb{R}^2$ on (x, y)-space. Consider the energy

$$\mathcal{E}(u, v) = \int_{\mathbb{R}^2} \frac{u_x^2 + u_y^2 + v_x^2 + v_y^2}{2} \, \mathrm{d}x \, \mathrm{d}y = \int_{\mathbb{R}^2} \frac{|\nabla\mathbf{u}|^2}{2} \, \mathrm{d}x \, \mathrm{d}y$$

subject to the constraint $u_x + v_y = \nabla \cdot \mathbf{u} = 0$, where $\nabla \cdot \mathbf{u}$ means the divergence of $\mathbf{u}$. This is just the Dirichlet energy (II.2.3) with $\mathcal{H} \equiv 0$, but now $\mathbf{u}$ must satisfy a subsidiary condition. Then $\mathcal{E}$ is augmented to become the Lagrangian

$$\int_\Omega \left(\frac{|\nabla\mathbf{u}|^2}{2} + \lambda(x, y) \nabla \cdot \mathbf{u} \right) \mathrm{d}x \, \mathrm{d}y.$$

The associated gradient flow now reads

$$\begin{cases} u_t = \Delta u + \lambda_x \,, \\ v_t = \Delta v + \lambda_y \,, \end{cases}$$

or in vector notation,

$$\mathbf{u}_t = \Delta\mathbf{u} + \nabla\lambda,$$

where the *pressure*-like variable λ is always such that $\nabla \cdot \mathbf{u} = 0$.

II.3 Singular singularly perturbed systems

In many areas of the natural sciences, mathematical modeling of systems with different time scales frequently arise. This comes as a result of studying differential equations where some variables have derivatives with much larger magnitude compared to those of other variables.

Singularly perturbed systems. Consider a system of ODEs with a small parameter $0 < \varepsilon \ll 1$ taking the form

$$\begin{cases} \varepsilon \dfrac{\mathrm{d}\mathbf{x}}{\mathrm{d}t} = \mathbf{f}(\mathbf{x}, \mathbf{y}, \varepsilon), \\ \dfrac{\mathrm{d}\mathbf{y}}{\mathrm{d}t} = \mathbf{g}(\mathbf{x}, \mathbf{y}, \varepsilon), \end{cases} \tag{II.3.1}$$

where $t \in \mathbb{R}$, vectors $\mathbf{x} \in \mathbb{R}^m$, $\mathbf{y} \in \mathbb{R}^n$, and right-hand sides $\mathbf{f} \in \mathbb{R}^m \times \mathbb{R}^n \to \mathbb{R}^m$, $\mathbf{g} \in \mathbb{R}^m \times \mathbb{R}^n \to \mathbb{R}^n$. Such equations form a *singularly perturbed system* since when $\varepsilon = 0$, the ability to specify an arbitrary initial condition for $\mathbf{x}(t)$ is lost.

In the language of *fast-slow systems* [Kue15], (II.3.1) is called an (m, n)- *fast-slow vector field*, where $\mathbf{x}$ is a *fast variable* and $\mathbf{y}$ is a *slow variable*. With $\tau = t/\varepsilon$ we get an equivalent form

$$\begin{cases} \dfrac{\mathrm{d}\mathbf{x}}{\mathrm{d}\tau} = \mathbf{f}(\mathbf{x}, \mathbf{y}, \varepsilon), \\ \dfrac{\mathrm{d}\mathbf{y}}{\mathrm{d}\tau} = \varepsilon\mathbf{g}(\mathbf{x}, \mathbf{y}, \varepsilon). \end{cases} \tag{II.3.2}$$

We refer to t as the slow time scale or *slow time* and to τ as the fast time scale or *fast time*.

Degenerate systems. The usual approach to the qualitative study of (II.3.1) and (II.3.2) is to first consider their *degenerate systems*, which are obtained by setting $\varepsilon = 0$. For System (II.3.1), we obtain the *reduced problem*

$$\begin{cases} 0 = \mathbf{f}(\mathbf{x}, \mathbf{y}, 0), \\ \dot{\mathbf{y}} = \mathbf{g}(\mathbf{x}, \mathbf{y}, 0), \end{cases}$$

where $\cdot$ means derivative with respect to t. This describes the dynamics of the slow variable $\mathbf{y}$ on the critical manifold $\{(\mathbf{x}, \mathbf{y}) \in \mathbb{R}^m \times \mathbb{R}^n : \mathbf{f}(\mathbf{x}, \mathbf{y}, 0) = 0\}$. In other words, the reduced system can be seen as an ODE for $\mathbf{y}$ with an algebraic constraint.

Setting $\varepsilon = 0$ in (II.3.2), on the other hand, yields the *layer problem*

$$\begin{cases} \mathbf{x}' = \mathbf{f}(\mathbf{x}, \mathbf{y}, 0), \\ \mathbf{y}' = 0, \end{cases}$$

where $'$ means differentiation with respect to τ. It pertains to the dynamics of the fast variable $\mathbf{x}$ on the so-called *layers*, which are areas where $\mathbf{y}$ is fixed.

From the reduced and layer problems (which are mathematically simpler), one draws conclusions about the qualitative behavior of the full system (II.3.1) or (II.3.2) for sufficiently small ε.

Singular singularly perturbed systems. [SSM14, Section 5.1] A singularly perturbed differential system with $0 < \varepsilon \ll 1$ can often be written in the form

$$\varepsilon \dot{\mathbf{z}} = \mathbf{Z}(\mathbf{z}, t, \varepsilon), \tag{II.3.3}$$

where $\mathbf{z} \in \mathbb{R}^{m+n}$, $t \in \mathbb{R}$ and the vector-valued function $\mathbf{Z}$ is sufficiently smooth. Assume that for $\varepsilon = 0$ the degenerate system $\mathbf{Z}(\mathbf{z}, t, 0) = 0$ has a family of solutions

$$\mathbf{z} = \boldsymbol{\psi}(\boldsymbol{\nu}, t), \quad \boldsymbol{\nu} \in \mathbb{R}^m, \quad t \in \mathbb{R}.$$

If $m > 0$, then (II.3.3) is called a *singular singularly perturbed system*. In words, these are singularly perturbed systems whose degenerate equations have an isolated but not simple solution.

A simple example is the ODE

$$\varepsilon \frac{\mathrm{d}\mathbf{z}}{\mathrm{d}t} = A\mathbf{z},$$

where A is an $(m+n) \times (m+n)$ singular matrix. The degenerate equation $A\mathbf{z} = 0$ has an m-parameter family of solutions (since $m = \dim x - \operatorname{rank} A$).

We close this section with an illustration to have a better idea of the problem and gain some insights in handling singular singularly perturbed systems. Consider the system

$$\varepsilon \begin{pmatrix} \dot{z_1} \\ \dot{z_2} \end{pmatrix} = A(\varepsilon) \begin{pmatrix} z_1 \\ z_2 \end{pmatrix}, \quad \text{where } A(\varepsilon) := \begin{pmatrix} 2 & -0 \\ 6 + 3\varepsilon & -3 \end{pmatrix}.$$

At first, it seems that there are two fast variables z_1 and z_2. With $\varepsilon = 0$, the linear algebraic system

$$2z_1 - z_2 = 0, \quad 6z_1 - 3z_2 = 0,$$

has, apart from the trivial solution, a one-parameter family of solutions $z_1 = s$ and $z_2 = 2s$, where $s \in \mathbb{R}$. Hence, no isolated solution exists for the degenerate system. Notice that the matrix A is singular, i.e. $\det A(0) = 0$, which actually motivates the terminology singular singularly perturbed system.

In this particular example, we can extract a slow variable to obtain a $(1, 1)$- fast-slow system. The rows of matrix $A(0)$ are proportional, with proportionality constant equal to 3. This inspires us to introduce a new variable $x := z_2 - 3z_1$, and obtain a differential equation for the (new) slow variable x. The solution to the full problem is then obtained by using either of the two equations for z_1 or z_2 as a fast equation. Here, we choose the z_2-equation and use $x - z_2 = -3z_1$ to obtain the new system

$$\begin{cases} \dot{x} = -x + z_2, \\ \varepsilon \dot{z_2} = -(2 + \varepsilon)x - (1 - \varepsilon)z_2. \end{cases}$$

This system possesses the one-dimensional attractive slow invariant manifold $z_2 = kx$. Inserting this to the equations above gives

$$\varepsilon k(-1 + k)x = -(2 + \varepsilon)x - (1 - \varepsilon)kx,$$

which implies

$$\varepsilon k^2 + (1 - 2\varepsilon)k + 2 + \varepsilon = 0.$$

With $k = k_0 + \varepsilon k_1 + O(\varepsilon^2)$, and equating the powers of ε, we compute that $k_0 = -2$ and $k_1 = -9$. Thus, the invariant manifold has the form

$$z_2 = -(2 + 9\varepsilon + O(\varepsilon^2))x = -(2 + 9\varepsilon + O(\varepsilon^2))(z_2 - 3z_1),$$

or equivalently,

$$z_2 = (2 + 3\varepsilon + O(\varepsilon^2))z_1.$$

Chapter III

The Filament Based Lamellipodium Model

Contents

In this chapter, we present the FBLM and refer to e.g. [Man+15] for more details. An overview of the full model is discussed in the first section, followed by a description of the mechanisms of filaments in the second one. The heart of the FBLM resides in Section III.3, where filament movement is derived from a minimization of the potential energy of the system subject to some constraints. It is written in the form of a *generalized gradient flow*, c.f. Equation (II.2.1). In the last section, a strong formulation (i.e. differential equations) of the FBLM is presented together with an interpretation of each term appearing in the equations.

III.1 Overview of the FBLM

Lamellipodia are layers of the cytoplasm with small aspect ratios (about 100-200 nm thickness vs. several μm lateral and inward extension). Their flatness is not necessarily due to flat substrates since their shape is preserved in three-dimensional (3D) space (on cells in suspension). Simulations in [SW15] of a 3D model discussing the interplay between actin dynamics and cell membrane deformation were able to predict pieces of flat lamellipodia without prescribed geometric restrictions. On the other

hand, a projection of the 3D actin network to a flat substrate shows two dominant filament directions (see Figure III.1). These directions are nearly symmetric with respect to the direction of the leading edge, and are around 70 degrees apart. Finally, the density of actin filaments in the lamellipodium is very high, as can be seen in the lamellipodium piece in Figure III.1. The statements in this paragraph motivate the idealizations discussed below.

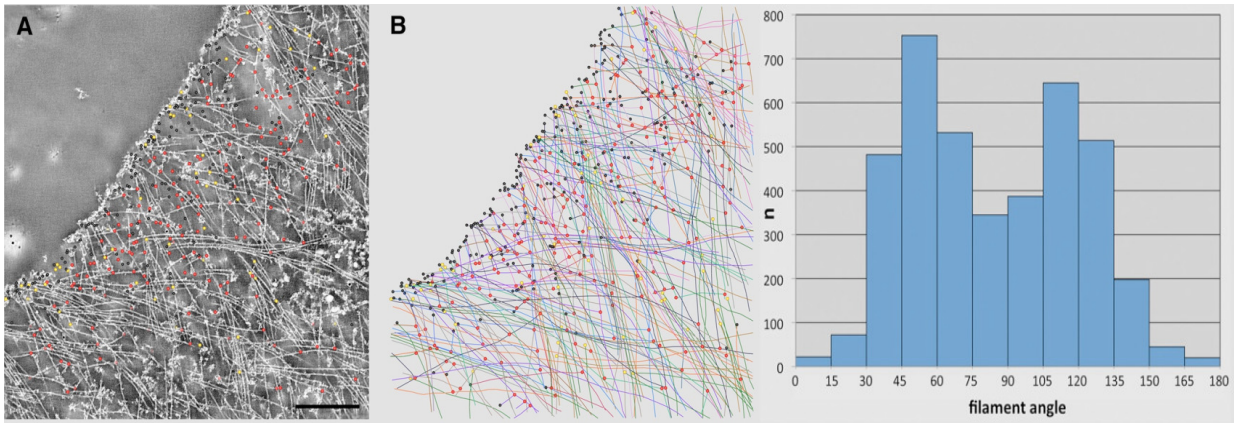

Figure III.1: Actin filament organization in a treadmilling lamellipodium. Left: Electron microscopy and tomography of a piece of lamellipodium. Center: Map of filament network. Right: Angular distribution of filaments relative to the leading edge. *Image reproduced / adapted with permission from Journal of cell science* [Vin+12].

Basic modeling assumptions of the FBLM are that the lamellipodium is a two-dimensional structure, and that the actin filament network consists of two families of locally parallel curves intersecting each other transversally. Filaments are categorized into *clockwise* (right-going) and *counterclockwise* (left-going) families, which we denote by the superscripts + and −, respectively. These superscripts are omitted whenever we concentrate on one filament family, and the quantities related to the other family are then indicated by the superscript $*$. Each of these families cover a ring-shaped domain between two closed curves: the cell membrane and the cell interior (see Figure III.2).

From a microscopic description of a discrete number of filaments, a homogenisation limit is adopted in [OS10b] in order to work with continuous quantities. Filaments are then labeled by the continuum variable $\alpha \in [0, 2\pi)$, and are parametrised by their arclength

$$\mathbf{F}(\alpha, s, t) \in \mathbb{R}^2, \quad (\alpha, s) \in \mathscr{B}(t) := \{(\alpha, s) \in \mathbb{T}^1 \times \mathbb{R} : -L(\alpha, t) \leq s \leq 0\}, \quad t \geq 0. \tag{III.1.1}$$

Here, we identify the one-dimensional torus $\mathbb{T}^1$ with the interval $[0, 2\pi)$. The coordinate s denotes *arc length* along the filament (at a fixed time), i.e.

$$|\partial_s \mathbf{F}| = 1. \tag{III.1.2}$$

This means that the distance between two material points remains constant. One may interpret the coordinate s as a *monomer counter* along a filament (see Figure III.3). It is increasing outwards: $s = -L$ corresponds to the *pointed end* of the filament, assumed to be in the cell interior (inner boundary), while $s = 0$ corresponds to the *barbed end* of the filament, assumed to be always in contact with the leading edge (outer boundary) of the lamellipodium. The inner boundary is artificial since the rear end

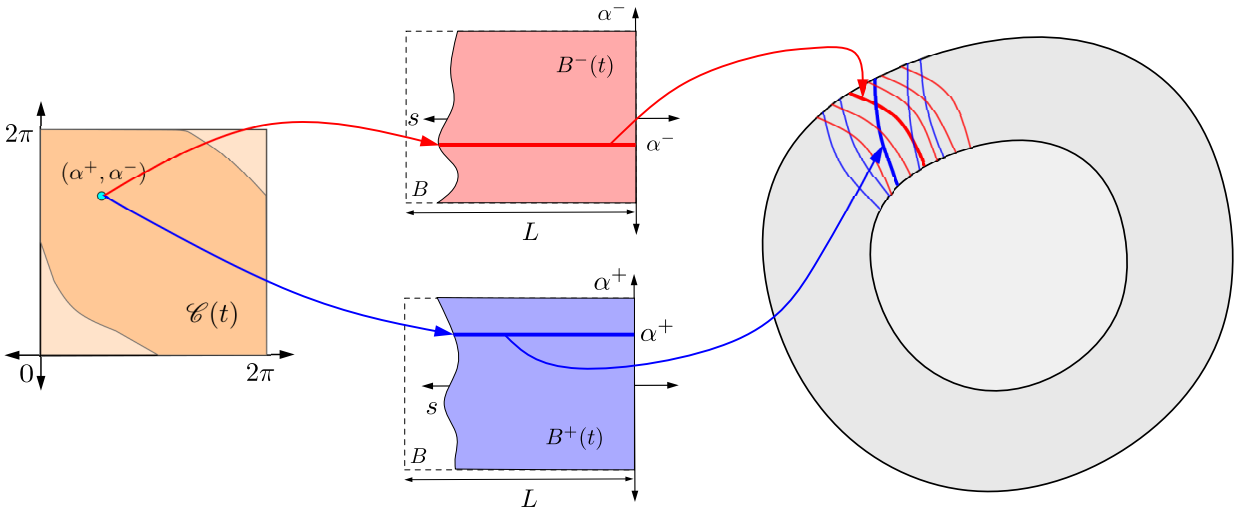

Figure III.2: Functional framework of the model

of the lamellipodium is typically not well-defined. However, we require the outer boundary to be the same for both families, which leads to the *tethering constraint*,

$$\left\{\mathbf{F}^+(\alpha, 0, t) : \alpha \in \mathbb{T}^1\right\} = \left\{\mathbf{F}^-(\alpha, 0, t) : \alpha \in \mathbb{T}^1\right\}, \quad t \geq 0. \tag{III.1.3}$$

The *maximal length* of the filament with label α at time t is denoted by $L(\alpha, t)$. The term *maximal length* is used since in this continuum description $\mathbf{F}(\alpha, \cdot, t)$ represents an ensemble of filaments with varying lengths.

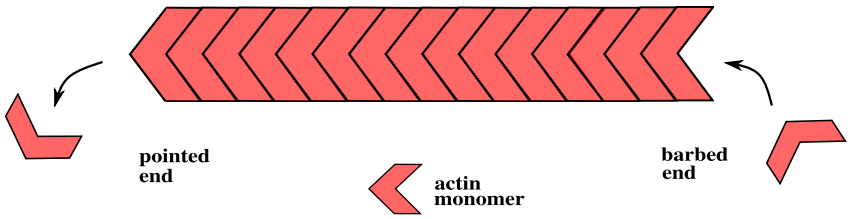

Figure III.3: Actin monomers treadmill through a filament

III.2 Filament mechanics

An important feature of the FBLM is the interplay between macroscopic aspects of cell migration and the meshwork structure. Individual accounts of filaments are employed to systematically derive a continuum model, making the FBLM adaptive to the inclusion of information or assumptions on subprocesses. In this section, submodels of the FBLM are presented which deal with filament mechanisms. In particular, we discuss the length distribution, crossings, polymerization, and density of filaments.

III.2.1 Filament length distribution

The length distribution of filaments is described by the density

$$\eta(\alpha, s, t) > 0.$$

The values $\eta(\alpha, 0, t) > 0$ give the number density of barbed ends along the leading edge. The map $s \mapsto \eta(\alpha, s, t)$ is nondecreasing, indicating the fact that all barbed ends touch the leading edge. The ratio $\eta(\alpha, s, t)/\eta(\alpha, 0, t) \in (0, 1]$ gives the proportion of filaments with length at least $-s$ (since $s \in [-1, 0]$). Another interpretation of η is that of a filament length density with respect to (α, s).

III.2.2 Filament crossings

The set $\mathscr{L}^{\pm}(t) := \mathbf{F}^{\pm}(\mathscr{B}^{\pm}(t), t)$ is the area covered by the $\pm$-family. The two are not necessarily the same. The lamellipodium area at time t is therefore given by $\mathscr{L}(t) = \mathscr{L}^{+}(t) \cup \mathscr{L}^{-}(t)$. The transformation from (α, s) to Eulerian coordinates $\mathbf{x} \in \mathbb{R}^2$ is given by $\mathbf{x} = \mathbf{F}(\alpha, s, t)$, and the area element satisfies

$$\mathrm{d}\mathbf{x} = |\det(\partial_\alpha \mathbf{F}, \partial_s \mathbf{F})| \, \mathrm{d}(\alpha, s) = \left|(\partial_\alpha \mathbf{F})^{\perp} \cdot \partial_s \mathbf{F}\right| \mathrm{d}(\alpha, s).$$

At this point we have to decide about the orientation of the leading edge curve, which we choose as *clockwise* (right-going). This implies that $\partial_\alpha \mathbf{F}^{\perp}$ is an outward normal vector, and that

$$\mathrm{d}\mathbf{x} = \partial_\alpha \mathbf{F}^{\perp} \cdot \partial_s \mathbf{F} \, \mathrm{d}(\alpha, s).$$

The filament length density ϱ with respect to Eulerian coordinates has to satisfy the equality $\varrho \, \mathrm{d}\mathbf{x} = \eta \, \mathrm{d}(\alpha, s)$. Hence, it is given by

$$\varrho[\mathbf{F}] = \frac{\eta}{\partial_\alpha \mathbf{F}^{\perp} \cdot \partial_s \mathbf{F}}, \tag{III.2.1}$$

and we assume that

$$\partial_\alpha \mathbf{F}^{\perp} \cdot \partial_s \mathbf{F} > 0. \tag{III.2.2}$$

Crossing filaments occur in the set $\mathscr{C}(t) = \mathscr{L}^{+}(t) \cap \mathscr{L}^{-}(t)$. The corresponding reduced domains $\mathscr{B}^{\pm}_{\mathscr{C}}(t)$ have to be determined such that $\mathbf{F}^{\pm}(\mathscr{B}^{\pm}_{\mathscr{C}}(t), t) = \mathscr{C}(t)$. We expect that both families provide simple coverings of $\mathscr{C}(t)$, which implies the existence of maps $\psi^{\pm} : \mathscr{B}^{\mp}_{\mathscr{C}}(t) \to \mathscr{B}^{\pm}_{\mathscr{C}}(t)$ such that

$$\mathbf{F}^{\mp} = \mathbf{F}^{\pm} \circ \psi^{\pm}. \tag{III.2.3}$$

III.2.3 Polymerization on barbed ends

Actin monomers move away from the leading edge with the variable polymerization speed $v(\alpha, t)$. Therefore, $s \in [-L, 0]$ is just a geometric parameter and not a Lagrangian variable. The Lagrangian variable is given by

$$\sigma = s + \int_0^t v(\alpha, \tau) \, \mathrm{d}\tau.$$

Therefore, the material derivative (i.e. time derivative for fixed (α, σ)) is

$$D_t := \partial_t + \frac{\partial s}{\partial t}\partial_s = \partial_t - v(\alpha, t)\partial_s \tag{III.2.4}$$

and the velocity of monomers relative to the substrate is $D_t\mathbf{F}$. This is also called the *ground speed* of monomers.

III.2.4 Model for filament density

The leading edge is assumed to be a rectifiable curve, parametrized by

$$x = X^{\pm}(\alpha, t) := \int_0^{\alpha} |\partial_\alpha \mathbf{F}^{\pm}(\alpha', 0, t)| \, \mathrm{d}\alpha'.$$

Denoting the number density of the clockwise filament ends by $u(x, t)$, the requirement

$$u \, \mathrm{d}x = \eta^+(s = 0) \, \mathrm{d}\alpha,$$

for the plus-family implies

$$\eta^+(\alpha, 0, t) = |\partial_\alpha \mathbf{F}^+(\alpha, 0, t)| u(X^+(\alpha, t), t),$$

where we recall η from Section III.2.1. Differentiating with respect to t gives

$$\partial_t \eta^+(s = 0) = |\partial_\alpha \mathbf{F}^+(s = 0)|(\partial_t u + \partial_x(\partial_t X^+ u)),$$

where $\partial_t X^+$ can be interpreted as the *lateral flow velocity* of the filament ends. An analogous computation holds for the number density $v(x, t)$ of the counterclockwise filament ends. Introducing

$$u^+(\alpha, t) = u(X^+(\alpha, t), t) \quad \text{and} \quad u^-(\alpha, t) = v(X^-(\alpha, t), t),$$

the length distribution of filaments at the leading edge evolves through the equation

$$\partial_t \eta^{\pm}(s = 0) = |\partial_\alpha \mathbf{F}^{\pm}(s = 0)| \left(\frac{(\kappa_{\mathrm{br}}/\kappa_{\mathrm{cap}}) u^{\mp} \circ \psi^{\mp}(s = 0)}{1 + u^{\pm} + u^{\mp} \circ \psi^{\mp}(s = 0)} - u^{\pm} \right), \tag{III.2.5}$$

where κ_{br} and κ_{cap} are the branching and the capping rates, respectively. Assuming that the processes regulating the length distribution are fast and are therefore always in equilibrium, we can compute the s-dependence of $\eta^{\pm}$:

$$\eta^{\pm}(\alpha, s, t) = \eta(\alpha, 0, t) \exp\left(-\frac{\kappa_{\mathrm{sev}} s^2}{2v^{\pm}(\alpha, t)}, \right) \tag{III.2.6}$$

where $\eta(\alpha, 0, t)$ is determined by (III.2.5), and with constant severing rate κ_{sev}. Finally, the lamellipodium region is defined by asking the density to be above a threshold value $\eta_{\min} > 0$, i.e. we define the maximal length by

$$\eta^{\pm}(\alpha, -L^{\pm}(\alpha, t), t) = \eta_{\min} > 0. \tag{III.2.7}$$

Finally, one can compute explicitly

$$L(t) := -\frac{\kappa_{\mathrm{cap,eff}}(t)}{\kappa_{\mathrm{sev}}} + \sqrt{\frac{\kappa_{\mathrm{cap,eff}}(t)^2}{\kappa_{\mathrm{sev}}^2} + \frac{2v}{\kappa_{\mathrm{sev}}} \log\left(\frac{\eta(0, t)}{\eta_{\min}} \right)},$$

where we refer to [Man+15] for more details on the derivation. Note that in this case, a faster polymerization speed leads to a wider lamellipodia.

III.3 Modeling filament movement

The main unknowns of the model are the positions and deformations of filaments. A quasi-stationary force balance is assumed, which relies on the fact that viscous forces in the cytosol dampen elastic oscillations in the filament network. This situation gets us into the *friction-dominated regime*, a typical idealization in biology. It is derived from Newton's second law of motion (force = mass × acceleration) when force is much larger than the acceleration term, which we now neglect in the model formulation.

Mathematically, we minimize a potential energy containing contributions from the bending of filaments, repulsion between filaments of the same family, stretching and twisting of cross-links, and stretching of filament-to-substrate adhesions. This is coupled to age-structured population models for the distributions of cross-links and adhesions, with the building and breaking of these connections modeled as stochastic processes.

A fast turnover of cross-links and adhesions compared to other mechanisms (e.g. polymerization and depolymerization) allowed carrying out a formal limit procedure [OS10b], and a rigorous one for a simplified model problem [MO11]. Both has led to friction models. The filament movement is therefore reproduced in the form of a *generalized gradient flow*. The FBLM is phrased as

$$(\mathbf{F}^+(\cdot,\cdot,t),\mathbf{F}^-(\cdot,\cdot,t)) = \lim_{\Delta t\to 0} \operatorname*{argmin}_{(\mathbf{G}^+,\mathbf{G}^-)\in\mathscr{G}(t)} \mathcal{E}^{\mathrm{tot}}(t)[\mathbf{G}^+,\mathbf{G}^-], \tag{III.3.1}$$

where the set of all admissible deformations is defined by

$$\mathscr{G}(t) := \left\{(\mathbf{G}^+,\mathbf{G}^-) \;\middle|\; \mathbf{G}^\pm : \mathscr{B}^\pm(t)\to\mathbb{R}^2,\ |\partial_s\mathbf{G}^\pm| = 1,\ \{\mathbf{G}^+(s=0)\} = \{\mathbf{G}^-(s=0)\}\right\}, \tag{III.3.2}$$

with admissibility conditions occurring as a consequence of the inextensibility (III.1.2) and tethering (III.1.3) constraints. Problem (III.3.1) determines the positions and deformations $(\mathbf{F}^+,\mathbf{F}^-)$ for given densities (η^+,η^-), which is in turn the solution of (III.2.5)-(III.2.7). The total energy $\mathcal{E}^{\mathrm{tot}}$ consists of two parts: the *potential energy* and *friction effects*, written as

$$\mathcal{E}^{\mathrm{tot}}(t)[\mathbf{F}^+,\mathbf{F}^-] := \mathcal{E}^{\mathrm{pot}}(t)[\mathbf{F}^+,\mathbf{F}^-] + \mathcal{E}^{\mathrm{fric}}(t,\Delta t)[\mathbf{F}^+,\mathbf{F}^-]. \tag{III.3.3}$$

Below, these functionals are discussed.

Potential energy. The total potential energy

$$\mathcal{E}^{\mathrm{pot}}(t)[\mathbf{F}^+,\mathbf{F}^-] := \mathcal{E}^B(t)[\mathbf{F}^+] + \mathcal{E}^B(t)[\mathbf{F}^-] + \mathcal{E}^C(t)[\mathbf{F}^+] + \mathcal{E}^C(t)[\mathbf{F}^-] + \mathcal{E}^T(t)[\mathbf{F}^+,\mathbf{F}^-] \tag{III.3.4}$$

consists of the following contributions:

1.1. **Filament bending.** Filaments are described as Euler-Bernoulli beams and we postulate that the potential energy for filament bending takes the form of *Kirchhoff bending energy* from standard linearized beam theory:

$$\mathcal{E}^B(t)[\mathbf{F}] := \frac{\mu^B}{2}\int_{\mathscr{B}(t)} |\partial_s^2\mathbf{F}|^2\eta\,\mathrm{d}(\alpha,s), \tag{III.3.5}$$

with the bending stiffness $\mu^B > 0$, and the density η appears as a weight. In particular, a larger value of η causes a part of the structure to become more resistant to bending.

1.2. **Pressure between locally parallel filaments.** It has been shown that actin filaments usually carry negative electric charges, which provides a repulsive Coulomb force. The potential energy describing pressure caused by repulsion between filaments of the same family is postulated to be

$$\mathcal{E}^C(t)[\mathbf{F}] := \int_{\mathscr{L}(t)} \Phi(\varrho)\varrho \,\mathrm{d}x = \int_{\mathscr{B}(t)} \Phi\left(\frac{\eta}{(\partial_\alpha \mathbf{F})^\perp \cdot \partial_s \mathbf{F}}\right) \eta \,\mathrm{d}(\alpha, s), \tag{III.3.6}$$

where Φ is the *electrostatic potential*. The connection (III.2.1) between the actin densities in Euler and, respectively, Lagrange coordinates is employed.

1.3. **Twisting of cross-links.** We account for the elastic energy in branches turned away from the equilibrium angle. The set $\mathscr{C}(t)$ of all crossing filament pairs is given by

$$\mathscr{C}(t) := \left\{(\alpha^+, \alpha^-) \in \mathbb{T}^1 \times \mathbb{T}^1 \;\middle|\; \exists s^\pm = S^\pm(\alpha^+, \alpha^-, t) : \mathbf{F}^-(\alpha^-, s^-, t) = \mathbf{F}^+(\alpha^+, s^+, t)\right\}, \tag{III.3.7}$$

which has already been introduced in Section III.2.2. Note that $s^\pm = S^\pm(\alpha^+, \alpha^-, t)$ is equivalent to $(\alpha^+, s^+) = \psi^+(\alpha^-, s^-)$ and $(\alpha^-, s^-) = \psi^-(\alpha^+, s^+)$. The potential energy in twisted cross-links is

$$\mathcal{E}^T(t)[\mathbf{F}^+, \mathbf{F}^-] := \frac{\mu^T}{2} \int_{\mathscr{C}(t)} (\phi - \phi_0)^2 \eta^+ \eta^- \,\mathrm{d}(\alpha^+, \alpha^-), \tag{III.3.8}$$

where $\eta^\pm = \eta^\pm(\alpha^\pm, S^\pm(\alpha^+, \alpha^-, t), t)$, and the angle $\phi \in [0, \pi]$ between crossing filaments is given by

$$\cos\phi(\alpha^+, \alpha^-, t) = \partial_s \mathbf{F}^+(\alpha^+, S^+(\alpha^+, \alpha^-, t), t) \cdot \partial_s \mathbf{F}^-(\alpha^-, S^-(\alpha^+, \alpha^-, t), t), \tag{III.3.9}$$

with equilibrium value $\phi_0 \in [0, \pi]$.

Friction effects. The filament-to-substrate *adhesions* and the interaction between filaments of different families via *cross-links* give rise to friction effects. The stretching energies are combined into

$$\mathcal{E}^{\mathrm{fric}}(t, \Delta t)[\mathbf{F}^+, \mathbf{F}^-] = \mathcal{E}^A(t, \Delta t)[\mathbf{F}^+] + \mathcal{E}^A(t, \Delta t)[\mathbf{F}^-] + \mathcal{E}^S(t, \Delta t)[\mathbf{F}^+, \mathbf{F}^-]. \tag{III.3.10}$$

2.1. **Adhesions to the substrate.** For simplicity, we assume that any point on an actin filament can be transiently connected to the substrate, resulting in friction between filament and substrate. Because of polymerization, a monomer which has the coordinate s at time t, had the coordinate $\sigma = s + \int_{t-\Delta t}^t v^\pm(\alpha, t')\,\mathrm{d}t'$ at time $t - \Delta t$. Therefore, if this monomer has been connected to the substrate at time $t - \Delta t$, then it has been displaced by

$$S_{\mathrm{adh}}[\mathbf{F}] := \mathbf{F}(\alpha, s, t) - \mathbf{F}\left(\alpha, s + \int_{t-\Delta t}^t v(\alpha, \tau)\,\mathrm{d}\tau, t - \Delta t\right),$$

and the connection has been stretched to the length of this displacement. The adhesion stretching energy reads as

$$\mathcal{E}^A(t, \Delta t)[\mathbf{F}] = \frac{\mu^A}{2\Delta t} \int_{\mathscr{B}(t)} |S_{\mathrm{adh}}[\mathbf{F}]|^2 \eta \,\mathrm{d}(\alpha, s), \tag{III.3.11}$$

with friction coefficient μ^A.

2.2. **Stretching of cross-links.** We are interested in the displacement $\mathbf{F}^+(\alpha^+, s^+, t) - \mathbf{F}^-(\alpha^-, s^-, t)$, where the two monomers have been at the same place, and have been connected there at time $t - \Delta t$. Recalling the set $\mathscr{C}(t)$ of crossing pairs in (III.3.7), together with the approximation $\int_{t-\Delta t}^{t} v^\pm \approx v^\pm \Delta t$, we have

$$\begin{aligned} & s^\pm + v^\pm \Delta t = S^\pm(\alpha^+, \alpha^-, t - \Delta t) \\ & \iff \mathbf{F}^+(\alpha^+, s^+ + v^+\Delta t, t - \Delta t) = \mathbf{F}^-(\alpha^-, s^- + v^-\Delta t, t - \Delta t). \end{aligned} \tag{III.3.12}$$

The displacement above can be written as

$$S_{\mathrm{scl}}[\mathbf{F}^+, \mathbf{F}^-] := \mathbf{F}^+(\alpha^+, S^+ - v^+\Delta t, t) - \mathbf{F}^-(\alpha^-, S^- - v^-\Delta t, t).$$

A stretching energy for the cross-links now reads

$$\mathcal{E}^S(t, \Delta t)[\mathbf{F}^+, \mathbf{F}^-] = \frac{\mu^S}{2\Delta t} \int_{\mathscr{C}(t-\Delta t)} |S_{\mathrm{scl}}[\mathbf{F}^+, \mathbf{F}^-]|^2 \eta^+ \eta^- \,\mathrm{d}(\alpha^+, \alpha^-), \tag{III.3.13}$$

where $\eta^\pm = \eta^\pm(\alpha^\pm, S^\pm, t - \Delta t)$.

III.3.1 Weak formulation

The displacements $\mathbf{F}^\pm(\cdot, \cdot, t)$ at time t has to satisfy the variational equation

$$\delta\mathcal{E}^{\mathrm{tot}}(t)[\mathbf{F}^+, \mathbf{F}^-](\boldsymbol{\delta}\mathbf{F}^+, \boldsymbol{\delta}\mathbf{F}^-) = 0 \tag{III.3.14}$$

for all admissible variations $\boldsymbol{\delta}\mathbf{F}^\pm$ in (III.3.2), where $\delta\mathcal{E}^{\mathrm{tot}}(t)$ is the variation of the total energy (III.3.3). In the derivation of a strong formulation of (III.3.14), the constraints are enforced by a Lagrange multiplier approach. For the extension of filaments, we introduce the Lagrange multiplier $\lambda_{\mathrm{inext}}(\alpha, s, t)$ and add the contribution

$$\mathcal{E}^{\mathrm{inext}}(t)[\mathbf{F}, \lambda_{\mathrm{inext}}] = \frac{1}{2} \int_{\mathscr{B}(t)} \lambda_{\mathrm{inext}}(\alpha, s, t)(|\partial_s \mathbf{F}|^2 - 1)\eta \,\mathrm{d}(\alpha, s) \tag{III.3.15}$$

to the total energy functional. Note that in order to produce a smooth Lagrangian, we have replaced the constraint by $|\partial_s \mathbf{F}|^2 = 1$. The other constraint involving an equality between sets has to be rewritten as a system of local equations. The deviation between the outer edges of both filament families is described by the functional

$$\mathcal{E}^{\mathrm{tether}}(t)[\mathbf{F}^+, \mathbf{F}^-, \lambda_{\mathrm{tether}}] = \int_{\mathbb{T}^1} \lambda_{\mathrm{tether}}(\alpha^+, t)(\mathbf{F}^+(\alpha^+, 0, t) - \mathbf{F}^-(\hat{\alpha}(\alpha^+, t), 0, t)) \cdot \boldsymbol{\nu}(\alpha^+, t) \,\mathrm{d}\alpha, \tag{III.3.16}$$

where $\hat{\alpha}(\alpha^+, t)$ has to be chosen such that $\mathbf{F}^+(\alpha^+, 0, t) - \mathbf{F}^-(\hat{\alpha}(\alpha^+, t), 0, t)$ is parallel to the unit normal vector

$$\boldsymbol{\nu}(\alpha^+, t) := \frac{\partial_\alpha \mathbf{F}^+(\alpha^+, 0, t)^\perp}{|\partial_\alpha \mathbf{F}^+(\alpha^+, 0, t)|} \tag{III.3.17}$$

along the barbed ends of the clockwise filaments. Recall from Section III.2.2 that we have chosen a clockwise parametrization by α of the leading edge ($s = 0$), so that $\boldsymbol{\nu}$ is an outward pointing normal vector. Below, the variations of energy and additional functionals are computed individually.

Bending. The variation of the bending energy in (III.3.5) reads

$$\delta\mathcal{E}^B(t)[\mathbf{F}]\boldsymbol{\delta}\mathbf{F} = \mu^B \int_{\mathscr{B}(t)} \eta\partial_s^2\mathbf{F}\cdot\partial_s^2\boldsymbol{\delta}\mathbf{F}\,\mathrm{d}(\alpha,s). \tag{III.3.18}$$

Pressure. For the variation of the pressure energy, we recall ϱ in (III.2.1) and take its variation:

$$\delta\varrho(t)[\mathbf{F}]\boldsymbol{\delta}\mathbf{F} = \frac{-\eta}{(\partial_\alpha\mathbf{F}^\perp\cdot\partial_s\mathbf{F})^2}\,(\partial_\alpha\mathbf{F}^\perp\cdot\partial_s\boldsymbol{\delta}\mathbf{F} - \partial_s\mathbf{F}^\perp\cdot\partial_\alpha\boldsymbol{\delta}\mathbf{F}),$$

where we used the fact that $\mathbf{x}^\perp\cdot\mathbf{y} = \mathbf{x}^{\perp\perp}\cdot\mathbf{x}^\perp = -\mathbf{x}\cdot\mathbf{y}^\perp$. Denoting *pressure* by $p(\varrho) := \Phi'(\varrho)\varrho^2$, we compute

$$\delta\mathcal{E}^C(t)[\mathbf{F}]\boldsymbol{\delta}\mathbf{F} = \int_{\mathscr{B}(t)} p(\varrho)(\partial_s\mathbf{F}^\perp\cdot\partial_\alpha\boldsymbol{\delta}\mathbf{F} - \partial_\alpha\mathbf{F}^\perp\cdot\partial_s\boldsymbol{\delta}\mathbf{F})\,\mathrm{d}(\alpha,s). \tag{III.3.19}$$

Twisting. Before finding the variation of the twisting energy, observe that the formula for the angle between filaments is only valid if the constraint $|\partial_s\mathbf{F}| = 1$ holds. In the Lagrange multiplier approach, however, variations which violate this condition are also allowed. Hence, we reformulate the definition (III.3.9) of the angle as

$$\cos\phi(\alpha^+,\alpha^-,t) = \frac{\partial_s\mathbf{F}^+}{|\partial_s\mathbf{F}^+|}(s = S^+(\alpha^+,\alpha^-,t))\cdot\frac{\partial_s\mathbf{F}^-}{|\partial_s\mathbf{F}^-|}(s = S^-(\alpha^+,\alpha^-,t)). \tag{III.3.20}$$

Denoting $T[\mathbf{F}^+,\mathbf{F}^-] := \phi - \phi_0$ and using the identity $\left(\delta\frac{\mathbf{x}}{|\mathbf{x}|}\right)_{|\mathbf{x}|=1} = (\mathbf{x}^\perp\cdot\boldsymbol{\delta}\mathbf{x})\mathbf{x}^\perp$, we compute that

$$\begin{aligned}\partial_{\mathbf{F}^+}T[\mathbf{F}^+,\mathbf{F}^-]\boldsymbol{\delta}\mathbf{F}^+ &= -\frac{1}{\sqrt{1-\cos^2\phi}}((\partial_s\mathbf{F}^+)^\perp\cdot\partial_s\boldsymbol{\delta}\mathbf{F}^+)(\partial_s\mathbf{F}^+)^\perp\cdot\partial_s\mathbf{F}^-\\ &= -\frac{1}{\sin\phi}(\partial_s\mathbf{F}^{+\perp}\cdot\partial_s\mathbf{F}^-)(\partial_s\mathbf{F}^{+\perp}\cdot\partial_s\boldsymbol{\delta}\mathbf{F}^+).\end{aligned}$$

The last equality holds from our requirement that $\phi\in(0,\pi)$, so that $|\sin\phi| = \sin\phi$. If θ is the angle between $\partial_s\mathbf{F}^{+\perp}$ and $\partial_s\mathbf{F}^-$, then

$$\partial_s\mathbf{F}^{+\perp}\cdot\partial_s\mathbf{F}^- = \cos\theta = \cos\left(\frac{\pi}{2}-\phi\right) = \sin\phi,$$

where we used $|\partial_s\mathbf{F}^{+\perp}| = |\partial_s\mathbf{F}^-| = 1$. It follows that

$$\partial_{\mathbf{F}^+}T[\mathbf{F}^+,\mathbf{F}^-]\boldsymbol{\delta}\mathbf{F}^+ = -\partial_s\mathbf{F}^{+\perp}\cdot\partial_s\boldsymbol{\delta}\mathbf{F}^+,$$

where $\partial_s\mathbf{F}^+$ and $\partial_s\boldsymbol{\delta}\mathbf{F}^+$ are evaluated at $(\alpha^+, S^+(\alpha^+,\alpha^-,t),t)$. Similar computations hold for the the other family. Therefore,

$$\delta\mathcal{E}^T[\mathbf{F}^+,\mathbf{F}^-]\boldsymbol{\delta}\mathbf{F}^\pm = \mp\mu^T\int_{\mathscr{C}(t)}(\phi-\phi_0)(\partial_s\mathbf{F}^{\pm\perp}\cdot\partial_s\boldsymbol{\delta}\mathbf{F}^\pm)\eta^+\eta^-\,\mathrm{d}(\alpha^+,\alpha^-). \tag{III.3.21}$$

The sign in the last term is due to the fact that the superscript + indicates the family of clockwise filaments. More precisely, if ϑ is the angle between $\partial_s\mathbf{F}^{-\perp}$ and $\partial_s\mathbf{F}^+$, then

$$\partial_s\mathbf{F}^{-\perp}\cdot\partial_s\mathbf{F}^+ = \cos\vartheta = \cos\left(\frac{\pi}{2}+\phi\right) = \sin(-\phi) = -\sin\phi.$$

Adhesion. For convenience, we use the notation $\widehat{\mathbf{F}} := \mathbf{F}\left(\alpha, s - \int_{t-\Delta t}^{t} v(\alpha,\tau)\,\mathrm{d}\tau, t-\Delta t\right)$. The variation of the stretching energy of the adhesions reads

$$\delta\mathcal{E}^A(t,\Delta t)[\mathbf{F}]\boldsymbol{\delta}\mathbf{F} = \frac{\mu^A}{\Delta t}\int_{\mathscr{B}(t)}\left(\mathbf{F}-\widehat{\mathbf{F}}\right)\cdot\boldsymbol{\delta}\mathbf{F}\eta\,\mathrm{d}(\alpha,s).$$

Sending $\Delta t \to 0$, a material derivative occurs:

$$\lim_{\Delta t\to 0}\delta\mathcal{E}^A(t,\Delta t)[\mathbf{F}]\boldsymbol{\delta}\mathbf{F} = \mu^A\int_{\mathscr{B}(t)} D_t\mathbf{F}\cdot\boldsymbol{\delta}\mathbf{F}\eta\,\mathrm{d}(\alpha,s), \tag{III.3.22}$$

where we recall the definition of the material derivative $D_t := \partial_t - v\partial_s$ in (III.2.4).

Stretching. For cross-link stretching, the variation of the energy (III.3.13) in the direction $\boldsymbol{\delta}\mathbf{F}^+$ is

$$\begin{aligned}\delta\mathcal{E}^S(t,\Delta t)[\mathbf{F}^+,\mathbf{F}^-]\boldsymbol{\delta}\mathbf{F}^+ = \frac{\mu^S}{\Delta t}\int_{\mathscr{C}(t-\Delta t)}&(\mathbf{F}^+(\alpha^+,S^+-v^+\Delta t,t)-\mathbf{F}^-(\alpha^-,S^--v^-\Delta t,t))\cdot\\ &\cdot\boldsymbol{\delta}\mathbf{F}^+(\alpha^+,S^+-v^+\Delta t,t)\,\eta^+\eta^-\,\mathrm{d}(\alpha^+,\alpha^-).\end{aligned}$$

The next step is the limit $\Delta t \to 0$. As the monomers were assumed to have been connected at time $t-\Delta t$ (see (III.3.12)), or in particular, $\mathbf{F}^+(\alpha^+,S^+,t-h) = \mathbf{F}^-(\alpha^-,S^-,t-h)$, we have

$$\begin{aligned}&\frac{1}{\Delta t}\left[\mathbf{F}^+(\alpha^+,S^+-v^+\Delta t,t)-\mathbf{F}^-(\alpha^-,S^--v^-\Delta t,t)\right]\\ &=\frac{\mathbf{F}^+(\alpha^+,S^+-v^+\Delta t,t)-\mathbf{F}^+(\alpha^+,S^+,t-\Delta t)}{\Delta t}+\frac{\mathbf{F}^-(\alpha^-,S^-,t-\Delta t)-\mathbf{F}^-(\alpha^-,S^--v^-\Delta t,t)}{\Delta t}.\end{aligned}$$

As $\Delta t \to 0$, we get the difference

$$D_t^+\mathbf{F}^+(\alpha^+,S^+,t) - D_t^-\mathbf{F}^-(\alpha^-,S^-,t),$$

where the definition of material derivatives $D_t^\pm = \partial_t - v^\pm\partial_s$ in (III.2.4) is employed. This is the *relative velocity* between monomers on crossing filaments. An analogous computation holds for the minus family. In summary,

$$\begin{aligned}&\lim_{\Delta t\to 0}\delta\mathcal{E}^S(t,\Delta t)[\mathbf{F}^+,\mathbf{F}^-]\boldsymbol{\delta}\mathbf{F}^\pm\\ &=\pm\mu^S\int_{\mathscr{C}(t)}(D_t^+\mathbf{F}^+(\alpha^+,S^+,t)-D_t^-\mathbf{F}^-(\alpha^-,S^-,t))\cdot\boldsymbol{\delta}\mathbf{F}^\pm(\alpha^\pm,S^\pm,t)\eta^+\eta^-\,\mathrm{d}(\alpha^+,\alpha^-),\end{aligned}\tag{III.3.23}$$

where again $\eta^\pm = \eta^\pm(\alpha^\pm,S^\pm,t-\Delta t)$.

In the following, we compute the variations of the additional functionals arising from the inextensibility (III.3.15) and tethering (III.3.16) constraints.

Inextensibility. The variation of the functional (III.3.15) is

$$\delta\mathcal{E}^{\text{inext}}(t)[\mathbf{F}, \lambda_{\text{inext}}](\boldsymbol{\delta}\mathbf{F}, \delta\lambda_{\text{inext}}) = \int_{\mathscr{B}(t)} \left(\lambda_{\text{inext}}\eta\partial_s\mathbf{F}\cdot\partial_s\boldsymbol{\delta}\mathbf{F} + (|\partial_s\mathbf{F}|^2 - 1)\eta\delta\lambda_{\text{inext}}\right) \mathrm{d}(\alpha, s), \tag{III.3.24}$$

where the second term in the integral corresponds to the inextensibility constraint (III.1.2).

Tethering. Let us split the integral (III.3.16) into two and perform a change of variables $\hat{\alpha}(\alpha^+, t) = \alpha^-$ so that $(\alpha^+, t) = \hat{\alpha}^{-1}(\alpha^-, t)$ in the second term. We compute

$$\begin{aligned}\mathcal{E}^{\text{tether}}(t)[\mathbf{F}^+, \mathbf{F}^-] = &\int_{\mathbb{T}^1} \lambda_{\text{tether}}(\alpha^+, t)\mathbf{F}^+(\alpha^+, 0, t)\cdot\boldsymbol{\nu}(\alpha^+, t)\,\mathrm{d}\alpha^+ \\ &- \int_{\mathbb{T}^1} \lambda_{\text{tether}}(\hat{\alpha}^{-1}(\alpha^-, t), t)\mathbf{F}^-(\alpha^-, 0, t)\cdot\boldsymbol{\nu}(\hat{\alpha}^{-1}(\alpha^-, t), t)\frac{\partial\hat{\alpha}^{-1}}{\partial\alpha^-}(\alpha^-, t)\,\mathrm{d}\alpha^-.\end{aligned} \tag{III.3.25}$$

Computing the variations in the directions $\boldsymbol{\delta}\mathbf{F}^+$ and $\boldsymbol{\delta}\mathbf{F}^-$, respectively, yields

$$\delta\mathcal{E}^{\text{tether}}(t)[\mathbf{F}^+, \mathbf{F}^-]\boldsymbol{\delta}\mathbf{F}^+ = \int_{\mathbb{T}^1} \lambda_{\text{tether}}(\alpha^+, t)\boldsymbol{\nu}(\alpha^+, t)\cdot\boldsymbol{\delta}\mathbf{F}^+(\alpha^+, 0, t)\,\mathrm{d}\alpha^+,$$

and

$$\begin{aligned}&\delta\mathcal{E}^{\text{tether}}(t)[\mathbf{F}^+, \mathbf{F}^-]\boldsymbol{\delta}\mathbf{F}^- \\ &= -\int_{\mathbb{T}^1} \lambda_{\text{tether}}(\hat{\alpha}^{-1}(\alpha^-, t), t)\,\frac{\partial\hat{\alpha}^{-1}}{\partial\alpha^-}(\alpha^-, t)\,\boldsymbol{\nu}(\hat{\alpha}^{-1}(\alpha^-, t), t)\cdot\boldsymbol{\delta}\mathbf{F}^-(\alpha^-, 0, t)\,\mathrm{d}\alpha^-.\end{aligned}$$

Once the outer edges of the two families coincide, we can replace $\hat{\alpha}^{-1}(\alpha^-, t)$ by the index of the crossing clockwise filament for a given α^- at $s = 0$ and time t, which we shall denote by $a_0^+(\alpha^-, t) := a^+(\alpha^-, 0, t)$. Therefore, the term which guarantees that all pointed ends touch the leading edge gives

$$\delta\mathcal{E}^{\text{tether}}(t)[\mathbf{F}^+, \mathbf{F}^-]\boldsymbol{\delta}\mathbf{F}^\pm = \pm\int_{\mathbb{T}^1} \lambda^\pm_{\text{tether}}\boldsymbol{\nu}^\pm\cdot\boldsymbol{\delta}\mathbf{F}^\pm(\alpha^\pm, 0, t)\,\mathrm{d}\alpha, \tag{III.3.26}$$

with the Lagrange multipliers $\lambda^+_{\text{tether}} := \lambda_{\text{tether}}(\alpha^+, t)$ and $\lambda^-_{\text{tether}} := \lambda_{\text{tether}}(a_0^+(\alpha^-, t), t)\frac{\partial a_0^+}{\partial\alpha^-}(\alpha^-, t)$. The unit normal vectors are

$$\boldsymbol{\nu}^+ = \boldsymbol{\nu}(\alpha^+, t), \quad \text{and} \quad \boldsymbol{\nu}^- = \boldsymbol{\nu}(a_0^+(\alpha^-, t), t), \tag{III.3.27}$$

where the outward pointing normal vector $\boldsymbol{\nu}(\alpha^+, t)$ can be computed from $\partial_\alpha\mathbf{F}^+(\alpha^+, 0, t)^\perp$ as in (III.3.17).

Weak form of the FBLM. Collecting the variations (III.3.18)-(III.3.19), (III.3.21)-(III.3.24), and (III.3.26), the full weak formulation for the position $\mathbf{F}^{\pm}$ reads

$$
\begin{aligned}
0 = &\int_{B^{\pm}(t)} \Big(\underbrace{\mu^B \partial_s^2 \mathbf{F}^{\pm} \cdot \partial_s^2 \boldsymbol{\delta}\mathbf{F}^{\pm}}_{\text{bending}} + \underbrace{\mu^A D_t^{\pm} \mathbf{F}^{\pm} \cdot \boldsymbol{\delta}\mathbf{F}^{\pm}}_{\text{adhesion}} + \underbrace{\lambda^{\pm}_{\text{inext}} \partial_s \mathbf{F}^{\pm} \cdot \partial_s \boldsymbol{\delta}\mathbf{F}^{\pm}}_{\text{inextensibility}} \Big) \eta^{\pm} \, \mathrm{d}(\alpha, s) \\
&+ \int_{B^{\pm}(t)} \underbrace{p(\varrho^{\pm}) \left(\partial_s \mathbf{F}^{\pm\perp} \cdot \partial_\alpha \boldsymbol{\delta}\mathbf{F}^{\pm} - \partial_\alpha \mathbf{F}^{\pm\perp} \cdot \partial_s \boldsymbol{\delta}\mathbf{F}^{\pm} \right)}_{\text{pressure}} \mathrm{d}(\alpha, s) \\
&+ \int_{\mathscr{C}(t)} \Big(\underbrace{\mu^S (D_t^{\pm} \mathbf{F}^{\pm} - D_t^{\mp} \mathbf{F}^{\mp}) \cdot \boldsymbol{\delta}\mathbf{F}^{\pm}}_{\text{cross-link stretching}} \mp \underbrace{\mu^T (\phi - \phi_0) \partial_s \mathbf{F}^{\pm\perp} \cdot \partial_s \boldsymbol{\delta}\mathbf{F}^{\pm}}_{\text{cross-link twisting}} \Big) \eta^+ \eta^- \, \mathrm{d}(\alpha^+, \alpha^-) \\
&\pm \int_{\mathbb{T}^1} \underbrace{\lambda^{\pm}_{\text{tether}} \boldsymbol{\nu}^{\pm} \cdot \boldsymbol{\delta}\mathbf{F}^{\pm}|_{s=0}}_{\text{tethering}} \, \mathrm{d}\alpha,
\end{aligned}
\tag{III.3.28}
$$

where now there are no restrictions on the variations $\boldsymbol{\delta}\mathbf{F}^+$ and $\boldsymbol{\delta}\mathbf{F}^-$. From the first three integrals, the Euler-Lagrange equations are derived. The last integral corresponds to the leading edge of the lamellipodium which contributes boundary conditions to a strong formulation of the problem. Notice that we have not put forces on the inner ends of the lamellipodium, i.e. at $s = -L^{\pm}$.

III.3.2 Domain transformations

To derive the strong formulation of (III.3.28), mappings between integration domains have to be introduced. The coordinate transformations for crossing filaments are summarized in Figure III.4.

We define the transformation from $\mathscr{C}(t)$ to $\mathscr{B}^+_{\mathscr{C}}(t)$ by $(\alpha, s) = (\alpha^+, S^+(\alpha^+, \alpha^-, t))$ and introduce its inverse $(\alpha^+, \alpha^-) = (\alpha, a^-(\alpha, s, t))$. In other words, $a^-(\alpha, s, t)$ is the index of the minus-filament crossing the filament with label α at location s and time t. The argument of $\mathbf{F}^-$ in this case is $(\alpha^-, S^-(\alpha^+, \alpha^-, t)) =: \psi^-(\alpha, s, t)$. Analogously, $\mathscr{C}(t)$ is transformed to $\mathscr{B}^-_{\mathscr{C}}(t)$ through the map $(\alpha, s) = (\alpha^-, S^-(\alpha^+, \alpha^-, t))$, with inverse $(\alpha^+, \alpha^-) = (a^+(\alpha, s, t), \alpha)$. Notice that a^+ and a^- are inverse mappings of each other at $s = 0$.

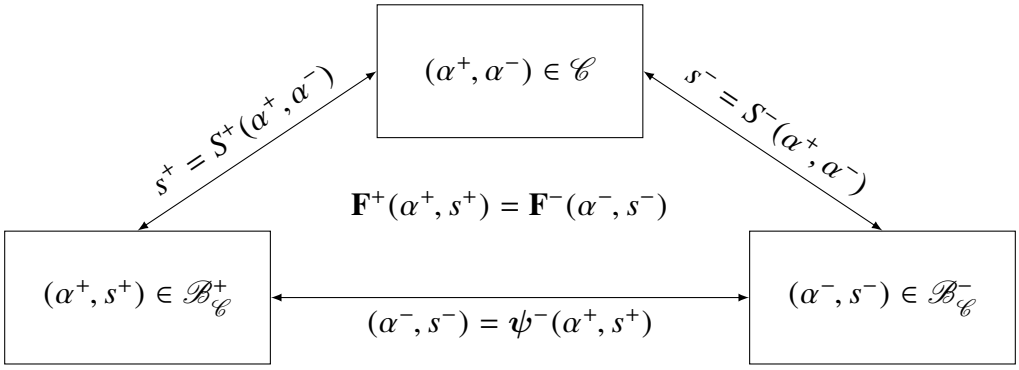

Figure III.4: Coordinate transformations for crossing filaments

Modified stiffness parameters. Going back to the variation of the twisting energy of cross-links, Equation (III.3.21) transforms to

$$\delta\mathcal{E}^T[\mathbf{F}^+,\mathbf{F}^-]\delta\mathbf{F}^\pm = \mp\int_{\mathscr{B}(t)^\pm(t)} \widehat{\mu}^{T,\pm}(\phi-\phi_0)(\partial_s\mathbf{F}^{\pm\perp}\cdot\partial_s\delta\mathbf{F}^\pm)\eta^\pm(\eta^\mp\circ\psi^\mp)\,\mathrm{d}(\alpha,s),$$

with the modified stiffness parameter

$$\widehat{\mu}^{T,\pm} = \mu^T\mathbb{1}_{B^\pm_{\mathscr{C}}(t)}\left|\frac{\partial a^\mp}{\partial s}\right|, \tag{III.3.29}$$

where $\mathbb{1}_A$ denotes the indicator function for a set A. Integration by parts yields the desired form

$$\begin{aligned}\delta\mathcal{E}^T[\mathbf{F}^+,\mathbf{F}^-]\delta\mathbf{F}^\pm = \pm\int_{\mathscr{B}(t)^\pm(t)} &\partial_s(\widehat{\mu}^{T,\pm}\eta^\pm(\eta^\mp\circ\psi^\mp)(\phi-\phi_0)\partial_s\mathbf{F}^{\pm\perp})\cdot\delta\mathbf{F}^\pm\,\mathrm{d}(\alpha,s)\\ &\mp\int_{\mathbb{T}^1}\widehat{\mu}^{T,\pm}\eta^\pm(\eta^\mp\circ\psi^\mp)(\phi-\phi_0)\partial_s\mathbf{F}^{\pm\perp}\cdot\delta\mathbf{F}^\pm\Big|_{s=-L^\pm}^{s=0}\,\mathrm{d}\alpha.\end{aligned}$$

On the other hand, the limit in (III.3.23) becomes

$$\lim_{\Delta t\to 0}\delta\mathcal{E}^S[\mathbf{F}^+,\mathbf{F}^-]\delta\mathbf{F}^\pm = \int_{\mathscr{B}(t)^\pm(t)}\widehat{\mu}^{S,\pm}(D_t^\pm\mathbf{F}^\pm - D_t^\mp\mathbf{F}^\mp\circ\psi^\mp)\cdot\delta\mathbf{F}^\pm\,\eta^\pm(\eta^\mp\circ\psi^\mp)\,\mathrm{d}(\alpha,s),$$

with the modified stiffness parameter

$$\widehat{\mu}^{S,\pm} = \mu^S\mathbb{1}_{B^\pm_{\mathscr{C}}(t)}\left|\frac{\partial a^\mp}{\partial s}\right|. \tag{III.3.30}$$

The additional terms $\left|\frac{\partial a^\mp}{\partial s}\right|$ in (III.3.29) and (III.3.30) can be interpreted as the number of crossings per unit length.

III.4 Euler-Lagrange equations

The Euler-Lagrange equations read

$$\begin{aligned}0 = &\underbrace{\mu^B\partial_s^2(\eta\partial_s^2\mathbf{F})}_{\text{bending}} - \underbrace{\partial_s(\eta\lambda_{\text{inext}}\partial_s\mathbf{F})}_{\text{inextensibility}} + \underbrace{\mu^A\eta D_t\mathbf{F}}_{\text{adhesion}} + \underbrace{\partial_s(p(\varrho)\partial_\alpha\mathbf{F}^\perp) - \partial_\alpha(p(\varrho)\partial_s\mathbf{F}^\perp)}_{\text{pressure}}\\ &\pm\underbrace{\partial_s\left(\widehat{\mu}^T\eta(\eta^*\circ\psi^*)(\phi-\phi_0)\partial_s\mathbf{F}^\perp\right)}_{\text{cross-link twisting}} + \underbrace{\widehat{\mu}^S\eta(\eta^*\circ\psi^*)(D_t\mathbf{F}-D_t^*\mathbf{F}^*\circ\psi^*)}_{\text{cross-link stretching}}.\end{aligned} \tag{III.4.1}$$

The terms in the first row correspond to standard linear models for the deformation of beams. The first term corresponds to bending, the second to stretching (with the right amount to satisfy the inextensibility constraint $|\partial_s\mathbf{F}| = 1$), and the third to friction caused by filament-to-substrate adhesions. The fourth corresponds to a Coulomb-like repulsion between filaments of the same family. All these terms are evaluated at (α, s, t), and none of them generates coupling between the different filaments. In

contrast, the terms on the second line describe the filament cross-links between filaments of different families, where the modified stiffness parameters $\widehat{\mu}^T$ and $\widehat{\mu}^S$ are determined by (III.3.29) and (III.3.30), respectively. These connections allow communication between the two filament families which is important for structural stability. The last term in (III.4.1) shows that the macroscopic effect of the resistance against stretching of cross-links is friction caused by the relative motion of the two filament families.

Solutions of (III.4.1) are subjected to the boundary conditions

$$\mu^B \eta \partial_s^2 \mathbf{F} = 0, \qquad s = -L, 0, \tag{III.4.2}$$

$$\begin{aligned} &- \mu^B \partial_s(\eta \partial_s^2 \mathbf{F}) - p(\varrho)\partial_\alpha \mathbf{F}^\perp + \eta \lambda_{\text{inext}} \partial_s \mathbf{F} \mp \widehat{\mu}^T \eta(\eta^* \circ \psi^*)(\phi - \phi_0)\partial_s \mathbf{F}^\perp \\ &\quad = \begin{cases} 0 & \text{for } s = -L, \\ \mp \lambda_{\text{tether}} \boldsymbol{\nu} & \text{for } s = 0. \end{cases} \end{aligned} \tag{III.4.3}$$

The first boundary condition (III.4.2) models the absence of torque on both filament ends. As mentioned, we do not put forces on the pointed ends of the filaments ($s = -L$), while at the barbed ends ($s = 0$), the Lagrange multiplier λ_{tether} has to be determined such that the tethering constraint is satisfied.

III.4.1 Area constraint

The most abundant molecule in cells is water, essentially an incompressible material at least under normal conditions. Water accounts for 70% or more of the total cell mass, and as a consequence, changing the volume of the cell would require a large amount of force. It is therefore reasonable to assume that the cell maintains a constant area, instead of membrane tension [OS10a] or myosin pulling [Man+15] in the previous model versions. The FBLM with area constraint has already been considered in a study of the limit of short filaments [Hen17]. Mathematically, we impose

$$\frac{\mathrm{d}}{\mathrm{d}t} A(t)[\mathbf{F}] = 0, \quad \text{for } t > 0, \tag{III.4.4}$$

where the current total area $A(t)$ enclosed by the cell at time t can be computed with the help of Green's theorem:

$$A(t)[\mathbf{F}] = \frac{1}{2} \int_{\mathbb{T}^1} \mathbf{F}(\alpha, 0, t) \cdot \partial_\alpha \mathbf{F}(\alpha, 0, t)^\perp \, \mathrm{d}\alpha, \tag{III.4.5}$$

where $\partial_\alpha \mathbf{F}(\alpha, 0, t)^\perp$ is the outward normal vector with respect to the leading edge (c.f Section III.2.2). Indeed, suppose $\Omega \subset \mathbb{R}^2$ is the plane region covered by the cell with area A and boundary $\partial\Omega := \{\mathbf{F}(\alpha, 0, t) : \alpha \in \mathbb{T}^1\}$. Then

$$A[\mathbf{F}] = \iint_\Omega \mathrm{d}x = \frac{1}{2} \iint_\Omega \boldsymbol{\nabla} \cdot x \, \mathrm{d}x = \frac{1}{2} \int_{\partial\Omega} x \cdot \boldsymbol{\nu} \, \mathrm{d}\gamma,$$

where γ is the length of $\partial\Omega$ and $\boldsymbol{\nu}$ is a unit outward normal vector with respect to $\partial\Omega$. With a change of variables, we obtain

$$A[\mathbf{F}] = \frac{1}{2} \int_{\mathbb{T}^1} \mathbf{F}(\alpha, 0, t) \cdot \boldsymbol{\nu} |\mathbf{F}(\alpha, 0, t)| \, \mathrm{d}\alpha = \frac{1}{2} \int_{\mathbb{T}^1} \mathbf{F}(\alpha, 0, t) \cdot \partial_\alpha \mathbf{F}(\alpha, 0, t)^\perp \, \mathrm{d}\alpha.$$

To enforce the area constraint, we introduce a Lagrange multiplier $\lambda_{\text{area}}(t)$ and add the contribution

$$\mathcal{E}^{\text{area}}(t)[\mathbf{F}, \lambda_{\text{area}}] = \lambda_{\text{area}}(t)(A(t)[\mathbf{F}] - A_0), \tag{III.4.6}$$

with $A(t)$ in (III.4.5) and prescribed constant area $A_0 > 0$. The variation of (III.4.6) reads

$$\delta\mathcal{E}^{\text{area}}(t)[\mathbf{F}, \lambda_{\text{area}}](\boldsymbol{\delta}\mathbf{F}, \delta\lambda_{\text{area}}) = (A(t)[\mathbf{F}] - A_0)\delta\lambda_{\text{area}} + \frac{\lambda_{\text{area}}}{2}\int_{\mathbb{T}^1}\Big(\boldsymbol{\delta}\mathbf{F}(\alpha,0,t)\cdot\partial_\alpha\mathbf{F}(\alpha,0,t)^\perp - \mathbf{F}(\alpha,0,t)^\perp\cdot\partial_\alpha\boldsymbol{\delta}\mathbf{F}(\alpha,0,t)\Big)\,\mathrm{d}\alpha.$$

Applying integration by parts to the second term yields

$$\delta\mathcal{E}^{\text{area}}(t)[\mathbf{F}, \lambda_{\text{area}}](\boldsymbol{\delta}\mathbf{F}, \delta\lambda_{\text{area}}) = (A(t)[\mathbf{F}] - A_0)\delta\lambda_{\text{area}} + \lambda_{\text{area}}\int_{\mathbb{T}^1}\partial_\alpha\mathbf{F}(\alpha,0,t)^\perp\cdot\boldsymbol{\delta}\mathbf{F}(\alpha,0,t)\,\mathrm{d}\alpha.$$

Notice that the second term on the right hand side vanishes when $A(t)[\mathbf{F}] = A_0$ for all variations $\delta\lambda_{\text{area}}$, which is equivalent to the constraint (III.4.4). Incorporating the additional functional (III.4.6) to the FBLM (III.4.1)-(III.4.3) modifies the second boundary condition to

$$\begin{aligned} &-\mu^B\partial_s(\eta\partial_s^2\mathbf{F}) - p(\varrho)\partial_\alpha\mathbf{F}^\perp + \eta\lambda_{\text{inext}}\partial_s\mathbf{F} \mp \eta(\eta^*\circ\psi^*)\widetilde{\mu}^T(\phi-\phi_0)\partial_s\mathbf{F}^\perp \\ &\quad= \begin{cases} 0 & \text{for } s = -L, \\ (\mp\lambda_{\text{tether}} - \widetilde{\lambda}_{\text{area}})\boldsymbol{\nu} & \text{for } s = 0, \end{cases} \end{aligned} \tag{III.4.7}$$

where the outward unit normal vector $\boldsymbol{\nu}$ is defined in (III.3.17) and $\widetilde{\lambda}_{\text{area}} := \lambda_{\text{area}}|\partial_\alpha\mathbf{F}(\alpha,0,t)|$.

In the next chapter, the FBLM with area constraint, i.e. equations (III.4.1)-(III.4.2) and (III.4.7) shall be utilized.

Chapter IV

Short filament approximation to the FBLM

Contents

The motivation for the present chapter is a significant simplification of the FBLM to propose a model for the simulation of large cell ensembles. Cells exhibiting lamellipodia typically have about a hundred μm of circumference yet contain a lamellipodial breadth of only a few μm (order of magnitude as in [VSB99; SIC78]). We exploit this information to justify the assumption that the width of lamellipodium on the cell periphery is *small* compared to the cell circumference.

An approximation to the FBLM with vanishing lamellipodium is therefore realized. The model derivation follows the framework presented in Section III.3 while retaining only a minimal number of effects to represent realistic cell organelle mechanics. In particular, the formulation only includes contributions from filament tethering, adhesion to the substrate, polymerization, area constraint, and cross-link twisting. The cell boundary is described by a curve carrying a finite number of degrees of freedom, and the dynamics is a coupled interaction between the evolution of the curve and solutions of PDEs for filament directions and crossings along the curve. A challenging step is to identify an appropriate scaling such that a nontrivial result can be established.

It is worth noting that the thinness of the dense strip provokes shortness of filaments, which gives rise to their stiffness. In contrast to this paradigm, the previous works [HMS17; Hen17] assumed a large filament bending stiffness μ^B to produce rigid filaments.

The chapter is organized as follows. In the first section, a formal limit of the full FBLM with a constant maximal filament length $L \to 0$ is carried out. Starting from Section IV.2, the solutions of the limiting problem are used as ansatz to derive a variational form of the model. Sections IV.3–IV.5 contain detailed discussions of each potential energy contribution, along with constraints, where model problems are considered to explain system mechanics. The last section presents weak and strong formulations of the FBLM with rigid and short filaments, where we obtain a circular-shaped cell as equilibria.

IV.1 Formal limit for short filaments

With only a thin (and dense) lamellipodium, it is a reasonable assumption that filaments are of the same constant length $0 < L \ll 1$. For simplicity, we consider constant and equal polymerization speeds v for both filament families. We further assume that there are no filament pointed ends inside the modeled part of the lamellipodium, with the consequence that the length distributions η and η^* both equal to one. The coordinate change

$$(\alpha, s, t) \mapsto (\alpha, Ls, t)$$

fixes the new domain $B := \{(\alpha, s) : \alpha \in [0, 2\pi), s \in [-1, 0]\}$ and introduces the *small parameter* L into the equations. The computational domain B is now time-independent and rectangular, in contrast to the time-varying and non-rectangular domain $B(t)$ in (III.1.1). The inextensibility constraint (III.1.2) is transformed to

$$|\partial_s \mathbf{F}(\alpha, s, t)| = L. \tag{IV.1.1}$$

In the new coordinates, the FBLM (III.4.1), (III.4.2), (III.4.7) simplifies to

$$\begin{cases} \mu^B \partial_s^4 \mathbf{F} - L^2 \partial_s(\lambda_{\text{inext}} \partial_s \mathbf{F}) + L^4 \mu^A \widetilde{D_t} \mathbf{F} + L^3(\partial_s(p(\varrho)\partial_\alpha \mathbf{F}^\perp) - \partial_\alpha(p(\varrho)\partial_s \mathbf{F}^\perp)) \\ \qquad \pm L^2 \partial_s(\widehat{\mu}^T(\phi - \phi_0)\partial_s \mathbf{F}^\perp) + L^4 \widehat{\mu}^S \widetilde{D_t}(\mathbf{F} - \mathbf{F}^*) = 0, \quad -1 < s < 0, \\ \partial_s^2 \mathbf{F} = 0, \quad \text{for } s = -1, 0, \\ -\mu^B \partial_s^3 \mathbf{F} + L^2 \lambda_{\text{inext}} \partial_s \mathbf{F} - L^3 p(\varrho)\partial_\alpha \mathbf{F}^\perp \mp L^2 \widehat{\mu}^T(\phi - \phi_0)\partial_s \mathbf{F}^\perp \\ \qquad = \begin{cases} 0 & \text{for } s = -1, \\ L^3(\mp \lambda_{\text{tether}} - \widetilde{\lambda}_{\text{area}})\boldsymbol{\nu} & \text{for } s = 0, \end{cases} \end{cases} \tag{IV.1.2}$$

with the modified material derivative

$$\widetilde{D_t} := \partial_t - \frac{v}{L}\partial_s.$$

Sending $L \to 0$ in the reparametrized FBLM (IV.1.2), the solutions of the formal limit

$$\begin{cases} \partial_s^4 \mathbf{F} = 0, & \text{for } -1 < s < 0, \\ \partial_s^3 \mathbf{F} = 0, & \text{for } s = -1, 0, \\ \partial_s^2 \mathbf{F} = 0, & \text{for } s = -1, 0, \end{cases} \tag{IV.1.3}$$

with constraint (IV.1.1) can be written as

$$\mathbf{F}(\alpha, s, t) = \mathbf{z}(\alpha, t) + Ls\boldsymbol{\omega}(\varphi(\alpha, t)), \quad (\alpha, s) \in B, \quad t \geq 0, \tag{IV.1.4}$$

where $\{\mathbf{z}(\alpha, \cdot) : 0 \leq \alpha < 2\pi\} \subset \mathbb{R}^2$ corresponds to the curve traced by the barbed ends of the filaments, assumed to be in contact with the leading edge of the cell. The unit vector $\boldsymbol{\omega}(\varphi) = (\cos\varphi, \sin\varphi)^T$ is the filament direction dependent on the angle-valued function $\varphi(\alpha, t) \in \mathbb{R}$. The other filament family is parametrized similarly, replacing $\mathbf{F}$, $\mathbf{z}$ and φ in (IV.1.3) by $\mathbf{F}^*$, $\mathbf{z}^*$ and φ^*, respectively. As mentioned in the beginning of this chapter, the shortness of filaments, i.e. smallness of L, led to rigid filaments.

One approach to formulate the FBLM with rigid filaments from equations (IV.1.2) and (IV.1.4) is to begin with the derivation of the *total force* and *total torque* balances [HMS17, Section 3]. Using the first equation in (IV.1.2), the total force balance is obtained by integration with respect to s from -1 to 0 and subsequent application of boundary conditions, while the total torque balance is found by its integration against $(\mathbf{F} - \mathbf{z})^\perp = Ls\boldsymbol{\omega}^\perp$. Substitution of ansatz (IV.1.4) to the total balances results to equations for $\mathbf{z}$ and φ, where the coupling in α happens only indirectly through the interaction between the two filament families.

A different strategy shall be adopted here: We systematically derive the rigid filament version starting from the formulation of a Lagrangian functional that accounts for the potential energy of the system (involving only filament-to-substrate adhesions and twisting of cross-links) along with constraints (filament tethering and prescribed area). This framework exposes the mechanisms of each effect more clearly and provides insights on how to achieve desirable steady states, i.e. those consistent with the results of the full FBLM.

IV.2 Variational problem for FBLM with rigid filaments

In this section, the FBLM with the rigid filament ansatz (IV.1.4) is formulated. However, we shall not include all the effects found in the reparametized version (IV.1.2), but only consider elastic contributions from stretching filament-to-substrate adhesions, twisting of cross-links, and constraints from filament tethering and prescribed cell area.

Area constraint. The cell is assumed to maintain a constant area, or in particular,

$$\frac{\mathrm{d}}{\mathrm{d}t} A(t)[\mathbf{z}] = 0, \quad \text{for } t > 0, \tag{IV.2.1}$$

where the current total area enclosed by the cell can be computed with the help of Stokes' theorem,

$$A(t)[\mathbf{z}] = \frac{1}{2} \int_0^{2\pi} \mathbf{z} \cdot \partial_\alpha \mathbf{z}^\perp \, \mathrm{d}\alpha, \tag{IV.2.2}$$

with the outward normal vector $\partial_\alpha \mathbf{z}^\perp$ to the leading edge.

Filament tethering. Filament barbed ends of both families are assumed to tether to the leading edge of the cell. Instead of employing a Lagrange multiplier technique (c.f. III.3.1), it shall be directly

incorporated in the problem formulation. As a consequence, the outer curves of the filament families must coincide at each point in time. Mathematically,

$$\{\mathbf{z}(\alpha,t) : \alpha \in [0,2\pi)\} = \{\mathbf{z}^*(\alpha,t) : \alpha \in [0,2\pi)\}, \quad \forall t \geq 0, \tag{IV.2.3}$$

where we recall that the superscript $*$ denotes the terms corresponding to the $*$-filament family.

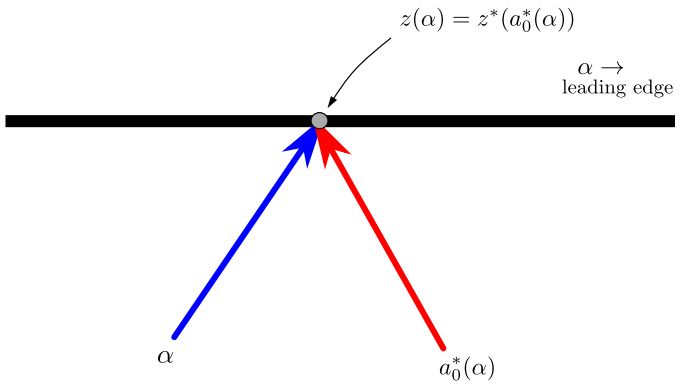

Figure IV.1: Polymerizing filament barbed ends tether to the leading edge

Filament crossings. Connections between two opposing filament families are essential to prevent the structure from disintegrating. The maps introduced in Section III.3.2 are adapted to fit our simplifications. We define a scalar function

$$a^* : B \times [0,\infty) \to [0,2\pi), \tag{IV.2.4}$$

such that $a^*(\alpha,s,t)$ is the index of the $*$-filament crossing the filament with label α at location s and time t. Similarly,

$$a : B \times [0,\infty) \to [0,2\pi), \tag{IV.2.5}$$

gives the index of the non-$*$ filament crossing the filament with label α^* at location s^* and time t. We shall also use the notations

$$a_0^*(\alpha,t) := a^*(\alpha,0,t), \quad \text{and} \quad a_0(\alpha^*,t) := a(\alpha^*,0,t), \tag{IV.2.6}$$

for filaments crossing at the leading edge (where $s, s^* = 0$). The parametrization of the curve is chosen such that a_0^* is an increasing function of α, consequently, $\partial_\alpha a_0^* > 0$.

Going back to filament tethering (IV.2.3), we enforce the equality of sets by assuming that for a fixed clockwise filament with label α, there exists a $*$-filament with label $a_0^*(\alpha,t)$ defined in (IV.2.6) such that

$$\mathbf{z}(\alpha,t) = \mathbf{z}^*(a_0^*(\alpha,t),t). \tag{IV.2.7}$$

Setting $\alpha^* = a_0^*(\alpha)$, the relation (IV.2.7) can be written in a different way,

$$\mathbf{z}(a_0(\alpha^*,t),t) = \mathbf{z}^*(\alpha^*,t). \tag{IV.2.8}$$

Therefore, the scalar functions $a_0^*(\alpha, t)$ and $a_0(\alpha^*, t)$ in (IV.2.6) are inverses of each other, i.e.

$$\alpha = a_0(a_0^*(\alpha, t), t) \quad \text{and} \quad \alpha^* = a_0^*(a_0(\alpha^*, t), t). \tag{IV.2.9}$$

By (IV.2.8), the $*$-filament crossing the filament with label α at $s = 0$ and time t is given by

$$\begin{aligned}\mathbf{F}^*(\alpha^*, s, t) &= \mathbf{z}^*(\alpha^*, t) + Ls\boldsymbol{\omega}(\varphi^*(a_0(\alpha^*, t), t)) \\ &= \mathbf{z}(a_0(\alpha^*, t), t) + Ls\boldsymbol{\omega}(\varphi^*(a_0(\alpha^*, t), t)).\end{aligned} \tag{IV.2.10}$$

This parametrization has the following advantage: Instead of working with two vector unknowns $\mathbf{z}$ and $\mathbf{z}^*$ constrained by the equality of sets in (IV.2.3), one has to find only a vector $\mathbf{z}$ and a scalar a_0^* and use either of the two vector equations (IV.2.7) or (IV.2.8) to find $\mathbf{z}^*$.

Variational formulation. The set of all admissible deformations is defined by

$$\begin{aligned}\mathscr{G}(t) := \Big\{(\mathbf{F}, \mathbf{F}^*) = (\mathbf{z} + Ls\boldsymbol{\omega}, \mathbf{z} + Ls\boldsymbol{\omega}^*)\Big|(\mathbf{z}, \varphi, \varphi^*, a_0^*) \in \mathbb{R}^2 \times \mathbb{R} \times \mathbb{R} \times [0, 2\pi), s \in [-1, 0], \\ \text{(IV.2.1) and (IV.2.7) hold}\Big\},\end{aligned}$$

with the notations $\boldsymbol{\omega} := \boldsymbol{\omega}(\varphi)$ and $\boldsymbol{\omega}^* := \boldsymbol{\omega}(\varphi^*)$. The dynamics of the filaments $(\mathbf{F}, \mathbf{F}^*)$ is governed by the equation

$$(\mathbf{F}(\cdot, \cdot, t), \mathbf{F}^*(\cdot, \cdot, t)) = \lim_{\Delta t \to 0} (\mathbf{F}_{\Delta t}(\cdot, \cdot, t), \mathbf{F}^*_{\Delta t}(\cdot, \cdot, t)), \tag{IV.2.11}$$

where

$$(\mathbf{F}_{\Delta t}(\cdot, \cdot, t), \mathbf{F}^*_{\Delta t}(\cdot, \cdot, t)) := \operatorname{argmin}_{(\mathbf{y}, \psi, \psi^*, b_0^*) \in \mathscr{G}} \mathcal{E}^{\text{tot}}(t, \Delta t)[\mathbf{y}, \psi, \psi^*, b_0^*]. \tag{IV.2.12}$$

The potential energy $\mathcal{E}^{\text{tot}}$ of the network arises from the combined effects of resistance against stretching substrate adhesions and the twisting of cross-links:

$$\mathcal{E}^{\text{tot}}(t, \Delta t)[\mathbf{z}, \varphi, \varphi^*, a_0^*] = \mathcal{E}^{A}(t, \Delta t)[\mathbf{z}, \varphi] + \mathcal{E}^{A*}(t, \Delta t)[\mathbf{z}, \varphi^*, a_0^*] + \mathcal{E}^{T}(t)[\mathbf{z}, \varphi, \varphi^*, a_0^*]. \tag{IV.2.13}$$

The contributions on the right-hand side of the energy above are discussed in the next sections. Here we have decided to skip the pressure term for the following reasons: Mechanically, when filaments are short, repulsion between them is not as significant compared to the effects of adhesion and twisting. Mathematically, it leads to complicated terms which do not fit our present purpose of a simplified model. Nevertheless, we have dedicated Chapter V to discuss its effects on a reduced version of the FBLM. Finally, the pressure term has been included in [Man+15] to stabilize the model in the sense of smoothing in the α-direction which we have, at least for the filament direction angles, achieved through cross-link twisting (c.f. Equation (IV.6.4)).

System (IV.2.11)-(IV.2.13) is a constrained minimization problem, which is solved by introducing the Lagrangian

$$\mathcal{L}[\mathbf{z}, \varphi, \varphi^*, a_0^*, \lambda_{\text{area}}] := \mathcal{E}^{\text{tot}}(t, \Delta t)[\mathbf{z}, \varphi, \varphi^*, a_0^*, \lambda_{\text{area}}] + \mathcal{E}^{\text{area}}(t)[\mathbf{z}, \lambda_{\text{area}}], \tag{IV.2.14}$$

with the Lagrange multiplier $\lambda_{\text{area}}(t)$, and the additional functional

$$\mathcal{E}^{\text{area}}(t)[\mathbf{z}, \lambda_{\text{area}}] = \lambda_{\text{area}}(t)(A(t)[\mathbf{z}] - A_0), \tag{IV.2.15}$$

for a given constant area $A_0 > 0$. Unconstrained stationary points of the Lagrangian must satisfy the first order necessary condition for optimality, i.e. that the first variation of (IV.2.14) vanishes. Then, the displacement $\mathbf{z}(\cdot, t)$, the angles $\varphi(\cdot, t)$, $\varphi^*(\cdot, t)$, and the label a_0^* have to satisfy the variational equation

$$\lim_{\Delta t \to 0} \delta\mathcal{L}[\mathbf{z}, \varphi, \varphi^*, a_0^*](\boldsymbol{\delta}\mathbf{z}, \delta\varphi, \delta\varphi^*, \delta a_0^*) = 0, \tag{IV.2.16}$$

for all admissible variations $(\boldsymbol{\delta}\mathbf{z}, \delta\varphi, \delta\varphi^*, \delta a_0^*) \in \mathcal{G}$, where $\delta\mathcal{L}$ is the variation of the functional (IV.2.14). As promised, each contribution in (IV.2.14) is examined in the subsequent sections. Variations of each functional are also computed to write the weak form (IV.2.16). Model problems are also included to reveal the interplay between the mechanical effects.

IV.3 Resistance against stretching filament-to-substrate adhesions

This section focuses on how the filament-to-substrate adhesion energy, which has already been introduced in (III.3.11), affects the rigid filament version of the FBLM. Hence, in the next subsections, we investigate the FBLM with rigid filaments and a potential energy consisting of only the resistance against stretching substrate adhesions. A discussion of a system of equations for the filament direction angles, along with its equilibria takes us into degenerate situations which were already observed in [OSS08]. First, let us compute for the variation of the total adhesion energy.

Adhesion energy for F−filaments. For clockwise filaments, the energy from stretching substrate adhesions reads

$$\mathcal{E}^A(t, \Delta t)[\mathbf{z}, \varphi] = \frac{\mu^A}{2\Delta t} \int_0^{2\pi} \int_{-1}^{0} |S_{\text{adh}}[\mathbf{z}, \varphi]|^2 \, \mathrm{d}s \, \mathrm{d}\alpha, \tag{IV.3.1}$$

with the displacement (see light blue line in Figure IV.2)

$$\begin{aligned} S_{\text{adh}}[\mathbf{z}, \varphi] &:= \mathbf{z}(\alpha, t) + Ls\boldsymbol{\omega}(\varphi(\alpha, t)) - \left(\mathbf{z}(\alpha, t - \Delta t) + L\left(s + \frac{v}{L}\Delta t\right)\boldsymbol{\omega}(\varphi(\alpha, t - \Delta t))\right) \\ &= \mathbf{z} - \widehat{\mathbf{z}} - v(\Delta t)\widehat{\boldsymbol{\omega}} + Ls(\boldsymbol{\omega} - \widehat{\boldsymbol{\omega}}). \end{aligned} \tag{IV.3.2}$$

Here we used the notations

$$\mathbf{z} := \mathbf{z}(\alpha, t), \quad \boldsymbol{\omega} := \boldsymbol{\omega}(\varphi(\alpha, t)), \quad \widehat{\mathbf{z}} := \mathbf{z}(\alpha, t - \Delta t), \quad \widehat{\boldsymbol{\omega}} := \boldsymbol{\omega}(\varphi(\alpha, t - \Delta t)). \tag{IV.3.3}$$

Notice that the $(1/L)$ appearing in (IV.3.2) with the polymerization speed v is a consequence of the rescaling $s \mapsto Ls$ implemented in the beginning of the present chapter. Evaluating the inner definite integral in (IV.3.1), the adhesion energy becomes

$$\mathcal{E}^A(t, \Delta t)[\mathbf{z}, \varphi] = \frac{\mu^A}{2\Delta t} \int_0^{2\pi} \left(|\mathbf{z} - \widehat{\mathbf{z}} - v(\Delta t)\widehat{\boldsymbol{\omega}}|^2 - L(\mathbf{z} - \widehat{\mathbf{z}} - v(\Delta t)\widehat{\boldsymbol{\omega}}) \cdot (\boldsymbol{\omega} - \widehat{\boldsymbol{\omega}}) + \frac{L^2}{3}|\boldsymbol{\omega} - \widehat{\boldsymbol{\omega}}|^2\right) \mathrm{d}\alpha.$$

Its variation is computed through the chain rule:

$$\delta\mathcal{E}^A(t,\Delta t)[\mathbf{z},\varphi](\boldsymbol{\delta z},\delta\varphi) = \frac{\mu^A}{\Delta t}\int_0^{2\pi}\Big((\mathbf{z}-\widehat{\mathbf{z}}-v(\Delta t)\widehat{\boldsymbol{\omega}})\cdot\boldsymbol{\delta z} - \frac{L}{2}(\boldsymbol{\omega}-\widehat{\boldsymbol{\omega}})\cdot\boldsymbol{\delta z} \\ - \frac{L}{2}(\mathbf{z}-\widehat{\mathbf{z}}-v(\Delta t)\widehat{\boldsymbol{\omega}})\cdot\boldsymbol{\omega}^\perp\delta\varphi + \frac{L^2}{3}(\boldsymbol{\omega}-\widehat{\boldsymbol{\omega}})\cdot\boldsymbol{\omega}^\perp\delta\varphi\Big)\,\mathrm{d}\alpha.$$

Rearranging the terms and sending $\Delta t \to 0$ gives

$$\lim_{\Delta t\to 0}\delta\mathcal{E}^A(t,\Delta t)[\mathbf{z},\varphi](\boldsymbol{\delta z},\delta\varphi) \\ = \mu^A\int_0^{2\pi}\left(\left(\partial_t\mathbf{z} - v\boldsymbol{\omega} - \frac{L}{2}(\partial_t\varphi)\boldsymbol{\omega}^\perp\right)\cdot\boldsymbol{\delta z} + \left(\frac{L^2}{3}\partial_t\varphi - \frac{L}{2}\partial_t\mathbf{z}\cdot\boldsymbol{\omega}^\perp\right)\delta\varphi\right)\mathrm{d}\alpha. \tag{IV.3.4}$$

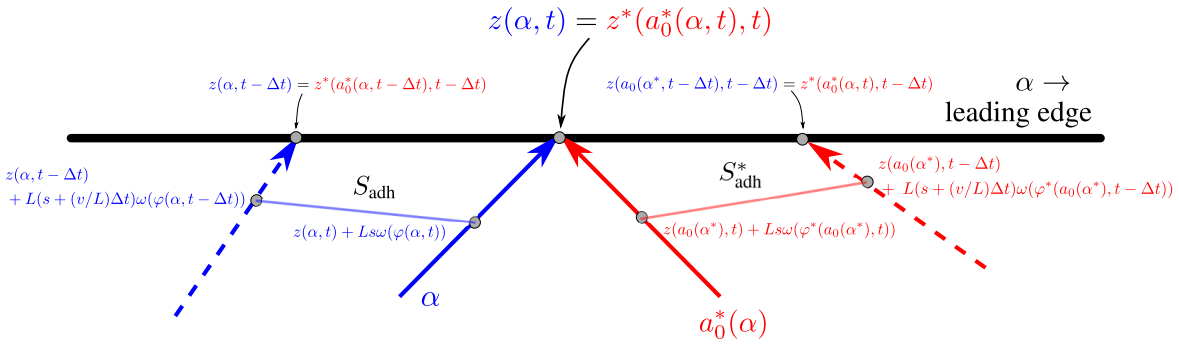

Figure IV.2: Present (solid lines) and past (dashed lines) positions and directions of clockwise (blue) and counterclockwise (red) rigid filaments, with sample monomer (gray circles) displacements caused by *actin filament treadmilling*.

Adhesion energy for $\mathbf{F}^*$−filaments. The adhesion energy from the $*$-filaments is given by

$$\mathcal{E}^{A*}(t,\Delta t)[\mathbf{z},\varphi^*,a_0] = \frac{\mu^A}{2\Delta t}\int_0^{2\pi}\int_{-1}^{0}\left|S^*_{\text{adh}}[\mathbf{z},\varphi^*,a_0]\right|^2\mathrm{d}s\,\mathrm{d}\alpha^*, \tag{IV.3.5}$$

with the displacement

$$S^*_{\text{adh}}[\mathbf{z},\varphi^*,a_0] = \mathbf{z}(a_0(\alpha^*,t),t) - \mathbf{z}(a_0(\alpha^*,t-\Delta t),t-\Delta t) - v(\Delta t)\boldsymbol{\omega}(\varphi^*(a_0(\alpha^*,t-\Delta t),t-\Delta t)) \\ + Ls\left(\boldsymbol{\omega}(\varphi^*(a_0(\alpha^*,t),t)) - \boldsymbol{\omega}(\varphi^*(a_0(\alpha^*,t-\Delta t),t-\Delta t))\right),$$

where we utilize the $\mathbf{F}^*$−filament parametrization in (IV.2.10). All the functions on the right hand side above are composed with a_0^* and a change of variables is performed so that the outer integral in (IV.3.5) is in terms of α and not in α^*. Consequently, (IV.3.5) is transformed to

$$\mathcal{E}^{A*}(t,\Delta t)[\mathbf{z},\varphi^*,a_0^*] = \frac{\mu^A}{2\Delta t}\int_0^{2\pi}\left(\int_{-1}^{0}\left|S^*_{\text{adh}}[\mathbf{z},\varphi^*,a_0^*]\right|^2\mathrm{d}s\right)\partial_\alpha a_0^*\;\mathrm{d}\alpha, \tag{IV.3.6}$$

where the relations in (IV.2.9) between α, α^*, a_0^* and a_0 allow us to write

$$S^*_{\mathrm{adh}}[\mathbf{z}, \varphi^*, a_0^*] := \mathbf{z} - \widehat{\mathbf{z}} \circ \widehat{a}_0 - v(\Delta t)\boldsymbol{\omega}(\widehat{\varphi}^* \circ \widehat{a}_0) + Ls(\boldsymbol{\omega}^* - \boldsymbol{\omega}(\widehat{\varphi}^* \circ \widehat{a}_0)).$$

For the notations, we recall (IV.3.3) and also introduce

$$\widehat{a}_0 := a_0(a_0^*(\alpha, t), t - \Delta t), \quad \boldsymbol{\omega}^* := \boldsymbol{\omega}(\varphi^*(\alpha, t)), \quad \widehat{\varphi}^* := \varphi^*(\alpha, t - \Delta t).$$

Evaluating the integral with respect to s in (IV.3.6), the adhesion energy for $*$-filaments reads

$$\begin{aligned}\mathcal{E}^{A*}(t, \Delta t)[\mathbf{z}, \varphi^*, a_0^*] = \frac{\mu^A}{2\Delta t} \int_0^{2\pi} \Big(&|\mathbf{z} - \widehat{\mathbf{z}} \circ \widehat{a}_0 - v(\Delta t)\boldsymbol{\omega}(\widehat{\varphi}^* \circ \widehat{a}_0)|^2 - L(\mathbf{z} - \widehat{\mathbf{z}} \circ \widehat{a}_0 \\ &- v(\Delta t)\boldsymbol{\omega}(\widehat{\varphi}^* \circ \widehat{a}_0)) \cdot (\boldsymbol{\omega}^* - \boldsymbol{\omega}(\widehat{\varphi}^* \circ \widehat{a}_0)) + \frac{L^2}{3}|\boldsymbol{\omega}^* - \boldsymbol{\omega}(\widehat{\varphi}^* \circ \widehat{a}_0)|^2 \Big) \partial_\alpha a_0^* \, \mathrm{d}\alpha.\end{aligned}$$

Its variation is computed as

$$\begin{aligned}&\delta\mathcal{E}^{A*}(t, \Delta t)[\mathbf{z}, \varphi^*, a_0^*](\delta\mathbf{z}, \delta\varphi^*, \delta a_0^*) \\ &= \frac{\mu^A}{\Delta t} \int_0^{2\pi} \Big((\mathbf{z} - \widehat{\mathbf{z}} \circ \widehat{a}_0 - v(\Delta t)\boldsymbol{\omega}(\widehat{\varphi}^* \circ \widehat{a}_0)) \cdot (\boldsymbol{\delta}\mathbf{z} + (\partial_\alpha \mathbf{z})(\partial_{\alpha^*} a_0)\delta a_0^*) \\ &\quad - \frac{L}{2}(\mathbf{z} - \widehat{\mathbf{z}} \circ \widehat{a}_0 - v(\Delta t)\boldsymbol{\omega}(\widehat{\varphi}^* \circ \widehat{a}_0)) \cdot \boldsymbol{\omega}^{*\perp}(\delta\varphi^* + (\partial_\alpha \varphi^*)(\partial_{\alpha^*} a_0)\delta a_0^*) \\ &\quad - \frac{L}{2}(\boldsymbol{\omega}^* - \boldsymbol{\omega}(\widehat{\varphi}^* \circ \widehat{a}_0)) \cdot (\boldsymbol{\delta}\mathbf{z} + (\partial_\alpha \mathbf{z})(\partial_{\alpha^*} a_0)\delta a_0^*) \\ &\quad + \frac{L^2}{3}(\boldsymbol{\omega}^* - \boldsymbol{\omega}(\widehat{\varphi}^* \circ \widehat{a}_0)) \cdot \boldsymbol{\omega}^{*\perp}(\delta\varphi^* + (\partial_\alpha \varphi^*)(\partial_{\alpha^*} a_0)\delta a_0^*) \Big) \partial_\alpha a_0^* \, \mathrm{d}\alpha + O(\Delta t).\end{aligned}$$

Passing to the limit $\Delta t \to 0$ and using the equality $\partial_\alpha a_0^* = 1/\partial_{\alpha^*} a_0$ allow us to arrive to the contribution

$$\begin{aligned}&\lim_{\Delta t \to 0} \delta\mathcal{E}^{A*}(t, \Delta t)[\mathbf{z}, \varphi^*, a_0^*](\delta\mathbf{z}, \delta\varphi^*, \delta a_0^*) \\ &= \mu^A \int_0^{2\pi} \Big[\Big(\Big(D_t\mathbf{z} - v\boldsymbol{\omega}^* - \frac{L}{2}(D_t\varphi^*)\boldsymbol{\omega}^{*\perp} \Big) \cdot \boldsymbol{\delta}\mathbf{z} + \Big(\frac{L^2}{3} D_t\varphi^* - \frac{L}{2} D_t\mathbf{z} \cdot \boldsymbol{\omega}^{*\perp} \Big) \delta\varphi^* \Big) \partial_\alpha a_0^* \\ &\quad + \Big(\Big(D_t\mathbf{z} - v\boldsymbol{\omega}^* - \frac{L}{2}(D_t\varphi^*)\boldsymbol{\omega}^{*\perp} \Big) \cdot \partial_\alpha \mathbf{z} + \Big(\frac{L^2}{3} D_t\varphi^* - \frac{L}{2} D_t\mathbf{z} \cdot \boldsymbol{\omega}^{*\perp} \Big) \partial_\alpha\varphi^* \Big) \delta a_0^* \Big] \mathrm{d}\alpha, \qquad \text{(IV.3.7)}\end{aligned}$$

where D_t denotes the *material derivative* (of a scalar or a vector) defined by

$$D_t := \Big(\partial_t - \frac{\partial_t a_0^*}{\partial_\alpha a_0^*} \, \partial_\alpha \Big). \qquad \text{(IV.3.8)}$$

Total adhesion energy. The variation of the total adhesion stretching energy ($\mathcal{E}^A + \mathcal{E}^{A*}$) for both filament families is the sum of (IV.3.4) and (IV.3.7), which reads

$$\begin{aligned}
&\lim_{\Delta t\to 0}\left(\delta\mathcal{E}^A(t,\Delta t)[\mathbf{z},\varphi](\boldsymbol{\delta}\mathbf{z},\delta\varphi)+\delta\mathcal{E}^{A*}(t,\Delta t)[\mathbf{z},\varphi^*,a_0^*](\boldsymbol{\delta}\mathbf{z},\delta\varphi^*,\delta a_0^*)\right)\\
&=\mu^A\int_0^{2\pi}\Bigg[\left(\partial_t\mathbf{z}-v\boldsymbol{\omega}-\frac{L}{2}(\partial_t\varphi)\boldsymbol{\omega}^\perp+\partial_\alpha a_0^*\left(D_t\mathbf{z}-v\boldsymbol{\omega}^*-\frac{L}{2}(D_t\varphi^*)\boldsymbol{\omega}^{*\perp}\right)\right)\cdot\boldsymbol{\delta}\mathbf{z}\\
&\quad+\left(\frac{L^2}{3}\partial_t\varphi-\frac{L}{2}\partial_t\mathbf{z}\cdot\boldsymbol{\omega}^\perp\right)\delta\varphi+\partial_\alpha a_0^*\left(\frac{L^2}{3}D_t\varphi^*-\frac{L}{2}D_t\mathbf{z}\cdot\boldsymbol{\omega}^{*\perp}\right)\delta\varphi^*\\
&\quad+\left(\left(D_t\mathbf{z}-v\boldsymbol{\omega}^*-\frac{L}{2}(D_t\varphi^*)\boldsymbol{\omega}^{*\perp}\right)\cdot\partial_\alpha\mathbf{z}+\left(\frac{L^2}{3}D_t\varphi^*-\frac{L}{2}D_t\mathbf{z}\cdot\boldsymbol{\omega}^{*\perp}\right)\partial_\alpha\varphi^*\right)\delta a_0^*\Bigg]\,\mathrm{d}\alpha. \qquad \text{(IV.3.9)}
\end{aligned}$$

For the rest of the present section, we concentrate on a model for rigid filaments which includes only the variation of the adhesion energy (IV.3.9).

IV.3.1 Rigid filaments with adhesion, polymerization, and filament tethering

A rigid filament version of the FBLM with adhesion, polymerization, and filament tethering is described by the weak formulation

$$\lim_{\Delta t\to 0}\left(\delta\mathcal{E}^A(t,\Delta t)[\mathbf{z},\varphi](\boldsymbol{\delta}\mathbf{z},\delta\varphi)+\delta\mathcal{E}^{A*}(t,\Delta t)[\mathbf{z},\varphi^*,a_0^*](\boldsymbol{\delta}\mathbf{z},\delta\varphi^*,\delta a_0^*)\right)=0 \qquad \text{(IV.3.10)}$$

for all admissible variations $\boldsymbol{\delta}\mathbf{z}$, $\delta\varphi$, $\delta\varphi^*$ and δa_0^*. In fact, (IV.3.10) is the variational form already introduced in (IV.2.16) but only with the adhesion energy.

Euler-Lagrange equations. The Euler-Lagrange equations corresponding to Problem (IV.3.10) constitute the following system:

$$\begin{cases}
\partial_t\mathbf{z}-v\boldsymbol{\omega}-\frac{L}{2}(\partial_t\varphi)\boldsymbol{\omega}^\perp+\partial_\alpha a_0^*\left(D_t\mathbf{z}-v\boldsymbol{\omega}^*-\frac{L}{2}(D_t\varphi^*)\boldsymbol{\omega}^{*\perp}\right)=0,\\
\left(D_t\mathbf{z}-v\boldsymbol{\omega}^*-\frac{L}{2}(D_t\varphi^*)\boldsymbol{\omega}^{*\perp}\right)\cdot\partial_\alpha\mathbf{z}+\left(\frac{L^2}{3}D_t\varphi^*-\frac{L}{2}D_t\mathbf{z}\cdot\boldsymbol{\omega}^{*\perp}\right)\partial_\alpha\varphi^*=0,\\
\frac{L^2}{3}\partial_t\varphi-\frac{L}{2}\partial_t\mathbf{z}\cdot\boldsymbol{\omega}^\perp=0,\\
\frac{L^2}{3}D_t\varphi^*-\frac{L}{2}D_t\mathbf{z}\cdot\boldsymbol{\omega}^{*\perp}=0.
\end{cases} \qquad \text{(IV.3.11)}$$

It is helpful to rewrite (IV.3.11) in a more convenient form, i.e. into explicit evolution equations for the unknowns $\mathbf{z}$, a_0^*, φ and φ^*. Inserting the last equation to the second one yields the equation

$$D_t\mathbf{z}-v\boldsymbol{\omega}^*-\frac{L}{2}(D_t\varphi^*)\boldsymbol{\omega}^{*\perp}=\zeta\partial_\alpha\mathbf{z}^\perp,\quad \text{for an unknown auxiliary scalar } \zeta.$$

This, and the first equation in System (IV.3.11) serve as equations for the vector unknown $\mathbf{z}$ and scalar unknowns a_0^* and ζ. The last two equations in (IV.3.11) are then used to eliminate the time derivatives of φ and φ^*. The result reads

$$\begin{cases}
M(\boldsymbol{\omega})\partial_t\mathbf{z}=v\boldsymbol{\omega}-\zeta\partial_\alpha a_0^*\,\partial_\alpha\mathbf{z}^\perp,\\
M(\boldsymbol{\omega}^*)D_t\mathbf{z}=v\boldsymbol{\omega}^*+\zeta\partial_\alpha\mathbf{z}^\perp,
\end{cases} \qquad \text{(IV.3.12)}$$

where the matrix M is defined by

$$M(\boldsymbol{\omega}) := I - \frac{3}{4}\Pi_{\boldsymbol{\omega}^\perp} = \Pi_{\boldsymbol{\omega}} + \frac{1}{4}\Pi_{\boldsymbol{\omega}^\perp} \quad \text{with } \Pi_{\boldsymbol{\omega}} := \boldsymbol{\omega} \otimes \boldsymbol{\omega}. \tag{IV.3.13}$$

Its inverse is just $M(\boldsymbol{\omega})^{-1} = \Pi_{\boldsymbol{\omega}} + 4\Pi_{\boldsymbol{\omega}^\perp}$. Multiplication of $M(\boldsymbol{\omega})^{-1}$ to the first and $M(\boldsymbol{\omega}^*)^{-1}$ to the second equation of (IV.3.12) isolates the time and material derivatives of $\mathbf{z}$, in particular,

$$\begin{cases} \partial_t \mathbf{z} = v\boldsymbol{\omega} - \zeta \partial_\alpha a_0^* M(\boldsymbol{\omega})^{-1} \partial_\alpha \mathbf{z}^\perp, \\ D_t \mathbf{z} = v\boldsymbol{\omega}^* + \zeta M(\boldsymbol{\omega}^*)^{-1} \partial_\alpha \mathbf{z}^\perp. \end{cases} \tag{IV.3.14}$$

Now let us return to the last two equations of System (IV.3.11). For these, we insert the scalar product of the first and second equations of (IV.3.14) with $\boldsymbol{\omega}^\perp$ and $\boldsymbol{\omega}^{*\perp}$, respectively. Gathering our calculations so far, we have transformed (IV.3.11) to

$$\begin{cases} \partial_t \mathbf{z} = v\boldsymbol{\omega} - \zeta \partial_\alpha a_0^* M(\boldsymbol{\omega})^{-1} \partial_\alpha \mathbf{z}^\perp, \\ D_t \mathbf{z} = v\boldsymbol{\omega}^* + \zeta M(\boldsymbol{\omega}^*)^{-1} \partial_\alpha \mathbf{z}^\perp, \\ \frac{L}{6} \partial_t \varphi = -\zeta \partial_\alpha a_0^* (\partial_\alpha \mathbf{z} \cdot \boldsymbol{\omega}), \\ \frac{L}{6} D_t \varphi^* = \zeta (\partial_\alpha \mathbf{z} \cdot \boldsymbol{\omega}^*), \end{cases} \tag{IV.3.15}$$

which is a closed system (two vector and two scalar equations) for the vector $\mathbf{z}$, scalar a_0^*, angles φ and φ^*, and a scalar auxiliary term ζ. Compared to System (IV.3.11), we now possess an extra scalar unknown ζ (with an extra equation). Nevertheless, it is more convenient to work with System (IV.3.15) since each equation comes only with one time derivative of an unknown. Moreover, observe that the dependence on L of the first two equations of (IV.3.15) only happens through their coupling with the last two equations.

Let us take another step and find explicit equations for the scalars ζ and a_0^*. We recall the material derivative D_t in (IV.3.8), and subtract the second equation from the first in (IV.3.15) to eliminate $\partial_t \mathbf{z}$. We obtain

$$v(\boldsymbol{\omega} - \boldsymbol{\omega}^*) - \frac{\partial_t a_0^*}{\partial_\alpha a_0^*} \partial_\alpha \mathbf{z} = \zeta \left(M(\boldsymbol{\omega}^*)^{-1} \partial_\alpha \mathbf{z}^\perp + \partial_\alpha a_0^* M(\boldsymbol{\omega})^{-1} \partial_\alpha \mathbf{z}^\perp \right). \tag{IV.3.16}$$

Projection of (IV.3.16) to $\partial_\alpha \mathbf{z}^\perp$ yields ζ,

$$\zeta := \zeta(\partial_\alpha \mathbf{z}, \boldsymbol{\omega}, \boldsymbol{\omega}^*, q) = \frac{v}{q} (\boldsymbol{\omega} - \boldsymbol{\omega}^*) \cdot \partial_\alpha \mathbf{z}^\perp, \tag{IV.3.17}$$

with the quadratic form q defined by

$$q := q(\partial_\alpha \mathbf{z}, \boldsymbol{\omega}, \boldsymbol{\omega}^*, \partial_\alpha a_0^*) = \left(M(\boldsymbol{\omega}^*)^{-1} \partial_\alpha \mathbf{z}^\perp + \partial_\alpha a_0^* M(\boldsymbol{\omega})^{-1} \partial_\alpha \mathbf{z}^\perp \right) \cdot \partial_\alpha \mathbf{z}^\perp. \tag{IV.3.18}$$

The estimate $q \geq 4\,(1 + \partial_\alpha a_0^*)\,|\partial_\alpha \mathbf{z}|^2$ along with $\partial_\alpha a_0^* > 0$ and $\partial_\alpha \mathbf{z} \neq 0$ assures that q remains positive. On the other hand, projection of (IV.3.16) to $\partial_\alpha \mathbf{z}$ produces an evolution equation for a_0^*,

$$\partial_t a_0^* = \frac{1}{|\partial_\alpha \mathbf{z}|^2} \left(v(\boldsymbol{\omega} - \boldsymbol{\omega}^*) - \left(M(\boldsymbol{\omega}^*)^{-1} \partial_\alpha \mathbf{z}^\perp + \partial_\alpha a_0^* M(\boldsymbol{\omega})^{-1} \partial_\alpha \mathbf{z}^\perp \right) \right) \cdot \partial_\alpha \mathbf{z}\, \partial_\alpha a_0^*, \tag{IV.3.19}$$

which describes how the $*$-filaments are transported in the leading edge of the lamellipodium.

Explicit evolution equations. The second vector equation in (IV.3.15) is replaced by equations (IV.3.17) and (IV.3.19) to finally arrive to the closed system of (explicit) equations:

$$\begin{cases} \partial_t \mathbf{z} = v\boldsymbol{\omega} - \zeta \partial_\alpha a_0^* M(\boldsymbol{\omega})^{-1} \partial_\alpha \mathbf{z}^\perp, \\ \partial_t a_0^* = \frac{1}{|\partial_\alpha \mathbf{z}|^2} \left(v(\boldsymbol{\omega} - \boldsymbol{\omega}^*) - \zeta \left(M(\boldsymbol{\omega}^*)^{-1} \partial_\alpha \mathbf{z}^\perp + \partial_\alpha a_0^* M(\boldsymbol{\omega})^{-1} \partial_\alpha \mathbf{z}^\perp \right) \right) \cdot \partial_\alpha \mathbf{z}\, \partial_\alpha a_0^*, \\ \frac{L}{6} \partial_t \varphi = -\zeta \partial_\alpha a_0^* (\partial_\alpha \mathbf{z} \cdot \boldsymbol{\omega}), \\ \frac{L}{6} D_t \varphi^* = \zeta (\partial_\alpha \mathbf{z} \cdot \boldsymbol{\omega}^*), \end{cases} \tag{IV.3.20}$$

where the matrix M is defined in (IV.3.13) and ζ in (IV.3.17). We close this subsection with some observations regarding System (IV.3.20).

Preliminary observations on System (IV.3.20)**.** When the polymerization speed $v = 0$, the term ζ vanishes, and consequently, all the time derivatives of the unknowns $\mathbf{z}$, a_0^*, φ and φ^* become zero. There is no movement at all, which should not be a surprise because the whole network relies on actin polymerization to evolve.

On the other hand, the first equation in (IV.3.20) can be rearranged to

$$\partial_t \mathbf{z} = \left(v - \zeta \partial_\alpha a_0^* (\partial_\alpha \mathbf{z}^\perp \cdot \boldsymbol{\omega}) \right) \boldsymbol{\omega} - 4\zeta \partial_\alpha a_0^* (\partial_\alpha \mathbf{z} \cdot \boldsymbol{\omega}) \boldsymbol{\omega}^\perp.$$

This is the evolution of the curve $\mathbf{z}$ decomposed into its components in the filament direction $\boldsymbol{\omega}$ and its orthogonal complement $\boldsymbol{\omega}^\perp$. With $\zeta = 0$, the curve $\mathbf{z}$ moves only according to the filament direction $\boldsymbol{\omega}$ with constant speed v.

Meanwhile, the second equation in (IV.3.20) is a nonlinear transport model for a_0^*. It describes the lateral flow of filaments on the leading edge. If we focus only on the first term on its right-hand side (e.g. $\zeta = 0$), we notice that the difference between the directions $\boldsymbol{\omega}$ and $\boldsymbol{\omega}^*$ multiplied by v is the forward speed in the parameter space caused by polymerization. Its scalar product with $\partial_\alpha \mathbf{z}$ projects it onto the membrane. This is consistent with the meaning of a_0^*: the label of $*$-filament crossing non-* filament at the leading edge. Finally, time evolution of the filament direction angles φ and φ^*, along with the auxiliary term ζ, are analyzed and interpreted in the next subsection.

IV.3.2 A singular singularly perturbed system for filament direction angles

In the language of *singular perturbation theory* (c.f. Section II.3), the angle equations of (IV.3.20), together with ζ in (IV.3.17), yield the system

$$\begin{cases} -\frac{1}{q} v \partial_\alpha a_0^* \, (\partial_\alpha \mathbf{z} \cdot \boldsymbol{\omega}) \, (\boldsymbol{\omega} - \boldsymbol{\omega}^*) \cdot \partial_\alpha \mathbf{z}^\perp = \frac{L}{6} \partial_t \varphi, \\ \frac{1}{q} v (\partial_\alpha \mathbf{z} \cdot \boldsymbol{\omega}^*) \, (\boldsymbol{\omega} - \boldsymbol{\omega}^*) \cdot \partial_\alpha \mathbf{z}^\perp = \frac{L}{6} D_t \varphi^*, \end{cases} \tag{IV.3.21}$$

which constitute a *singularly perturbed system* with a small parameter L.

Degenerate system. The degenerate system corresponding to (IV.3.21) is found by setting $L = 0$, i.e.

$$\begin{cases} -v \partial_\alpha a_0^* \, (\partial_\alpha \mathbf{z} \cdot \boldsymbol{\omega}) \, (\boldsymbol{\omega} - \boldsymbol{\omega}^*) \cdot \partial_\alpha \mathbf{z}^\perp = 0, \\ v (\partial_\alpha \mathbf{z} \cdot \boldsymbol{\omega}^*) \, (\boldsymbol{\omega} - \boldsymbol{\omega}^*) \cdot \partial_\alpha \mathbf{z}^\perp = 0. \end{cases} \tag{IV.3.22}$$

We decide to rewrite the tangent vector $\partial_\alpha \mathbf{z}$ to better understand the terms on the left-hand sides of the equations above:

$$\partial_\alpha \mathbf{z} = |\partial_\alpha \mathbf{z}| \boldsymbol{\omega}(\vartheta), \tag{IV.3.23}$$

where ϑ is the direction angle of $\partial_\alpha \mathbf{z}$ and we recall that $\boldsymbol{\omega}$ is the vector $\boldsymbol{\omega}(\cdot) = (\cos(\cdot), \sin(\cdot))^\top$. In these coordinates, the degenerate system (IV.3.22) becomes

$$\begin{cases} -v\partial_\alpha a_0^* \, |\partial_\alpha \mathbf{z}|^2 \cos(\varphi - \vartheta) \, (\sin(\varphi - \vartheta) - \sin(\varphi^* - \vartheta)) = 0, \\ v|\partial_\alpha \mathbf{z}|^2 \cos(\varphi^* - \vartheta) \, (\sin(\varphi - \vartheta) - \sin(\varphi^* - \vartheta)) = 0. \end{cases} \tag{IV.3.24}$$

Below, solutions of this system are discussed.

Case 1. $v = 0$. Without polymerization, there is no movement. This has already been mentioned in the paragraphs below System (IV.3.20), when all time derivatives of the unknowns vanish: $\partial_t \mathbf{z} = \partial_t a_0^* = \partial_t \varphi = \partial_t \varphi^* = 0$.

Case 2. $\partial_\alpha a_0^* = 0$. This makes a_0^* constant, which is not allowed in our parametrization (c.f. (IV.2.6) where we have chosen $\partial_\alpha a_0^* > 0$).

Case 3. $|\partial_\alpha \mathbf{z}| = 0$. The tangent vector $\partial_\alpha \mathbf{z}$ vanishes, which implies that $\mathbf{z}$ is constant in α. This means that the cell is reduced to a single point, which we shall not consider here.

Case 4. $\cos(\varphi - \vartheta) = 0$ and $\cos(\varphi^* - \vartheta) = 0$. This implies that

$$\varphi = \vartheta + \frac{k_1 \pi}{2} \quad \text{and} \quad \varphi^* = \vartheta + \frac{k_2 \pi}{2},$$

for some integers k_1 and k_2. In particular, filaments of both families are orthogonal to the membrane. But since φ and φ^* are the direction angles of crossing clockwise and counterclockwise filaments, respectively, then they must coincide, i.e.

$$\varphi = \varphi^* = \vartheta + \frac{\pi}{2}.$$

Case 5. $\sin(\varphi - \vartheta) - \sin(\varphi^* - \vartheta) = 0$. Its equivalent formulation $(\boldsymbol{\omega} - \boldsymbol{\omega}^*) \cdot \partial_\alpha \mathbf{z}^\perp = 0$ reflects the fact that crossing filaments are symmetric with respect to the outward normal vector to the cell membrane.

Symmetric filaments with respect to the leading edge. Let us focus on Case 5, along with the assumptions that v, $\partial_\alpha a_0^*$ and $|\partial_\alpha \mathbf{z}|$ are all nonzero. If in addition $\cos(\varphi - \vartheta) = 0$, then symmetry implies $\cos(\varphi^* - \vartheta) = 0$ and we are back to Case 4. Hence we also assume that $\cos(\varphi - \vartheta)$ and $\cos(\varphi^* - \vartheta)$ are both non-zero. Now, the equation

$$\sin(\varphi - \vartheta) - \sin(\varphi^* - \vartheta) = 0$$

has the general solution

$$\varphi^* - \vartheta = n\pi + (-1)^n (\varphi - \vartheta), \quad n \in \mathbb{Z}.$$

When $n = 0$, then $\varphi^* = \varphi$, which means that crossing filaments coincide. Because of our choice of orientations for φ and φ^* (right- and left-going, respectively), this is only possible when the filaments are orthogonal to the membrane, which is the situation in Case 4. Again due to the filament orientations, we are left to consider the case when $n = 1$, i.e.

$$\varphi^* = 2\vartheta - \varphi + \pi. \tag{IV.3.25}$$

Assuming that the direction angle ϑ is given, we have just found a one-parameter family of solutions (where φ serves as a *parameter*) to the degenerate system (IV.3.24). This makes (IV.3.21) a *singular singularly perturbed* system of equations for φ and φ^*. In the following, we use (IV.3.25) to find a quasi-stationary equation for φ.

Now, observe that one can take a linear combination of the equations in (IV.3.21) to eliminate their left-hand sides. In particular,

$$\frac{L}{6}(\partial_t\varphi)(\partial_\alpha\mathbf{z}\cdot\boldsymbol{\omega}^*) + \frac{L}{6}(D_t\varphi^*)(\partial_\alpha a_0^*)(\partial_\alpha\mathbf{z}\cdot\boldsymbol{\omega}) = 0,$$

which we rearrange to

$$(\partial_\alpha\mathbf{z}\cdot\boldsymbol{\omega}^*)\partial_t\varphi + \partial_\alpha a_0^*\,(\partial_\alpha\mathbf{z}\cdot\boldsymbol{\omega})\left(\partial_t\varphi^* - \frac{\partial_t a_0^*}{\partial_\alpha a_0^*}\,\partial_\alpha\varphi^*\right) = 0,$$

again recalling the material derivative D_t in (IV.3.8). Inserting φ^* in (IV.3.25) to the equation above yields an evolution equation for φ,

$$|\partial_\alpha\mathbf{z}|\cos(\varphi-\vartheta)\left((1+\partial_\alpha a_0^*)\partial_t\varphi - 2\partial_\alpha a_0^*\,\partial_t\vartheta + \partial_t a_0^*\,(2\partial_\alpha\vartheta - \partial_\alpha\varphi)\right) = 0. \tag{IV.3.26}$$

Explicit evolution equation for φ. A difficulty however in Equation (IV.3.26) is the appearance of the time derivatives of ϑ and a_0^*. We appeal to the evolution equations for $\mathbf{z}$ and a_0^* in (IV.3.20) to remove this issue. Before that, we shall need the time derivative of Equation (IV.3.23):

$$\partial_t(\partial_\alpha\mathbf{z}) = \partial_t(|\partial_\alpha\mathbf{z}|)\,\boldsymbol{\omega}(\vartheta) + |\partial_\alpha\mathbf{z}|\,\boldsymbol{\omega}(\vartheta)^\perp\,\partial_t\vartheta.$$

Scalar product with $\boldsymbol{\omega}(\vartheta)^\perp$ yields an equation for the time derivative of ϑ:

$$\partial_t\vartheta = \frac{1}{|\partial_\alpha\mathbf{z}|}\,\partial_t(\partial_\alpha\mathbf{z})\cdot\boldsymbol{\omega}(\vartheta)^\perp = \frac{1}{|\partial_\alpha\mathbf{z}|^2}\,\partial_t(\partial_\alpha\mathbf{z})\cdot\partial_\alpha\mathbf{z}^\perp, \tag{IV.3.27}$$

where we used $|\partial_\alpha\mathbf{z}| \neq 0$, and reinserted (IV.3.23).

Now, let us go back to the first two equations in (IV.3.20). First, inserting φ^* from (IV.3.25) into these equations is equivalent to just setting $\zeta = 0$. This results to the system

$$\begin{cases} \partial_t\mathbf{z} = v\boldsymbol{\omega}(\varphi), \\ \partial_t a_0^* = \dfrac{2v}{|\partial_\alpha\mathbf{z}|}\cos(\varphi-\vartheta)\,\partial_\alpha a_0^*. \end{cases} \tag{IV.3.28}$$

Taking the α-derivative of the first equation above and assuming sufficient smoothness of $\mathbf{z}$, we obtain

$$\partial_\alpha(\partial_t\mathbf{z}) = \partial_t(\partial_\alpha\mathbf{z}) = v\boldsymbol{\omega}(\varphi)^\perp\partial_\alpha\varphi.$$

Substituting this to (IV.3.27), one has

$$\partial_t \vartheta = \frac{v\cos(\varphi-\vartheta)}{|\partial_\alpha \mathbf{z}|}\,\partial_\alpha\varphi. \tag{IV.3.29}$$

As a last step, let us insert (IV.3.28) and (IV.3.29) to (IV.3.26) to arrive to the equation

$$|\partial_\alpha \mathbf{z}|\cos(\varphi-\vartheta)\left((1+\partial_\alpha a_0^*)\,\partial_t\varphi - \frac{4v}{|\partial_\alpha \mathbf{z}|}\,\cos(\varphi-\vartheta)\,\partial_\alpha a_0^*\,(\partial_\alpha\varphi-\partial_\alpha\vartheta)\right)=0.$$

Because $|\partial_\alpha \mathbf{z}|$ and $\cos(\varphi-\vartheta)$ are both nonzero, we can divide the equation above by $|\partial_\alpha \mathbf{z}|\cos(\varphi-\vartheta)$. Furthermore, $\partial_\alpha a_0^* > 0$, so one can divide by $(1+\partial_\alpha a_0^*)$ and isolate the time derivative of φ. Finally, we have the desired form for the evolution of φ:

$$\partial_t\varphi = \frac{4v\cos(\varphi-\vartheta)\,\partial_\alpha a_0^*}{|\partial_\alpha \mathbf{z}|(1+\partial_\alpha a_0^*)}\,(\partial_\alpha\varphi-\partial_\alpha\vartheta)\,. \tag{IV.3.30}$$

Given $\mathbf{z}$, and hence ϑ, this can be interpreted as a transport equation for φ with speed

$$\varsigma(\partial_\alpha \mathbf{z},\varphi,\partial_\alpha a_0^*) = \frac{4v\cos(\varphi-\vartheta)\,\partial_\alpha a_0^*}{|\partial_\alpha \mathbf{z}|(1+\partial_\alpha a_0^*)}. \tag{IV.3.31}$$

Finally we scrutinize the last term involving $\partial_\alpha\vartheta$ in (IV.3.30). The scalar product of $\boldsymbol{\omega}(\vartheta)^\perp$ and the α-derivative of (IV.3.23) gives us

$$\partial_\alpha\vartheta = \frac{\partial_\alpha^2 \mathbf{z}\cdot\partial_\alpha \mathbf{z}^\perp}{|\partial_\alpha \mathbf{z}|^2}, \tag{IV.3.32}$$

which is related to the signed curvature $\varkappa$ of the curve $\mathbf{z}$ through

$$\varkappa(\partial_\alpha \mathbf{z}) = \frac{\partial_\alpha \mathbf{z}^\perp\cdot\partial_\alpha^2 \mathbf{z}}{|\partial_\alpha \mathbf{z}|^3} = \frac{1}{|\partial_\alpha \mathbf{z}|}\,\partial_\alpha\vartheta.$$

In summary, the filament directions evolve through a nonlinear transport with a source term related to the curvature of the outer edge of the lamellipodium.

Zeroth-order approximation of System (IV.3.20)**.** Let us end this subsection with a summary of our results. Equation (IV.3.25) for the angle φ^*, which is a solution of the degenerate system (IV.3.24), allowed us to find a quasi-stationary equation (IV.3.30) for the angle φ and also for the other unknowns $\mathbf{z}$ and a_0^*. Equations (IV.3.25), (IV.3.28) and (IV.3.30) constitute the zeroth-order approximation (since $L=0$) of model (IV.3.20). It is the system

$$\begin{cases} \partial_t \mathbf{z} = v\boldsymbol{\omega}(\varphi), \\ \partial_t a_0^* = \dfrac{2v}{|\partial_\alpha \mathbf{z}|}\cos(\varphi-\vartheta)\,\partial_\alpha a_0^*, \\ \partial_t\varphi = \dfrac{4v\cos(\varphi-\vartheta)\,\partial_\alpha a_0^*}{|\partial_\alpha \mathbf{z}|(1+\partial_\alpha a_0^*)}\,(\partial_\alpha\varphi-\partial_\alpha\vartheta)\,, \\ \varphi^* = 2\vartheta-\varphi+\pi. \end{cases} \tag{IV.3.33}$$

We reiterate that the values v, $\partial_\alpha a_0^*$, $\partial_\alpha \mathbf{z}$ and $\cos(\varphi-\vartheta)$ are all nonzero. In the next section we look at a steady configuration of System (IV.3.33) and interpret our results.

IV.3.3 Steady configuration for lamellipodium with rigid filaments

A non-trivial steady profile for the FBLM corresponds to the situation when there are only movements in the tangential directions with respect to the leading edge curve. Biologically, this pertains to the so-called *lateral flow* of filaments [Koe+08], a dynamic rotation of the barbed ends along the leading edge, caused by polymerization and the inclination of filaments. In this subsection, we look at steady configurations of System (IV.3.33).

Lamellipodium with steady shape. Components in the normal direction of $\partial_t \mathbf{z}$ must vanish, while the components in the tangential direction should be nonzero. On the other hand, to achieve lateral flow of filaments, $\partial_t a_0^*$ should not vanish and filament direction angles do not change in time, i.e. $\partial_t \varphi = 0$. Therefore, in *equilibrium*, we look for states of System (IV.3.33) that satisfy the following:

$$\begin{cases} \partial_t \mathbf{z} \cdot \partial_\alpha \mathbf{z}^\perp = 0, \\ \partial_t \mathbf{z} \cdot \partial_\alpha \mathbf{z} \neq 0, \\ \partial_t a_0^* \neq 0, \\ \partial_\alpha \varphi = \partial_\alpha \vartheta. \end{cases} \tag{IV.3.34}$$

The last condition implies that $\varphi(\alpha) = \vartheta(\alpha) + \theta$, where θ is a constant angle. In particular, this means that the filament directions are just rotations of the tangent vector. Indeed, one can write

$$\boldsymbol{\omega}(\varphi) = \boldsymbol{\omega}(\vartheta + \theta) = \boldsymbol{\omega}(\vartheta)\cos\theta + \boldsymbol{\omega}(\vartheta)^\perp \sin\theta.$$

Plugging this result to the equations for $\mathbf{z}$, a_0^* and φ^* in System (IV.3.33) yields

$$\begin{cases} \partial_t \mathbf{z} = (v\cos\theta)\boldsymbol{\omega}(\vartheta) + (v\sin\theta)\boldsymbol{\omega}(\vartheta)^\perp, \\ \partial_t a_0^* = \dfrac{2v\cos\theta}{|\partial_\alpha \mathbf{z}|}\, \partial_\alpha a_0^*, \\ \varphi^* = \vartheta + \theta + \pi. \end{cases}$$

Now, to satisfy the first equation in (IV.3.34), $\sin\theta$ must vanish, which forces $\theta = 0$. The system above then reduces to the equations for a steady shape:

$$\begin{cases} \partial_t \mathbf{z} = v\boldsymbol{\omega}(\vartheta), \\ \partial_t a_0^* = \dfrac{2v}{|\partial_\alpha \mathbf{z}|}\, \partial_\alpha a_0^*, \\ \varphi = \vartheta, \\ \varphi^* = \vartheta + \pi. \end{cases} \tag{IV.3.35}$$

The first equation is just

$$\partial_t \mathbf{z} = \frac{v}{|\partial_\alpha \mathbf{z}|}\, \partial_\alpha \mathbf{z},$$

which means that points on the curve $\mathbf{z}$ move in the tangential direction with speed $(v/|\partial_\alpha \mathbf{z}|)$. According to the last two equations in (IV.3.35), filaments of different families are antiparallel to each other and

are tangential to the membrane with relative flow speed $(2v/|\partial_\alpha \mathbf{z}|)$. In this case, the lamellipodium collapses into a dense ring. This degenerate situation has already been observed in the implementations of the rotationally symmetric FBLM in [OSS08], when adhesion is strong and there is no torsional stiffness. We have also mentioned its opposite extreme case: when adhesion is weak and there is no torsional stiffness, filaments become orthogonal to the membrane (see Case 4 after equation (IV.3.24)). The result is a dissolving lamellipodium with filaments in the radial direction, which is again supported with simulations in the rotationally symmetric case [OSS08].

Outlook. Let us close this section with the following remarks. First, one can choose α to be an arc length parametrization of the leading edge, with the consequence $|\partial_\alpha \mathbf{z}| = 1$. This transforms the first two equations in (IV.3.35) into

$$\begin{cases} \partial_t \mathbf{z} = v \partial_\alpha \mathbf{z}, \\ \partial_t a_0^* = 2v \partial_\alpha a_0^*, \end{cases}$$

which are linear transport models with constant speeds. Therefore, every possible (initial) shape is a solution, since points are merely transported around the curve and the cell shape no longer changes in time. Second, we have seen in equilibrium that filaments of different families become antiparallel and tangential to the membrane, which we have obtained by setting $L = 0$. For a nonvanishing L, we consider the Fourier expansion

$$\boldsymbol{\omega}(\varphi) = \Pi_{\boldsymbol{\tau}} \boldsymbol{\omega}(\varphi) + \Pi_{\boldsymbol{\nu}} \boldsymbol{\omega}(\varphi),$$

with the notations for orthogonal projections

$$\Pi_{\boldsymbol{\tau}} := \boldsymbol{\tau} \otimes \boldsymbol{\tau} = \frac{\partial_\alpha \mathbf{z}}{|\partial_\alpha \mathbf{z}|} \otimes \frac{\partial_\alpha \mathbf{z}}{|\partial_\alpha \mathbf{z}|}, \quad \text{and} \quad \Pi_{\boldsymbol{\nu}} := \boldsymbol{\nu} \otimes \boldsymbol{\nu} = \frac{\partial_\alpha \mathbf{z}^\perp}{|\partial_\alpha \mathbf{z}|} \otimes \frac{\partial_\alpha \mathbf{z}^\perp}{|\partial_\alpha \mathbf{z}|}, \tag{IV.3.36}$$

to the tangent $\boldsymbol{\tau}$ and to the outward normal $\boldsymbol{\nu}$ of the leading edge, respectively.

Substituting of the decomposition to the first equation in the original System (IV.3.15) and gathering its normal components, we require

$$\frac{1}{q} \, (\boldsymbol{\omega} - \boldsymbol{\omega}^*) \cdot \partial_\alpha \mathbf{z}^\perp \, \partial_\alpha a_0^* \, (|\partial_\alpha \mathbf{z}|^2 + 3(\partial_\alpha \mathbf{z} \cdot \boldsymbol{\omega})^2) = |\partial_\alpha \mathbf{z}|^2 \, \partial_\alpha \mathbf{z}^\perp \cdot \boldsymbol{\omega}$$

to achieve a steady shape. As symmetry is approached on the left-hand side, i.e. $(\boldsymbol{\omega} - \boldsymbol{\omega}^*) \cdot \partial_\alpha \mathbf{z}^\perp \to 0$, clockwise filaments become more and more tangential to the membrane, i.e. $\partial_\alpha \mathbf{z}^\perp \cdot \boldsymbol{\omega} \to 0$ on the right-hand side. By symmetry, counterclockwise filaments also become tangential to the membrane, i.e. $\partial_\alpha \mathbf{z}^\perp \cdot \boldsymbol{\omega}^* \to 0$. Consequently, the *densities* (c.f. Equation (III.2.1))

$$\varrho := \frac{1}{\partial_\alpha \mathbf{z}^\perp \cdot \boldsymbol{\omega}}, \quad \text{and} \quad \varrho^* := \frac{1}{\partial_\alpha \mathbf{z}^\perp \cdot \boldsymbol{\omega}^*} \tag{IV.3.37}$$

approach infinity. The hope is that the issues raised in this paragraph can be resolved by the effects that are discussed in the next sections.

IV.4 Inclusion of the area constraint

In the present section, we compute for the variation of the additional functional (IV.2.15) that enforces the area constraint. We also include a short subsection to discuss how this constraint influences the model for rigid filaments in System (IV.3.20).

Calculating the variation of the cell area functional in (IV.2.2), one has

$$\delta A(t)[\mathbf{z}]\boldsymbol{\delta}\mathbf{z} = \frac{1}{2}\int_0^{2\pi} (\boldsymbol{\delta}\mathbf{z}\cdot\partial_\alpha\mathbf{z}^\perp + \mathbf{z}\cdot\partial_\alpha\boldsymbol{\delta}\mathbf{z}^\perp)\,\mathrm{d}\alpha = \int_0^{2\pi}\partial_\alpha\mathbf{z}^\perp\cdot\boldsymbol{\delta}\mathbf{z}\,\mathrm{d}\alpha.$$

Consequently, the variation of the area constraint functional in (IV.2.15) reads

$$\delta\mathcal{E}^{\mathrm{area}}(t)[\mathbf{z},\lambda_{\mathrm{area}}](\boldsymbol{\delta}\mathbf{z},\delta\lambda_{\mathrm{area}}) = \lambda_{\mathrm{area}}(t)\int_0^{2\pi}\partial_\alpha\mathbf{z}^\perp\cdot\boldsymbol{\delta}\mathbf{z}\,\mathrm{d}\alpha + \delta\lambda_{\mathrm{area}}(t)(A(t)[\mathbf{z}]-A_0). \tag{IV.4.1}$$

The second term on the right hand side vanishes when $A(t)[\mathbf{z}] = A_0$ for all variations $\delta\lambda_{\mathrm{area}}(t)$, which is exactly the area constraint (IV.2.1). In the sequel, we add this variation to the weak form of a model for rigid filaments with adhesion, polymerization and filament tethering in (IV.3.10).

IV.4.1 Rigid filaments with adhesion, polymerization, tethering and area constraint

The rigid filament version of the FBLM with adhesion, polymerization, tethering and area constraint is derived by including the variation (IV.4.1) to the weak form (IV.3.10). It reads

$$\begin{aligned}\lim_{\Delta t\to 0}\Big(\delta\mathcal{E}^A(t,\Delta t)[\mathbf{z},\varphi](\boldsymbol{\delta}\mathbf{z},\delta\varphi) + \delta\mathcal{E}^{A*}(t,\Delta t)[\mathbf{z},\varphi^*,a_0^*](\boldsymbol{\delta}\mathbf{z},\delta\varphi^*,\delta a_0^*)\Big)\\ + \delta\mathcal{E}^{\mathrm{area}}(t)[\mathbf{z},\lambda_{\mathrm{area}}](\boldsymbol{\delta}\mathbf{z},\delta\lambda_{\mathrm{area}}) = 0\end{aligned} \tag{IV.4.2}$$

for all admissible variations $\boldsymbol{\delta}\mathbf{z}$, $\delta\varphi$, $\delta\varphi^*$, δa_0^*, and $\delta\lambda_{\mathrm{area}}$. Mimicking the steps in Section IV.3.1 allows us to derive the corresponding Euler-Lagrange equations with the area constraint:

$$\begin{cases}\partial_t\mathbf{z} = v\boldsymbol{\omega} - \Big(\zeta\partial_\alpha a_0^* + \frac{1}{q}\widetilde{\lambda}_{\mathrm{area}}(M(\boldsymbol{\omega}^*)^{-1}\partial_\alpha\mathbf{z}^\perp)\cdot\partial_\alpha\mathbf{z}^\perp\Big)\,M(\boldsymbol{\omega})^{-1}\partial_\alpha\mathbf{z}^\perp,\\ \partial_t a_0^* = \Big[v(\boldsymbol{\omega}-\boldsymbol{\omega}^*) - \frac{1}{q}\widetilde{\lambda}_{\mathrm{area}}M(\boldsymbol{\omega})^{-1}\partial_\alpha\mathbf{z}^\perp\\ \qquad - \Big(\zeta - \frac{1}{q}\widetilde{\lambda}_{\mathrm{area}}(M(\boldsymbol{\omega})^{-1}\partial_\alpha\mathbf{z}^\perp)\cdot\partial_\alpha\mathbf{z}^\perp\Big)\Big(M(\boldsymbol{\omega}^*)^{-1}\partial_\alpha\mathbf{z}^\perp + \partial_\alpha a_0^* M(\boldsymbol{\omega})^{-1}\partial_\alpha\mathbf{z}^\perp\Big)\Big]\cdot\frac{\partial_\alpha\mathbf{z}}{|\partial_\alpha\mathbf{z}|^2}\,\partial_\alpha a_0^*,\\ \frac{L}{6}\partial_t\varphi = -\Big(\zeta\partial_\alpha a_0^* + \frac{1}{q}\widetilde{\lambda}_{\mathrm{area}}(M(\boldsymbol{\omega}^*)^{-1}\partial_\alpha\mathbf{z}^\perp)\cdot\partial_\alpha\mathbf{z}^\perp\Big)\,\partial_\alpha\mathbf{z}\cdot\boldsymbol{\omega},\\ \frac{L}{6}D_t\varphi^* = \Big(\zeta - \frac{1}{q}\widetilde{\lambda}_{\mathrm{area}}(M(\boldsymbol{\omega})^{-1}\partial_\alpha\mathbf{z}^\perp)\cdot\partial_\alpha\mathbf{z}^\perp\Big)\,\partial_\alpha\mathbf{z}\cdot\boldsymbol{\omega}^*,\end{cases} \tag{IV.4.3}$$

where $\widetilde{\lambda}_{\mathrm{area}} := (\lambda_{\mathrm{area}}/\mu^A)$, and we recall the terms ζ from (IV.3.17) and q from (IV.3.18). This is just System (IV.3.20) with an area constraint.

Equation for λ_{area}. The task left is to find an equation for the Lagrange multiplier λ_{area}. Integrating the projection of the first equation in (IV.4.3) to $\partial_\alpha \mathbf{z}^\perp$ on the interval $[0, 2\pi)$ with respect to α yields

$$\int_0^{2\pi} \left(v\boldsymbol{\omega} - \left(\zeta \partial_\alpha a_0^* + \frac{1}{q} \widetilde{\lambda}_{\text{area}} (M(\boldsymbol{\omega}^*)^{-1} \partial_\alpha \mathbf{z}^\perp) \cdot \partial_\alpha \mathbf{z}^\perp \right) M(\boldsymbol{\omega})^{-1} \partial_\alpha \mathbf{z}^\perp \right) \cdot \partial_\alpha \mathbf{z}^\perp \, \mathrm{d}\alpha = \int_0^{2\pi} \partial_t \mathbf{z} \cdot \partial_\alpha \mathbf{z}^\perp \, \mathrm{d}\alpha = 0,$$

where the last equality follows from the area constraint (IV.2.1). Solving for λ_{area}, one finds that it is equal to μ^A multiplied by an integral. In this case, we can drop the tildes in System (IV.4.3) for simplicity, and write

$$\lambda_{\text{area}} = \frac{v}{\Lambda} \int_0^{2\pi} \left(\boldsymbol{\omega} - \frac{1}{q} (\boldsymbol{\omega} - \boldsymbol{\omega}^*) \cdot \partial_\alpha \mathbf{z}^\perp \partial_\alpha a_0^* \, (M(\boldsymbol{\omega})^{-1} \partial_\alpha \mathbf{z}^\perp) \right) \cdot \partial_\alpha \mathbf{z}^\perp \, \mathrm{d}\alpha, \tag{IV.4.4}$$

where

$$\Lambda = \int_0^{2\pi} \frac{1}{q} \, (M(\boldsymbol{\omega}^*)^{-1} \partial_\alpha \mathbf{z}^\perp) \cdot \partial_\alpha \mathbf{z}^\perp (M(\boldsymbol{\omega})^{-1} \partial_\alpha \mathbf{z}^\perp) \cdot \partial_\alpha \mathbf{z}^\perp \, \mathrm{d}\alpha.$$

For the remainder of this subsection, we scrutinize System (IV.4.3)-(IV.4.4).

Degenerate system and remarks. As in Section IV.3.2, we consider the degenerate system for the angle equations in (IV.4.3) (c.f. System (IV.3.22)) obtained by setting $L = 0$:

$$\begin{cases} -\left(\zeta \partial_\alpha a_0^* + \frac{1}{q} \lambda_{\text{area}} (M(\boldsymbol{\omega}^*)^{-1} \partial_\alpha \mathbf{z}^\perp) \cdot \partial_\alpha \mathbf{z}^\perp \right) \partial_\alpha \mathbf{z} \cdot \boldsymbol{\omega} = 0, \\ \left(\zeta - \frac{1}{q} \lambda_{\text{area}} (M(\boldsymbol{\omega})^{-1} \partial_\alpha \mathbf{z}^\perp) \cdot \partial_\alpha \mathbf{z}^\perp \right) \partial_\alpha \mathbf{z} \cdot \boldsymbol{\omega}^* = 0, \end{cases} \tag{IV.4.5}$$

As we do not want the filaments to be orthogonal to the membrane, i.e. $\partial_\alpha \mathbf{z} \cdot \boldsymbol{\omega} \neq 0$ or $\partial_\alpha \mathbf{z} \cdot \boldsymbol{\omega}^* \neq 0$, the second equation implies that

$$\zeta - \frac{1}{q} \lambda_{\text{area}} (M(\boldsymbol{\omega})^{-1} \partial_\alpha \mathbf{z}^\perp) \cdot \partial_\alpha \mathbf{z}^\perp = 0. \tag{IV.4.6}$$

The term ζ from (IV.3.17) thus allows us to write (IV.4.6) as

$$v(\boldsymbol{\omega} - \boldsymbol{\omega}^*) \cdot \partial_\alpha \mathbf{z}^\perp = \lambda_{\text{area}} (M(\boldsymbol{\omega})^{-1} \partial_\alpha \mathbf{z}^\perp) \cdot \partial_\alpha \mathbf{z}^\perp. \tag{IV.4.7}$$

Inserting this to the first equation in (IV.4.5) leaves us with $\lambda_{\text{area}} = 0$, and consequently from (IV.4.7), we obtain $(\boldsymbol{\omega} - \boldsymbol{\omega}^*) \cdot \partial_\alpha \mathbf{z}^\perp = 0$. However, this requirement forces $\boldsymbol{\omega} \cdot \partial_\alpha \mathbf{z}^\perp = 0$ and $\boldsymbol{\omega}^* \cdot \partial_\alpha \mathbf{z}^\perp = 0$ as one can see in (IV.4.4). The density of filaments again becomes infinite, and the problems we encountered in the previous section are still unresolved.

We speculate that adding the area constraint is not enough to control the cell shape and the density of filaments, since it only controls cell size. On the other hand, λ_{area} is a global variable, so its inclusion is not expected to have control over local quantities (in the variable α). In the next section, another effect is introduced which takes care of the issues still reflected in the present model (IV.4.3)-(IV.4.4).

IV.5 Resistance against cross-link twisting with preferred angle and symmetry at the leading edge

With the rigid filament ansatz, turning the cross-linked filaments away from the equilibrium angle $\phi_0 \in [0, \pi]$ is assumed to produce the energy

$$\mathcal{E}^T(t)[\mathbf{z}, \varphi, \varphi^*, a_0^*] = \frac{\mu^T}{2} \int_{\mathscr{C}(t)} \left(\varphi^*(a_0(\alpha^*, t), t) - \varphi(\alpha, t) - \phi_0\right)^2 \mathrm{d}(\alpha, \alpha^*), \tag{IV.5.1}$$

where the set of all crossing filament pairs is given by

$$\mathscr{C}(t) = \left\{(\alpha, \alpha') \in [0, 2\pi)^2 \,\middle|\, \exists s, s' \in [-1, 0] \text{ s.t. } \mathbf{F}(\alpha, s, t) = \mathbf{F}^*(\alpha', s', t))\right\}.$$

To derive the rigid filament version of the FBLM with adhesion, polymerization, tethering, area constraint and cross-link twisting, one can compute the variation of (IV.5.1), follow the steps in Section III.3.2 to map $\mathscr{C}(t)$ to B, and finally combine the result with (IV.3.9) and (IV.4.1). Here we proceed with approximations that exploit the smallness of L along with simplifying assumptions before computing the variation of the twisting energy.

The resistance against cross-link twisting is assumed to be very strong. However, for a curved membrane, we cannot expect the equilibrium angle at all crossings. Therefore, as an approximation, the equilibrium angle is enforced at the barbed ends and deviation from the former is penalized at the other crossings by an energy functional discussed below.

Now, assuming short ($0 < L \ll 1$) and rigid filaments with equilibrium angle ϕ_0 at the barbed ends, one has

$$\mathbf{F}(\alpha, s, t) = \mathbf{z}(\alpha, t) + Ls\boldsymbol{\omega}(\varphi(\alpha, t)), \quad \mathbf{F}^*(\alpha, s, t) = \mathbf{z}(\alpha, t) + Ls\boldsymbol{\omega}(\varphi(\alpha, t) + \phi_0), \tag{IV.5.2}$$

for $0 \le \alpha < 2\pi$ and $-1 \le s \le 0$. Here, α indicates filaments of the $\mathbf{F}$-family as in the ansatz (IV.1.4), whereas $\alpha^* = a_0^*(\alpha, t)$ indicates filaments of the $\mathbf{F}^*$-family as parametrized in (IV.2.10).

Filament crossings. Given $(\alpha, s) \in B$, we try to find (α', s') such that $\mathbf{F}(\alpha, s, t) = \mathbf{F}^*(\alpha', s', t)$. Since the filaments are short, we can assume that $\alpha' - \alpha = O(L)$ and approximate from (IV.5.2):

$$\begin{aligned}\mathbf{F}^*(\alpha', s', t) &= \mathbf{z}(\alpha, t) + (\alpha' - \alpha)\partial_\alpha \mathbf{z}(\alpha, t) + Ls'\boldsymbol{\omega}(\varphi(\alpha, t) + \phi_0) + O(L^2)\\ &\approx \mathbf{z}(\alpha, t) + (\alpha' - \alpha)\partial_\alpha \mathbf{z}(\alpha, t) + Ls'\boldsymbol{\omega}^*,\end{aligned}$$

where from now on $\boldsymbol{\omega}^* := \boldsymbol{\omega}(\varphi + \phi_0)$. This gives the approximate equation

$$Ls\boldsymbol{\omega} = (\alpha' - \alpha)\partial_\alpha \mathbf{z} + Ls'\boldsymbol{\omega}^*, \tag{IV.5.3}$$

where $\boldsymbol{\omega} := \boldsymbol{\omega}(\varphi)$. Scalar multiplication with $\boldsymbol{\omega}^{*\perp}$ yields $Ls\boldsymbol{\omega} \cdot \boldsymbol{\omega}^{*\perp} = (\alpha' - \alpha)\partial_\alpha \mathbf{z} \cdot \boldsymbol{\omega}^{*\perp}$, and since $\boldsymbol{\omega} \cdot \boldsymbol{\omega}^{*\perp} = -\sin\phi_0$, we compute that

$$\alpha' - \alpha = \frac{Ls \sin\phi_0}{\partial_\alpha \mathbf{z}^\perp \cdot \boldsymbol{\omega}^*}. \tag{IV.5.4}$$

At the barbed ends where $s = 0$, the labels are equal, i.e. $\alpha' = \alpha$, as expected.

Twisting energy. For the angle between filaments at the crossing, we approximate

$$\varphi(\alpha', t) + \phi_0 - \varphi(\alpha, t) \approx \phi_0 + (\alpha' - \alpha)\partial_\alpha \varphi.$$

With $\alpha^* = a_0^*(\alpha', t)$, the approximation above transforms the twisting energy (IV.5.1) into

$$\mathcal{E}^T(t)[\mathbf{z}, \varphi, a_0^*] = \frac{\mu^T}{2} \int_{\mathscr{C}(t)} (\alpha' - \alpha)^2 (\partial_\alpha \varphi)^2 \, \mathrm{d}(\alpha, \alpha^*). \tag{IV.5.5}$$

For further computation of the twisting energy, we make the simplifying symmetry assumption

$$\partial_\alpha \mathbf{z}^\perp \cdot \boldsymbol{\omega} = \partial_\alpha \mathbf{z}^\perp \cdot \boldsymbol{\omega}^* = |\partial_\alpha \mathbf{z}| \cos(\phi_0/2), \tag{IV.5.6}$$

which has already been enforced in the derivation of rigid filaments with adhesion, polymerization, tethering and vanishing length found in (IV.3.33) (c.f. Case 5 in Section IV.3.2). In particular, this means that crossing filaments at the leading edge meet with equilibrium angle ϕ_0 and are symmetric with respect to the normal direction $\partial_\alpha \mathbf{z}^\perp$.

The scalar product of (IV.5.3) with $\boldsymbol{\omega}^\perp$, i.e.

$$\alpha' - \alpha = \frac{L s' \sin \phi_0}{\partial_\alpha \mathbf{z}^\perp \cdot \boldsymbol{\omega}},$$

together with (IV.5.4) and symmetry (IV.5.6) imply that $s = s'$ and

$$-\frac{2L \sin(\phi_0/2)}{|\partial_\alpha \mathbf{z}|} \leq \alpha' - \alpha \leq 0.$$

We then continue to compute for the twisting energy (IV.5.5) by a coordinate transformation, where we introduce the variable $\mathbb{a} := \alpha' - \alpha$. It yields the functional

$$\begin{aligned}\mathcal{E}^T(t)[\mathbf{z}, \varphi, a_0^*] &= \frac{\mu^T}{2} \int_0^{2\pi} \int_{-(2L \sin(\phi_0/2)/|\partial_\alpha \mathbf{z}|)}^0 \mathbb{a}^2 (\partial_\alpha \varphi)^2 \partial_\alpha a_0^* \, \mathrm{d}\mathbb{a} \, \mathrm{d}\alpha \\ &= \widehat{\mu}^T \left(\frac{L\mu^A}{4}\right) \int_0^{2\pi} \frac{\partial_\alpha a_0^*}{|\partial_\alpha \mathbf{z}|^3} (\partial_\alpha \varphi)^2 \, \mathrm{d}\alpha,\end{aligned}$$

where the parameter $\widehat{\mu}^T := \dfrac{16\mu^T}{3\mu^A} L^2 \sin^3(\phi_0/2)$ is chosen to simplify the computations in the next section.

Variation of twisting energy and rescaling. As a simplification, we only consider the variation of the twisting energy with respect to φ:

$$\partial_\varphi \mathcal{E}^T[\mathbf{z}, \varphi, a_0^*]\delta\varphi = -\widehat{\mu}^T \left(\frac{L\mu^A}{2}\right) \int_0^{2\pi} \partial_\alpha \left(\frac{\partial_\alpha a_0^*}{|\partial_\alpha \mathbf{z}|^3} \, \partial_\alpha \varphi\right) \delta\varphi \, \mathrm{d}\alpha.$$

Finally we rescale μ^T to (μ^T/L^2) so that $\widehat{\mu}^T$ becomes $O(L)$. This is the same order as the lowest one in the variation with respect to angles of the adhesion energy in (IV.3.9). Adding the contribution above to the weak form (IV.4.2) completes the formulation of the variational problem (IV.2.16) of the present chapter.

IV.6 Zero-width limit for the lamellipodium

The rigid filament version of the FBLM with adhesion, polymerization, tethering, area constraint and cross-link twisting reads as the variational form

$$\lim_{\Delta t\to 0}\Big(\delta\mathcal{E}^A(t,\Delta t)[\mathbf{z},\varphi](\boldsymbol{\delta}\mathbf{z},\delta\varphi)+\delta\mathcal{E}^{A*}(t,\Delta t)[\mathbf{z},\varphi^*,a_0^*](\boldsymbol{\delta}\mathbf{z},\delta\varphi^*,\delta a_0^*)\Big)$$
$$+\,\delta\mathcal{E}^{\text{area}}(t)[\mathbf{z},\lambda_{\text{area}}](\boldsymbol{\delta}\mathbf{z},\delta\lambda_{\text{area}})+\partial_\varphi\mathcal{E}^T[\mathbf{z},\varphi,a_0^*]\delta\varphi=0 \tag{IV.6.1}$$

which must hold for all admissible variations $\boldsymbol{\delta}\mathbf{z}$, $\delta\varphi$, $\delta\varphi^*$, δa_0^*, and $\delta\lambda_{\text{area}}$. With the simplifications of equilibrium angle at the barbed ends (IV.5.2) and symmetry (IV.5.6) with respect to $\partial_\alpha\mathbf{z}^\perp$ of the previous section, we derive equations for $\mathbf{z}$, a_0^*, and φ in the limit $L\to 0$.

Euler-Lagrange equations for adhesion, area constraint, and twisting in the limit $L\to 0$. The strong form is derived from Equation (IV.6.1) with preferred angle and symmetry at the leading edge. Passing to the limit $L\to 0$, we obtain the final system

$$\partial_t\mathbf{z}-v\boldsymbol{\omega}+\partial_\alpha a_0^*(D_t\mathbf{z}-v\boldsymbol{\omega}^*)+\lambda_{\text{area}}\partial_\alpha\mathbf{z}^\perp=0, \tag{IV.6.2}$$
$$(D_t\mathbf{z}-v\boldsymbol{\omega}^*)\cdot\partial_\alpha\mathbf{z}=0, \tag{IV.6.3}$$
$$\partial_t\mathbf{z}\cdot\boldsymbol{\omega}^\perp+\partial_\alpha a_0^*D_t\mathbf{z}\cdot\boldsymbol{\omega}^{*\perp}+\widehat{\mu}^T\partial_\alpha\left(\frac{\partial_\alpha a_0^*}{|\partial_\alpha\mathbf{z}|^3}\,\partial_\alpha\varphi\right)=0, \tag{IV.6.4}$$

where we recall for convenience that $D_t:=\partial_t-\frac{\partial_t a_0^*}{\partial_\alpha a_0^*}\,\partial_\alpha$ and $\widehat{\mu}^T:=\frac{16\mu^T}{3\mu^A}\sin^3(\phi_0/2)$. Using (IV.6.3) in the scalar product of (IV.6.2) with $\partial_\alpha\mathbf{z}$ gives

$$\partial_t\mathbf{z}\cdot\partial_\alpha\mathbf{z}=v\boldsymbol{\omega}\cdot\partial_\alpha\mathbf{z},$$

which is not surprising, since it describes just the lateral flow of the $\mathbf{F}$-family due to polymerization. Inserting this to (IV.6.3), one can write

$$\partial_t a_0^*=\frac{v(\boldsymbol{\omega}-\boldsymbol{\omega}^*)\cdot\partial_\alpha\mathbf{z}}{|\partial_\alpha\mathbf{z}|^2}\,\partial_\alpha a_0^* \tag{IV.6.5}$$

for the evolution of a_0^* which, in a way, describes the lateral flow of the $\mathbf{F}^*$-family. This can be used to eliminate $\partial_t a_0^*$ from (IV.6.2) to get an equation for $\mathbf{z}$:

$$(1+\partial_\alpha a_0^*)\partial_t\mathbf{z}-v(I+\partial_\alpha a_0^*\,\Pi_{\boldsymbol{\tau}})\boldsymbol{\omega}-v\partial_\alpha a_0^*\Pi_{\boldsymbol{\nu}}\boldsymbol{\omega}^*+\lambda_{\text{area}}\partial_\alpha\mathbf{z}^\perp=0, \tag{IV.6.6}$$

where we recall from (IV.3.36) the notations $\Pi_{\boldsymbol{\tau}}:=\boldsymbol{\tau}\otimes\boldsymbol{\tau}=\frac{\partial_\alpha\mathbf{z}}{|\partial_\alpha\mathbf{z}|}\otimes\frac{\partial_\alpha\mathbf{z}}{|\partial_\alpha\mathbf{z}|}$ for the orthogonal projection to the tangent of the leading edge and $\Pi_{\boldsymbol{\nu}}$, with $\boldsymbol{\nu}:=\frac{\partial_\alpha\mathbf{z}^\perp}{|\partial_\alpha\mathbf{z}|}$, the projection to the outward normal.

Equations (IV.6.5) and (IV.6.6) can be used in (IV.6.4) to get a quasi-stationary equation for φ. Indeed, one can compute that

$$\widehat{\mu}^T\partial_\alpha\left(\frac{\partial_\alpha a_0^*}{|\partial_\alpha\mathbf{z}|^3}\,\partial_\alpha\varphi\right)+v\partial_\alpha a_0^*\left(\Pi_{\boldsymbol{\tau}}(\boldsymbol{\omega}-\boldsymbol{\omega}^*)\right)\cdot(\boldsymbol{\omega}-\boldsymbol{\omega}^*)^\perp-\lambda\partial_\alpha\mathbf{z}\cdot(\boldsymbol{\omega}+\boldsymbol{\omega}^*\partial_\alpha a_0^*)=0. \tag{IV.6.7}$$

A highlight of the equation above is the presence of a second-order derivative of φ with respect to α, which helps with regularity along the α-direction.

Finally for λ_{area} we project (IV.6.6) to $\partial_\alpha \mathbf{z}^\perp$ and integrate with respect to α from 0 to 2π:

$$\lambda_{\text{area}} \int_0^{2\pi} \frac{|\partial_\alpha \mathbf{z}|^2}{1+\partial_\alpha a_0^*}\,\mathrm{d}\alpha = v\int_0^{2\pi} \frac{1}{1+\partial_\alpha a_0^*}\,\left((I+\partial_\alpha a_0^*\,\Pi_{\boldsymbol{\tau}})\boldsymbol{\omega}+\partial_\alpha a_0^*\Pi_{\boldsymbol{\nu}}\boldsymbol{\omega}^*\right)\cdot\partial_\alpha\mathbf{z}^\perp\,\mathrm{d}\alpha,$$

where the integral $\int_0^{2\pi}\partial_t\mathbf{z}\cdot\partial_\alpha\mathbf{z}^\perp\,\mathrm{d}\alpha$ vanished due to the area constraint. Because

$$\left((I+\partial_\alpha a_0^*\,\Pi_{\boldsymbol{\tau}})\boldsymbol{\omega}+\partial_\alpha a_0^*\Pi_{\boldsymbol{\nu}}\boldsymbol{\omega}^*\right)\cdot\partial_\alpha\mathbf{z}^\perp = (\boldsymbol{\omega}+\partial_\alpha a_0^*\boldsymbol{\omega}^*)\cdot\partial_\alpha\mathbf{z}^\perp,$$

we expand and rearrange the terms into the equation

$$\lambda_{\text{area}} = \frac{v}{\Lambda}\int_0^{2\pi}\frac{1}{1+\partial_\alpha a_0^*}\,(\boldsymbol{\omega}+\partial_\alpha a_0^*\boldsymbol{\omega}^*)\cdot\partial_\alpha\mathbf{z}^\perp\,\mathrm{d}\alpha,$$

where

$$\Lambda := \int_0^{2\pi}\frac{|\partial_\alpha\mathbf{z}|^2}{1+\partial_\alpha a_0^*}\,\mathrm{d}\alpha.$$

Equilibria. We shall look for equilibria, where the shape of the cell does not change:

$$\mathbf{z}(\alpha,t)=\mathbf{z}_\infty(\alpha+\beta(t)),\quad \varphi(\alpha,t)=\varphi_\infty(\alpha+\beta(t)),\quad a_0^*(\alpha,t)=\alpha+b(t),$$

and we shall write $\mathbf{z}_\infty'(\alpha+\beta(t))=R\boldsymbol{\omega}(\vartheta_\infty)$, as well as $\varphi_\infty-\vartheta_\infty=\gamma$. Substitution to (IV.6.5) and (IV.6.6) and separating the tangential and orthogonal components gives

$$\begin{cases} R\dot b = v(\cos\gamma-\cos(\gamma+\phi_0)),\\ R\dot\beta = v\cos\gamma,\\ R\lambda_{\text{area}} = v(\sin\gamma+\sin(\gamma+\phi_0)),\end{cases}$$

where $\cdot$ means differentiation with respect to t. An initial conclusion is that R and γ cannot depend on α and therefore not on t (because they only depend on $\alpha+\beta(t)$), so all quantities in the above equations are constants. Now everything is substituted to (IV.6.7) to achieve the equation

$$\widehat{\mu}^T\varphi_\infty'' = R^3 v(\cos\phi_0)\sin(\pi-\phi_0-2\gamma). \tag{IV.6.8}$$

Since φ_∞ has to satisfy the boundary conditions

$$\varphi_\infty(2\pi)-\varphi_\infty(0)=2\pi,\qquad \varphi_\infty'(2\pi)-\varphi_\infty'(0)=0,$$

the right hand side of (IV.6.8) has to vanish, and we get the symmetry result

$$\gamma=\frac{\pi-\phi_0}{2}.$$

Consequentially, up to a phase shift,

$$\varphi_\infty=\vartheta_\infty+\frac{\pi-\phi_0}{2}=\alpha+\frac{vt}{R}\cos\left(\frac{\pi-\phi_0}{2}\right),$$

which corresponds to a circular-shaped cell, as expected. This result agrees with the numerical computations for long time solution in the rotationally symmetric case [OSS08], and the stationary cross-link dominated equilibrium in [HMS17]. The radius R is determined by the equation for λ_{area}, which is also anticipated since the area constraint provides control over the cell size.

Chapter summary. In this chapter, we have derived a model for rigid filaments with adhesion, polymerization, tethering, area constraint and cross-link twisting. With the simplifying assumptions of symmetry with respect to and equilibrium angle at the leading edge, the asymptotic model for small lamellipodium width produces a circular equilibrium consistent with numerical results for the full FBLM. We emphasize that this result is achieved with a prescribed area, as opposed to the previous FBLM versions with artificial tension energy acting on the cell membrane [OS10b] or pulling towards the center of the cell due to actin-myosin interaction [Man+15].

Chapter V

Pressure models

Contents

Existence of solutions of the FBLM has only been shown for the rotationally symmetric case and for short enough times [OS10a]. The rotational symmetry assumption has been made to reduce complexity, but its removal is expected not to cause significant difficulties. The restriction to sufficiently short time intervals, on the other hand, was more crucial. The model describes two intersecting families of locally parallel filaments and it relies on the assumption that filaments of the same family do not cross. The model analyzed in [OS10a] does not contain any mechanism to avoid such crossings, a situation where the local-in-time existence result seems to be optimal.

Heuristics dictate that the structure might break down due to the clustering or bundling of the filaments. Therefore, a repulsive force between parallel filaments, caused by Coulomb interaction, has been introduced in [Man+15; Lei15], and its derivation from a microscopic model based on individual filaments can be found in [Ram11]. With rotational symmetry, convergence to and stability of the steady state has been supported by a linear stability analysis [Lei15]. Without rotational symmetry and boundary conditions, the FBLM with pressure has been shown to possess smooth solutions for all times [Lei15]. Based on these works, the additional *pressure* term helped stabilize the model so that one can hope for global existence of solutions.

The discussion above serves as impetus to the present chapter, where we focus on the effects of the pressure term in the FBLM. The first section deals with a one-dimensional (1D) problem which will be the basis for the development of the ideas and strategies implemented in the subsequent sections. In Section V.2, a reduced model is derived systematically from contributions of the potential energy of the system and prescribed external forces. Section V.3 specializes on FBLM with rigid filaments and

pressure since we expect steady states of the reduced model to be straight lines. Instabilities brought about by the pressure term (and possibly nonconservative external forces) motivated the inclusion of an artificial tension energy of the filaments' center-of-mass curve. A bifurcation analysis is presented in Section V.4 where parameters for pressure and center-of-mass curve tension play the key roles.

V.1 1D model problem

To better understand the mechanisms of filament repulsion, it is helpful to demonstrate its effects in a simple situation. Instead of filaments, we consider k moving points with Lagrangian label $\alpha_j = j/k$ on the line with positions

$$x^n_{\text{left}} = x^n_1 < x^n_2 < \cdots < x^n_k = x^n_{\text{right}}. \tag{V.1.1}$$

The terms x^n_j are interpreted as approximations for the values $x(\alpha_j, t_n)$ of an increasing (with respect to the first coordinate), continuous function $x : [0,1] \times [0,\infty) \to \mathbb{R}$ where $t_n = n\tau$ and τ is a given time step. With only the Coloumb interaction, friction from filament-to-substrate adhesions and prescribed external forces, the dynamics is dictated by

$$(x^{n+1}_1, \ldots, x^{n+1}_k) = \text{argmin}_{(y_1,\ldots,y_k)} U^n(y_1, \ldots, y_k), \tag{V.1.2}$$

with the Lagrangian

$$U^n(y_1, \ldots, y_k) := \frac{1}{2k\tau} \sum_{j=1}^{k} (y_j - x^n_j)^2 + \frac{1}{k} \sum_{j=2}^{k} \Phi\left(\frac{1}{k(y_j - y_{j-1})}\right) - y_1 f_{\text{left}} + y_k f_{\text{right}}. \tag{V.1.3}$$

Here, Φ is an electrostatic potential, and $f_{\text{left}}, f_{\text{right}} > 0$ are constant external forces on the left-end and on the right-end points, respectively. The negative sign in front of $y_1 f_{\text{left}}$ and positive in front of $y_k f_{\text{right}}$ depict the fact that we have chosen the external forces to push inwards, thus preventing the structure from expanding indefinitely due to repulsion.

Euler-Lagrange equations for (V.1.2)**-**(V.1.3)**.** The Euler-Lagrange equations corresponding to Problem (V.1.2)-(V.1.3) are now derived. Passing to the limit $\tau \to 0$, we arrive to the system

$$\begin{cases} \frac{1}{k}\partial_t x_{\text{left}} + p(\varrho_2) - f_{\text{left}} = 0 & \text{for } x_{\text{left}}, \\ \frac{1}{k}\partial_t x_{\text{right}} - p(\varrho_k) + f_{\text{right}} = 0 & \text{for } x_{\text{right}}, \\ k(p(\varrho_{j+1}) - p(\varrho_j)) + \partial_t x_j = 0 & \text{for } x_2, \ldots, x_{k-1}, \end{cases}$$

where we define *pressure* by $p(\varrho) := \Phi'(\varrho)\varrho^2$ along with the notation $\varrho_j := (k(x_j(t) - x_{j-1}(t)))^{-1}$. Formally sending $k \to \infty$, a gradient flow (or steepest-descent curve c.f. (II.2.1)) emerges:

$$\partial_t x = -\partial_\alpha(p(\varrho)), \quad \varrho := \frac{1}{\partial_\alpha x(\alpha, t)}, \tag{V.1.4}$$

as the curve x tends to move in the direction of the fastest *decrease* [1] of $p(\varrho)$ with respect to α, which is now a continuous variable with values ranging from 0 to 1. In this continuum description, ϱ is

[1] if $\Phi' > 0$ or increase if $\Phi' < 0$

interpreted as *density* of points. Indeed, $\varrho > 0$ since x is an increasing function of α. Equation (V.1.4) is subject to the boundary conditions

$$\begin{cases} p(\varrho) = f_{\text{left}} & \text{for } \alpha = 0, \\ p(\varrho) = f_{\text{right}} & \text{for } \alpha = 1. \end{cases} \tag{V.1.5}$$

Coordinate change to Eulerian variables. A transformation to Eulerian coordinates allows us to understand System (V.1.4)-(V.1.5) in terms of its surrounding space. To this end, we introduce the map $\boldsymbol{\Psi}(\alpha, t) = (x, t) = (\Psi_1, \Psi_2)$, its inverse $\boldsymbol{\Xi} := \boldsymbol{\Psi}^{-1}$, $\boldsymbol{\Xi}(x, t) = (\alpha, t) = (\Xi_1, \Xi_2)$, and the notations

$$\widetilde{\varrho}(x, t) := \varrho(\alpha, t)|_{(\alpha,t)=\boldsymbol{\Xi}(x,t)}, \quad \text{and} \quad v(x, t) := \partial_t \Psi_1(\alpha, t)|_{(\alpha,t)=\boldsymbol{\Xi}(x,t)}. \tag{V.1.6}$$

The definition of ϱ in (V.1.4) implies that $\widetilde{\varrho} = 1/\partial_\alpha \Psi_1$. In the new coordinates, equation (V.1.4) transforms to $v = -(1/\widetilde{\varrho})\partial_x p(\widetilde{\varrho})$. Multiplying this by $\widetilde{\varrho}$, one has

$$\partial_x p(\widetilde{\varrho}) + \widetilde{\varrho} v = 0. \tag{V.1.7}$$

Continuity equation for (V.1.7)**.** It is helpful to find conserved quantities. Guided by the fact that the density of points in the structure remains unchanged through time, we consider the time derivative of $\widetilde{\varrho}$. Using chain rule, we compute that

$$\partial_t \widetilde{\varrho} = \frac{\mathrm{d}}{\mathrm{d}t} \varrho(\alpha, t)|_{(\alpha,t)=\boldsymbol{\Xi}(x,t)} = ((\partial_\alpha \varrho)\partial_t \Xi_1 + \partial_t \varrho)\,|_{(\alpha,t)=\boldsymbol{\Xi}(x,t)}, \tag{V.1.8}$$

where we used $\partial_t \Xi_2 = 1$. From the first equation in (V.1.6), we find

$$\partial_\alpha \varrho(\alpha, t)|_{(\alpha,t)=\boldsymbol{\Xi}(x,t)} = (\partial_x \widetilde{\varrho})\partial_\alpha \Psi_1.$$

On the other hand, we compute for the time derivative of ϱ defined in (V.1.4):

$$\partial_t \varrho(\alpha, t)|_{(\alpha,t)=\boldsymbol{\Xi}(x,t)} = -\frac{1}{(\partial_\alpha \Psi_1)^2}\, \partial_t \partial_\alpha \Psi_1.$$

Inserting the last two equations to (V.1.8) yields

$$\partial_t \widetilde{\varrho} = (\partial_x \widetilde{\varrho})(\partial_\alpha \Psi_1)\partial_t \Xi_1 - \frac{1}{(\partial_\alpha \Psi_1)^2}\, \partial_t \partial_\alpha \Psi_1. \tag{V.1.9}$$

Our goal is to write the right-hand side of (V.1.9) in the new variables. Differentiating the relation $x = \Psi_1(\Xi_1(x, t), t)$ with respect to t and x, we obtain the equations

$$0 = (\partial_\alpha \Psi_1)\partial_t \Xi_1 + \partial_t \Psi_1, \quad \text{and} \quad 1 = (\partial_\alpha \Psi_1)\partial_x \Xi_1,$$

respectively. Plugging these into (V.1.9) and assuming sufficient smoothness of Ψ_1 so that $\partial_t \partial_\alpha \Psi_1 = \partial_\alpha \partial_t \Psi_1$, one has

$$\partial_t \widetilde{\varrho} = -(\partial_x \widetilde{\varrho})\partial_t \Psi_1 - \frac{1}{\partial_\alpha \Psi_1}(\partial_\alpha \partial_t \Psi_1)\partial_x \Xi_1. \tag{V.1.10}$$

Notice that taking the x-derivative of v defined in (V.1.6) gives $\partial_x v = (\partial_\alpha \partial_t \Psi_1)\partial_x \Xi_1$. We also remember that $\widetilde{\varrho} = 1/\partial_\alpha \Psi_1$. The foregoing statements allow us to write (V.1.10) as $\partial_t \widetilde{\varrho} = -(\partial_x \widetilde{\varrho})v - \widetilde{\varrho}\partial_x v$, or more compactly, the *continuity equation*

$$\partial_t \widetilde{\varrho} = -\partial_x(\widetilde{\varrho} v). \tag{V.1.11}$$

Integrating with respect to x from x_{left} to x_{right} yields

$$\frac{\mathrm{d}}{\mathrm{d}t}\int_{x_{\text{left}}}^{x_{\text{right}}} \widetilde{\varrho}\,\mathrm{d}x = -\widetilde{\varrho} v\Big|_{x_{\text{left}}}^{x_{\text{right}}} = 0,$$

since v vanishes at the end points in the new coordinates. We can therefore assume, with appropriate scaling, that

$$\int_{x_{\text{left}}}^{x_{\text{right}}} \widetilde{\varrho}\,\mathrm{d}x = 1. \tag{V.1.12}$$

Free-boundary problem. We are ready to write the final equations with the help of the conservation equation above. Going back to Equation (V.1.7), we take another derivative with respect to x and drop the tildes for simplicity. We compute that

$$0 = \partial_x^2 p(\varrho) + \partial_x(\varrho v) = \partial_x^2 p(\varrho) - \partial_t \varrho,$$

where the last equality follows from the continuity equation (V.1.11). Gathering the results above, we arrive to the transformed system:

$$\begin{cases} \partial_t \varrho = \partial_x^2 p(\varrho) & \text{for } x_{\text{left}}(t) < x < x_{\text{right}}(t), \\ p(\varrho) = f_{\text{left}}, \quad \dot{x}_{\text{left}} = -\frac{1}{\varrho}\partial_x p(\varrho) & \text{for } x = x_{\text{left}}(t), \\ p(\varrho) = f_{\text{right}}, \quad \dot{x}_{\text{right}} = -\frac{1}{\varrho}\partial_x p(\varrho) & \text{for } x = x_{\text{right}}(t), \end{cases} \tag{V.1.13}$$

where $\cdot$ denotes differentiation with respect to time t. The first equation models nonlinear diffusion,

$$\partial_t \varrho = \partial_x^2 p(\varrho) = \partial_x(p'(\varrho)\partial_x \varrho), \tag{V.1.14}$$

where the nonnegativity of the diffusivity $p'(\varrho)$ is necessary for stability.

System (V.1.13) takes the form of a *free boundary problem*, which is a partial differential equation (PDE) for both an unknown function and an unknown domain. A classical example of such problems is the melting of a block of ice, where regions with temperature greater than the melting point of ice will be occupied by liquid water instead. The *free boundary* formed from the ice-liquid interface is not known at the outset of the problem and is governed dynamically by the solution of the PDE. In our case, the unknown density ϱ evolves through the PDE (V.1.14), and the unknown boundary points x_{left} and x_{right} are controlled by ϱ and the density-dependent pressure $p(\varrho)$. The pressure p is simultaneously prescribed at the boundaries. Below, we study traveling wave solutions to System (V.1.13).

Traveling wave solutions to System (V.1.15)**.** One of the most important properties of nonlinear parabolic systems (e.g. heat/diffusion equation) is their potential to admit traveling wave solutions. Traveling waves are solution profiles advancing in time without change in shape and with constant speed of propagation. In contrast to the linear hyperbolic wave equation, where any wave profile advances with a specific speed, nonlinear diffusion equations may only allow certain wave profiles to propagate, each with its own characteristic velocity.

To gain a better understanding of the long-time behavior of (V.1.13), we seek solutions in the form of a traveling wave,

$$\varrho(x,t) = w(x-ct), \tag{V.1.15}$$

where $z = x - ct$ is the *wave variable*, $w(z)$ is a *wave profile* and c is a constant *wave speed*. In a traveling frame moving with speed c, waves described by (V.1.15) appear stationary. Inserting the ansatz (V.1.15) to (V.1.7) gives

$$\partial_x p(w) + cw = 0. \tag{V.1.16}$$

Integrating with respect to x from x_{left} to x_{right} and imposing the boundary conditions in (V.1.13), one computes

$$f_{\text{right}} - f_{\text{left}} + c\int_{x_{\text{left}}}^{x_{\text{right}}} w\,\mathrm{d}x = 0.$$

The conservation equation in (V.1.12) then allows us to compute for the constant wave speed c,

$$c = f_{\text{left}} - f_{\text{right}}, \tag{V.1.17}$$

which is, unsurprisingly, just the difference between the external forces. For a consistency check, notice that the structure moves to the right whenever $f_{\text{left}} > f_{\text{right}}$, meaning we push stronger on the left. This implies that $c > 0$, and the wave $w(x-ct)$ goes to the right.

Boltzmann-Poisson pressure model. As a next step, let us now choose a potential $\Phi = \Phi(\varrho)$ such that $p'(\varrho) \geq 0$. The *Boltzmann-Poisson model* for mobile carrier density leads to $\Phi(\varrho) = \ln \varrho$, implying that $p(\varrho) = \varrho$. With this choice of Φ and the traveling wave ansatz (V.1.15), Equation (V.1.16) becomes

$$w' + cw = 0, \tag{V.1.18}$$

where $'$ denotes derivative with respect to z. The ODE above has the solution

$$w(x-ct) = w_0 \exp(-c(x-ct)), \tag{V.1.19}$$

for a given initial data w_0. The boundary conditions in (V.1.13) imply

$$w_{\text{left}} := w(x_{\text{left}} - ct) = f_{\text{left}}, \quad w_{\text{right}} := w(x_{\text{right}} - ct) = f_{\text{right}}, \quad t \geq 0,$$

and

$$\dot{x}_{\text{left}} = -\frac{w'}{w}\Big|_{x=x_{\text{left}}} = c, \quad \dot{x}_{\text{right}} = -\frac{w'}{w}\Big|_{x=x_{\text{right}}} = c, \quad t \geq 0,$$

where the last two equations follow from (V.1.18). Integrating $\dot{x}_{\text{left}}$ and $\dot{x}_{\text{right}}$ with respect to time gives $x_{\text{left}} = ct$ and $x_{\text{right}} = ct + L$ for some L. Then, at $t = 0$ the left endpoint $x_{\text{left}} = 0$. Substitution to (V.1.19), one finds that the initial data must be $w_0 = f_{\text{left}}$. Now, let us evaluate w in (V.1.19) at $x = x_{\text{right}}$. Straightforward computations yield $w_{\text{right}} = f_{\text{right}} = f_{\text{left}} \exp(-cL)$, from where we find the value of L:

$$L = \frac{1}{c} \ln\left(\frac{f_{\text{left}}}{f_{\text{right}}}\right) = \frac{1}{f_{\text{left}} - f_{\text{right}}} \ln\left(\frac{f_{\text{left}}}{f_{\text{right}}}\right), \tag{V.1.20}$$

where the last equation follows from (V.1.17). Remember that the external forces f_{left} and f_{right} are both assumed to be positive. Consequently, $L > 0$, which is to be interpreted as the length of the segment of moving points (V.1.1).

Summary. In summary, we find that traveling wave solutions of system (V.1.13) take the form

$$\begin{cases} \varrho(x,t) = f_{\text{left}} \exp(-c(x - ct)), & t \geq 0, \\ x \in [x_{\text{left}}, x_{\text{right}}] = [ct, ct + L], & t \geq 0, \end{cases} \tag{V.1.21}$$

with wave speed $c = f_{\text{left}} - f_{\text{right}} > 0$, and strip length L defined by (V.1.20). As an example, we plot ϱ at times $t = 0$ (blue curve) and $t = 1$ (red curve) in Figure V.1, where $f_{\text{left}} = 1.75$ and $f_{\text{right}} = 0.5$. The wave moves to the right with speed $c = 1.25$ and the length of the strip is $L = 1.0022$.

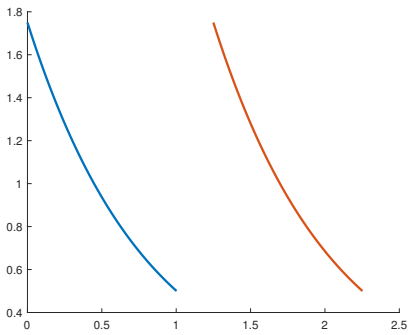

Figure V.1: Traveling wave solution (V.1.21) to System (V.1.13) plotted at times $t = 0$ (blue curve) and $t = 1$ (red curve), where the prescribed external forces are $f_{\text{left}} = 1.75$ and $f_{\text{right}} = 0.5$.

V.2 Reduced FBLM with pressure

Because repulsion acts only on filaments within the same family, we approximate a piece of lamellipodium by a strip consisting of just one filament family, with filaments of the same length, so that the maximal filament length L becomes constant and $\eta = \eta^* = 1$. In contrast to Section IV.1, we rescale

the Lagrange multiplier λ_{inext} so that it appears in the leading order problem of the FBLM (III.4.1) as L is formally sent to zero. More precisely,

$$\begin{cases} \mu^B \partial_s^4 \mathbf{F} = \partial_s(\lambda_{\text{inext}} \partial_s \mathbf{F}), & \text{for } -1 < s < 0, \\ \mu^B \partial_s^3 \mathbf{F} = \lambda_{\text{inext}} \partial_s \mathbf{F}, & \text{for } s = -1, 0, \\ \partial_s^2 \mathbf{F} = 0, & \text{for } s = -1, 0, \end{cases} \tag{V.2.1}$$

subject to the constraint $|\partial_s \mathbf{F}| = L$. We next linearize the nonlinear problem above around the trivial solution

$$\bar{\mathbf{F}}(\alpha, s) = \bar{\mathbf{z}}(\alpha) + L\left(s + \frac{1}{2}\right)\boldsymbol{\omega}(\bar{\varphi}(\alpha)), \quad \bar{\lambda} = 0, \tag{V.2.2}$$

where $\bar{\mathbf{z}}$ is the center-of-mass of the filament with direction $\boldsymbol{\omega}(\bar{\varphi}) := (\cos\bar{\varphi}, \sin\bar{\varphi})$. The constraint is rewritten as $|\partial_s \mathbf{F}|^2 = L^2$ for convenience. The linearization of (V.2.1) around (V.2.2) reads

$$\begin{cases} \mu^B \partial_s^4 \mathbf{F} = L(\partial_s \lambda_{\text{inext}})\boldsymbol{\omega}, & \text{for } -1 < s < 0, \\ \mu^B \partial_s^3 \mathbf{F} = L\lambda_{\text{inext}}\boldsymbol{\omega}, & \text{for } s = -1, 0, \\ \mu^B \partial_s^2 \mathbf{F} = 0, & \text{for } s = -1, 0, \end{cases} \tag{V.2.3}$$

subject to the linearized constraint

$$\boldsymbol{\omega} \cdot \partial_s^2 \mathbf{F} = 0, \quad -1 \le s \le 0. \tag{V.2.4}$$

This implies that $\partial_s^2 \mathbf{F} = c\boldsymbol{\omega}^\perp$ for some scalar c independent of s.

For a given $\boldsymbol{\omega}$, we look at the solutions of (V.2.3)-(V.2.4). Integrating the first equation with respect to s and using the first boundary condition give us $\mu^B \partial_s^3 \mathbf{F} = L\lambda_{\text{inext}}\boldsymbol{\omega}$ for $s \in [-1, 0]$. Integrating once more yields

$$\mu^B \partial_s^2 \mathbf{F} = L\boldsymbol{\omega} \int_{-1}^{s} \lambda_{\text{inext}}(\tilde{s})\, \mathrm{d}\tilde{s}. \tag{V.2.5}$$

With the second boundary condition, this becomes

$$\int_{-1}^{0} \lambda_{\text{inext}}(s)\, \mathrm{d}s = 0.$$

Taking the scalar product of (V.2.5) with $\boldsymbol{\omega}$ and applying the constraint (V.2.4) result to

$$\int_{-1}^{s} \lambda_{\text{inext}}(\tilde{s})\, \mathrm{d}\tilde{s} = 0 \quad \text{for all } s \in [-1, 0].$$

Consequently, $\lambda_{\text{inext}} = 0$ in $[-1, 0]$. Therefore, the right hand sides of the first two equations in (V.2.3) should vanish. This takes us back to the linear system (IV.1.3), however, the constraint (IV.1.1) is replaced by its linear version (V.2.4). Solutions to this reduced system can be written as

$$\mathbf{F}(\alpha, s, t) = \mathbf{z}(\alpha, t) + Ls_\ell \boldsymbol{\omega}(\varphi(\alpha, t)) + L^2 s_q b(\alpha, t)\boldsymbol{\omega}(\varphi(\alpha, t))^\perp, \tag{V.2.6}$$

with the Legendre polynomials (chosen for convenience)

$$s_\ell := s + \frac{1}{2}, \quad \text{and} \quad s_q := \frac{1}{2}\left(s + \frac{1}{2}\right)^2 - \frac{1}{24}, \quad s \in [-1, 0]. \tag{V.2.7}$$

These polynomials satisfy

$$\int_{-1}^{0} s_\ell \,\mathrm{d}s = 0, \quad \int_{-1}^{0} s_q \,\mathrm{d}s = 0, \quad \int_{-1}^{0} s_\ell s_q \,\mathrm{d}s = 0, \quad \frac{\mathrm{d}}{\mathrm{d}s} s_q = s_\ell. \tag{V.2.8}$$

The term $b(\alpha, t)$ dictates the amount of filament bending.

With the ansatz (V.2.6), we derive a description of a lamellipodium strip with one filament family that accounts for filament repulsion. As in the full model, the dynamics of the filaments is governed by a generalized gradient flow, which means that at each point in time, the positions and deformations of the filaments minimize a potential energy functional arising from the combined effects discussed below. The variations of each contribution is computed to derive the weak and strong formulations of the problem.

Filament bending. A straightforward computation from (V.2.6) yields $\partial_s \mathbf{F} = L\boldsymbol{\omega} + L^2 s_\ell b \boldsymbol{\omega}^\perp$, so that $\partial_s^2 \mathbf{F} = L^2 b \boldsymbol{\omega}^\perp$ with squared length $\left|\partial_s^2 \mathbf{F}\right|^2 = L^4 b^2$ and

$$\mathcal{E}^B(t)[b] = \frac{L^4 \mu^B}{2} \int_0^1 b^2 \,\mathrm{d}\alpha,$$

since $b = b(\alpha, t)$ is independent of s. Its variation is

$$\delta\mathcal{E}^B(t)[b]\delta b = \int_0^1 \mu^B L^4 b \,\delta b \,\mathrm{d}\alpha.$$

Adhesion to the substrate. Filament-to-substrate adhesions give rise to the energy

$$\mathcal{E}^A(t, \Delta t)[\mathbf{z}, \varphi, b] = \frac{\mu^A}{2\Delta t} \int_B \left|\mathbf{z} - \widehat{\mathbf{z}} + L s_\ell(\boldsymbol{\omega} - \widehat{\boldsymbol{\omega}}) + L^2 s_q(b\boldsymbol{\omega}^\perp - \widehat{b}\widehat{\boldsymbol{\omega}}^\perp) - v\Delta t \widehat{\boldsymbol{\omega}}\right|^2 \mathrm{d}(\alpha, s),$$

with the notations $\widehat{\mathbf{z}} := \mathbf{z}(\alpha, t - \Delta t)$, $\widehat{\boldsymbol{\omega}} := \boldsymbol{\omega}(\varphi(\alpha, t - \Delta t))$, and $\widehat{b} := b(\alpha, t - \Delta t)$. Here, we have rescaled v to v/L. The variation of the adhesion energy is

$$\begin{aligned}
\delta\mathcal{E}^A[\mathbf{z}, \varphi, b](\boldsymbol{\delta}\mathbf{z}, \delta\varphi, \delta b) = \frac{\mu^A}{\Delta t} \int_B \Big[&\Big(\mathbf{z} - \widehat{\mathbf{z}} + L s_\ell(\boldsymbol{\omega} - \widehat{\boldsymbol{\omega}}) + L^2 s_q(b\boldsymbol{\omega}^\perp - \widehat{b}\,\widehat{\boldsymbol{\omega}}^\perp) - v\Delta t \widehat{\boldsymbol{\omega}}\Big) \cdot \boldsymbol{\delta}\mathbf{z} \\
&+ L\Big(\mathbf{z} - \widehat{\mathbf{z}} + L s_\ell(\boldsymbol{\omega} - \widehat{\boldsymbol{\omega}}) + L^2 s_q(b\boldsymbol{\omega}^\perp - \widehat{b}\widehat{\boldsymbol{\omega}}^\perp) - v\Delta t \widehat{\boldsymbol{\omega}}^\perp\Big) \cdot (\boldsymbol{\omega}^\perp s_\ell - \boldsymbol{\omega} L s_q b)\delta\varphi \\
&+ L^2 s_q\Big(\mathbf{z} - \widehat{\mathbf{z}} + L s_\ell(\boldsymbol{\omega} - \widehat{\boldsymbol{\omega}}) + L^2 s_q(b\boldsymbol{\omega}^\perp - \widehat{b}\widehat{\boldsymbol{\omega}}^\perp) - v\Delta t \widehat{\boldsymbol{\omega}}\Big) \cdot \boldsymbol{\omega}^\perp \delta b\Big] \,\mathrm{d}(\alpha, s).
\end{aligned}$$

For convenience, let us introduce the notation

$$S_{i,j} := \int_{-1}^{0} s_\ell^i s_q^j \,\mathrm{d}s. \tag{V.2.9}$$

Remembering (V.2.8), one has $S_{1,0} = S_{0,1} = S_{1,1} = 0$. It follows that

$$\delta\mathcal{E}^A[\mathbf{z},\varphi,b](\delta\mathbf{z},\delta\varphi,\delta b) = \frac{\mu^A}{\Delta t}\int_0^1 \Big[\,(\mathbf{z}-\widehat{\mathbf{z}}-v\Delta t\widehat{\boldsymbol{\omega}})\cdot\boldsymbol{\delta}\mathbf{z} + \Big(L^2S_{2,0}(\boldsymbol{\omega}-\widehat{\boldsymbol{\omega}})\cdot\boldsymbol{\omega}^\perp - L^4S_{0,2}b(b\boldsymbol{\omega}^\perp-\widehat{b}\widehat{\boldsymbol{\omega}}^\perp)\cdot\boldsymbol{\omega}\Big)\delta\varphi + L^4S_{0,2}(b\boldsymbol{\omega}^\perp-\widehat{b}\widehat{\boldsymbol{\omega}}^\perp)\cdot\boldsymbol{\omega}^\perp\delta b\Big]\,\mathrm{d}\alpha.$$

Taking the limit as $\Delta t \to 0$,

$$\lim_{\Delta t\to 0}\delta\mathcal{E}^A(t,\Delta t)[\mathbf{z},\varphi,b](\delta\mathbf{z},\delta\varphi,\delta b) = \mu^A\int_0^1\Big[(\partial_t\mathbf{z}-v\boldsymbol{\omega})\cdot\boldsymbol{\delta}\mathbf{z} + \Big(L^2S_{2,0}-L^4S_{0,2}b^2\Big)\,\partial_t\varphi\,\delta\varphi + L^4S_{0,2}(\partial_t b)\delta b\Big]\,\mathrm{d}\alpha,$$

with the coefficients $S_{2,0} = 1/12$ and $S_{0,2} = 1/720$.

Pressure from filament repulsion. To compute for pressure, we first find the density ϱ. We shall need the derivative $\partial_\alpha\mathbf{F} = \partial_\alpha\mathbf{z} + Ls_\ell\boldsymbol{\omega}^\perp\partial_\alpha\varphi + L^2s_q\boldsymbol{\omega}^\perp\partial_\alpha b - L^2s_qb\boldsymbol{\omega}\partial_\alpha\varphi$ and its orthogonal complement

$$\partial_\alpha\mathbf{F}^\perp = \partial_\alpha\mathbf{z}^\perp - Ls_\ell\boldsymbol{\omega}\partial_\alpha\varphi - L^2s_q\boldsymbol{\omega}\partial_\alpha b - L^2s_qb\boldsymbol{\omega}^\perp\partial_\alpha\varphi$$

for the computation

$$\begin{aligned}\frac{1}{\varrho} = \partial_\alpha\mathbf{F}^\perp\cdot\partial_s\mathbf{F} &= (\partial_\alpha\mathbf{z}^\perp - Ls_\ell\boldsymbol{\omega}\partial_\alpha\varphi - L^2s_q\boldsymbol{\omega}\partial_\alpha b - L^2s_qb\boldsymbol{\omega}^\perp\partial_\alpha\varphi)\cdot(L\boldsymbol{\omega}+L^2s_\ell b\boldsymbol{\omega}^\perp)\\ &= L\partial_\alpha\mathbf{z}^\perp\cdot\boldsymbol{\omega} - L^2s_\ell\partial_\alpha\varphi - L^3s_q\partial_\alpha b + L^2s_\ell b\partial_\alpha\mathbf{z}\cdot\boldsymbol{\omega} - L^4s_\ell s_qb^2\partial_\alpha\varphi. \qquad \text{(V.2.10)}\end{aligned}$$

The energy arising from the pressure-like repulsion between filaments reads

$$\mathcal{E}^C(t)[\mathbf{z},\varphi,b] = \int_B \Phi\left(\varrho[\mathbf{z},\varphi,b]\right)\mathrm{d}(\alpha,s), \qquad \text{(V.2.11)}$$

with ϱ determined by (V.2.10). In what follows, we introduce the notation

$$P_{i,j} := \int_{-1}^0 s_\ell^i s_q^j\, p(\varrho)\,\mathrm{d}s, \quad \text{with } p(\varrho) := \Phi'(\varrho)\varrho^2. \qquad \text{(V.2.12)}$$

The variation of $\mathcal{E}^C$ is

$$\delta\mathcal{E}^C(t)[\mathbf{z},\varphi,b](\boldsymbol{\delta}\mathbf{z},\delta\varphi,\delta b) = \partial_{\mathbf{z}}\mathcal{E}^C(t)[\mathbf{z},\varphi,b]\boldsymbol{\delta}\mathbf{z} + \partial_\varphi\mathcal{E}^C(t)[\mathbf{z},\varphi,b]\delta\varphi + \partial_b\mathcal{E}^C(t)[\mathbf{z},\varphi,b]\delta b,$$

with terms on the right-hand side computed below. First, from (V.2.11), we have

$$\begin{aligned}\partial_{\mathbf{z}}\mathcal{E}^C[\mathbf{z},\varphi,b]\delta\mathbf{z} &= \int_B -p(\varrho)(L\partial_\alpha\delta\mathbf{z}^\perp\cdot\boldsymbol{\omega} + L^2s_\ell b\partial_\alpha\delta\mathbf{z}^\perp\cdot\boldsymbol{\omega}^\perp)\,\mathrm{d}(\alpha,s)\\ &= \int_B p(\varrho)(L\boldsymbol{\omega}^\perp - L^2s_\ell b\boldsymbol{\omega})\cdot\partial_\alpha\boldsymbol{\delta}\mathbf{z}\,\mathrm{d}(\alpha,s).\end{aligned}$$

Evaluating the integral with respect to s with the aid of integration by parts gives us

$$\begin{aligned}\partial_{\mathbf{z}}\mathcal{E}^C[\mathbf{z},\varphi,b]\boldsymbol{\delta}\mathbf{z} &= \int_0^1 (LP_{0,0}\boldsymbol{\omega}^\perp - L^2P_{1,0}b\boldsymbol{\omega})\cdot\partial_\alpha\boldsymbol{\delta}\mathbf{z}\,\mathrm{d}\alpha\\ &= (LP_{0,0}\boldsymbol{\omega}^\perp - L^2P_{1,0}b\boldsymbol{\omega})\cdot\delta\mathbf{z}\Big|_0^1 + \int_0^1 \left(-L\partial_\alpha(P_{0,0}\boldsymbol{\omega}^\perp) + L^2\partial_\alpha(P_{1,0}b\boldsymbol{\omega})\right)\cdot\boldsymbol{\delta}\mathbf{z}\,\mathrm{d}\alpha.\end{aligned}$$

The variation with respect to φ of (V.2.11) reads

$$\begin{aligned}\partial_\varphi\mathcal{E}^C[\mathbf{z},\varphi,b]\delta\varphi &= \int_B -p(\varrho)(L\partial_\alpha z^\perp\cdot\boldsymbol{\omega}^\perp\delta\varphi - L^2s_\ell\partial_\alpha\delta\varphi - L^2s_\ell b\partial_\alpha z^\perp\cdot\boldsymbol{\omega}\delta\varphi - L^4s_\ell s_q b^2\partial_\alpha\delta\varphi)\,\mathrm{d}(\alpha,s)\\ &= \int_0^1 (-LP_{0,0}\partial_\alpha z\cdot\boldsymbol{\omega}\delta\varphi + L^2P_{1,0}\partial_\alpha\delta\varphi + L^2P_{1,0}b\partial_\alpha z^\perp\cdot\boldsymbol{\omega}\delta\varphi + L^4P_{1,1}b^2\partial_\alpha\delta\varphi)\,\mathrm{d}\alpha.\end{aligned}$$

Integrating by parts once again, this is rewritten as

$$\begin{aligned}\partial_\varphi\mathcal{E}^C[\mathbf{z},\varphi,b]\delta\varphi = (L^2P_{1,0}+L^4P_{1,1}b^2)\delta\varphi\Big|_0^1 + \int_0^1 (&-LP_{0,0}\partial_\alpha z\cdot\boldsymbol{\omega} + L^2P_{1,0}b\partial_\alpha z^\perp\cdot\boldsymbol{\omega} - L^2\partial_\alpha P_{1,0}\\ &- L^4\partial_\alpha(P_{1,1}b^2))\delta\varphi\,\mathrm{d}\alpha.\end{aligned}$$

Finally, we find the variation of (V.2.11) with respect to b:

$$\begin{aligned}\partial_b\mathcal{E}^C[\mathbf{z},\varphi,b]\delta b &= \int_B p(\varrho)(L^3s_q\partial_\alpha(\delta b) - L^2s_\ell\partial_\alpha z\cdot\boldsymbol{\omega}\delta b + 2L^4s_\ell s_q b(\partial_\alpha\varphi)\delta b)\,\mathrm{d}(\alpha,s)\\ &= \int_0^1 (L^3P_{0,1}\partial_\alpha\delta b + (-L^2P_{1,0}\partial_\alpha z\cdot\boldsymbol{\omega} + 2L^4P_{1,1}b\partial_\alpha\varphi)\delta b)\,\mathrm{d}\alpha.\end{aligned}$$

Applying integration by parts to the expression above yields

$$\partial_b\mathcal{E}^C[\mathbf{z},\varphi,b]\delta b = L^3P_{0,1}\delta b\Big|_0^1 + \int_0^1 (-L^2P_{1,0}\partial_\alpha z\cdot\boldsymbol{\omega} + 2L^4P_{1,1}b\partial_\alpha\varphi - L^3\partial_\alpha P_{0,1})\delta b\,\mathrm{d}\alpha.$$

Forces on the layer ends. With only the effects introduced above (especially filament repulsion), the structure has a tendency to expand arbitrarily. We counteract this by introducing external forces along the first and last filaments of the strip, i.e. the filaments with label $\alpha = 0$ and $\alpha = 1$, respectively. To have control over the size of the structure, the forces must be assumed to push inwards. A contribution to the potential energy is produced by multiplying the external forces $\mathbf{g}_0$ and $\mathbf{g}_1$ by the displacements:

$$\begin{aligned}\mathcal{E}^f(t)[\mathbf{z},\varphi,b] = -\int_{-1}^0 \Big[&(\mathbf{z} + Ls_\ell\boldsymbol{\omega} + L^2s_qb\boldsymbol{\omega}^\perp)\big|_{\alpha=1}\cdot\mathbf{g}_1(s,t)\\ &+ (\mathbf{z} + Ls_\ell\boldsymbol{\omega} + L^2s_qb\boldsymbol{\omega}^\perp)\big|_{\alpha=0}\cdot\mathbf{g}_0(s,t)\Big]\,\mathrm{d}s,\end{aligned}\tag{V.2.13}$$

where $\mathbf{g}_0$ and $\mathbf{g}_1$ are prescribed below. The variation of the foregoing functional reads

$$\begin{aligned}&\delta\mathcal{E}^f(t)[\mathbf{z},\varphi,b](\boldsymbol{\delta}\mathbf{z},\delta\varphi,\delta b)\\ &= -\int_{-1}^0 \Big[\left(\boldsymbol{\delta}\mathbf{z} + Ls_\ell\boldsymbol{\omega}^\perp\delta\varphi - L^2s_q\left((\delta b)\boldsymbol{\omega}^\perp - L^2s_qb(\delta\varphi)\boldsymbol{\omega}\right)\right)\Big|_{\alpha=1}\cdot\mathbf{g}_1(s,t)\\ &\quad + \left(\boldsymbol{\delta}\mathbf{z} + Ls_\ell\boldsymbol{\omega}^\perp\delta\varphi - L^2s_q\left((\delta b)\boldsymbol{\omega}^\perp - L^2s_qb(\delta\varphi)\boldsymbol{\omega}\right)\right)\Big|_{\alpha=0}\cdot\mathbf{g}_0(s,t)\Big]\,\mathrm{d}s.\end{aligned}\tag{V.2.14}$$

The external forces are chosen to act in a direction orthogonal to the sides of the strip and to push the filaments inwards. Denoting the magnitude of these forces on the left and right ends by f_0 and f_1, respectively, one has

$$\mathbf{g}_0 = f_0\boldsymbol{\omega}(\varphi(\alpha=0))^\perp, \quad \text{and} \quad \mathbf{g}_1 = f_1\boldsymbol{\omega}(\varphi(\alpha=1))^\perp. \tag{V.2.15}$$

We emphasize that these forces depend on the deformation of the strip and that they are nonconservative. In particular, the choices (V.2.15) cannot be derived as variations of a functional. Nevertheless, the decision to prescribe (V.2.15) after computing the variation (V.2.14) produces much simpler boundary conditions compared to inserting (V.2.15) to the energy (V.2.13) and then finding its variation.

Now, for simplicity, let us further assume that f_0 and f_1 are constant in s. Substituting these to (V.2.14) and evaluation of the integral, one obtains the contribution

$$\delta\mathcal{E}^f(t)[\mathbf{z},\varphi,b](\boldsymbol{\delta}\mathbf{z},\delta\varphi,\delta b) = -Lf_1\boldsymbol{\omega}^\perp\cdot\boldsymbol{\delta}\mathbf{z}\Big|_{\alpha=1} + Lf_0\boldsymbol{\omega}^\perp\cdot\boldsymbol{\delta}\mathbf{z}\Big|_{\alpha=0}.$$

Euler-Lagrange equations. The combined variations of the functionals above produces the weak formulation of the problem:

$$\begin{aligned}
0 &= \lim_{\Delta t\to 0}\Big(\delta\mathcal{E}^B[b]\delta b + \delta\mathcal{E}^A[\mathbf{z},\varphi,b](\delta\mathbf{z},\delta\varphi,\delta b) + \delta\mathcal{E}^C[\mathbf{z},\varphi,b](\boldsymbol{\delta}\mathbf{z},\delta\varphi,\delta b) + \delta\mathcal{E}^f[\mathbf{z},\varphi,b](\boldsymbol{\delta}\mathbf{z},\delta\varphi,\delta b)\Big)\\
&= \Big((L(P_{0,0}-f_\alpha)\boldsymbol{\omega}^\perp - L^2P_{1,0}b\boldsymbol{\omega})\cdot\boldsymbol{\delta}\mathbf{z} + (L^2P_{1,0}+L^4P_{1,1}b^2)\delta\varphi + L^3P_{0,1}\delta b\Big)\Big|_0^1\\
&+ \int_0^1\Bigg(\Big(\mu^A(\partial_t\mathbf{z}-v\boldsymbol{\omega}) - L\partial_\alpha(P_{0,0}\boldsymbol{\omega}^\perp) + L^2\partial_\alpha(P_{1,0}b\boldsymbol{\omega})\Big)\cdot\boldsymbol{\delta}\mathbf{z}\\
&+ \Big(\mu^A\left(L^2S_{2,0}-L^4S_{0,2}b^2\right)\partial_t\varphi - LP_{0,0}\partial_\alpha\mathbf{z}\cdot\boldsymbol{\omega} + L^2P_{1,0}b\partial_\alpha\mathbf{z}^\perp\cdot\boldsymbol{\omega} - L^2\partial_\alpha P_{1,0} - L^4\partial_\alpha(P_{1,1}b^2)\Big)\delta\varphi\\
&+ \Big(\mu^AL^4S_{0,2}\,\partial_t b - L^2P_{1,0}\partial_\alpha\mathbf{z}\cdot\boldsymbol{\omega} + 2L^4P_{1,1}b\partial_\alpha\varphi - L^3\partial_\alpha P_{0,1}\Big)\delta b\Bigg)\,\mathrm{d}\alpha,
\end{aligned}$$

for all admissible variations $\boldsymbol{\delta}\mathbf{z}$, $\delta\varphi$ and δb. From here the Euler-Lagrange equations are derived:

$$\begin{cases}
\mu^A(\partial_t\mathbf{z}-v\boldsymbol{\omega}) - L\partial_\alpha(P_{0,0}\boldsymbol{\omega}^\perp) + L^2\partial_\alpha(P_{1,0}b\boldsymbol{\omega}) = 0,\\
\mu^AL^2(S_{2,0}-L^2S_{0,2}b^2)\,\partial_t\varphi - LP_{0,0}\partial_\alpha\mathbf{z}\cdot\boldsymbol{\omega} + L^2P_{1,0}b\partial_\alpha\mathbf{z}^\perp\cdot\boldsymbol{\omega} - L^2\partial_\alpha P_{1,0} - L^4\partial_\alpha(P_{1,1}b^2) = 0,\\
\mu^AL^4S_{0,2}\,\partial_t b - L^2P_{1,0}\partial_\alpha\mathbf{z}\cdot\boldsymbol{\omega} + 2L^4P_{1,1}b\partial_\alpha\varphi - L^3\partial_\alpha P_{0,1} + \mu^Bb = 0,
\end{cases} \tag{V.2.16}$$

with the boundary conditions

$$\begin{cases}
P_{0,0}\boldsymbol{\omega}^\perp - LP_{1,0}b\boldsymbol{\omega} = f_{0,1}\boldsymbol{\omega}^\perp & \text{for } \alpha = 0,1,\\
P_{1,0} + L^2P_{1,1}b^2 = 0 & \text{for } \alpha = 0,1,\\
P_{0,1} = 0 & \text{for } \alpha = 0,1,
\end{cases} \tag{V.2.17}$$

where S_{ij} and P_{ij} for $i,j = 0,1,2$ are defined in (V.2.9) and (V.2.12), respectively. Equilibrium states of System (V.2.16)-(V.2.17) involve $b = 0$, i.e. when filaments are straight. In fact, for an inextensible filament with only friction from adhesion and bending energy, convergence to a straight line segment and the existence of φ can be proved rigorously [Oel11]. In the next section, we look more closely at the states where $b = 0$.

V.3 Rigid filaments with pressure

The rigid filament version of the FBLM with pressure can be derived by setting $b = 0$ in System (V.2.16)-(V.2.17):

$$\begin{cases} \mu^A(\partial_t \mathbf{z} - v\boldsymbol{\omega}) - L\partial_\alpha(P_0\boldsymbol{\omega}^\perp) = 0, \\ \frac{L^2}{12}\mu^A\partial_t\varphi - LP_0\partial_\alpha\mathbf{z}\cdot\boldsymbol{\omega} - L^2\partial_\alpha P_1 = 0, \end{cases} \tag{V.3.1}$$

with the boundary conditions

$$\begin{cases} P_0\boldsymbol{\omega}^\perp = f_{0,1}\boldsymbol{\omega}^\perp & \text{for } \alpha = 0, 1, \\ P_1 = 0 & \text{for } \alpha = 0, 1, \end{cases} \tag{V.3.2}$$

and the *pressure* terms P_0 and P_1 now defined by

$$P_0 := \int_{-1}^{0} p(\widetilde{\varrho})\,\mathrm{d}s, \quad P_1 := \int_{-1}^{0} \left(s + \frac{1}{2}\right) p(\widetilde{\varrho})\,\mathrm{d}s, \quad \widetilde{\varrho} := \left(\partial_\alpha\mathbf{z}^\perp\cdot\boldsymbol{\omega} - L\left(s+\frac{1}{2}\right)\partial_\alpha\varphi\right)^{-1}.$$

As in Section V.1, we employ the Boltzmann-Poisson pressure model $\Phi(\widetilde{\varrho}) = \mu^P \ln\widetilde{\varrho}$ with stiffness parameter $\mu^P > 0$. Consequently, $p(\widetilde{\varrho}) := \Phi'(\widetilde{\varrho})\widetilde{\varrho}^2$ becomes $\mu^P\widetilde{\varrho}$. Substituting this to P_0 and P_1, we compute explicitly that

$$P_0 = -\frac{\mu^P}{L\partial_\alpha\varphi}\ln\left(1 - \frac{L\partial_\alpha\varphi}{\partial_\alpha\mathbf{z}^\perp\cdot\boldsymbol{\omega} + (L/2)\partial_\alpha\varphi}\right) \quad \text{and} \quad P_1 = -\frac{1}{L\partial_\alpha\varphi}\left(\mu^P - P_0\partial_\alpha\mathbf{z}^\perp\cdot\boldsymbol{\omega}\right).$$

Approximations for pressure terms. Approximation of P_0 and P_1 for small L utilizes the expansion

$$\ln(1-x) = -x - \frac{1}{2}x^2 - \frac{1}{3}x^3 - \cdots,$$

which converges for $x \in [-1, 1)$. For P_0 and P_1, we therefore consider the following:

$$|L\partial_\alpha\varphi| < \left|\partial_\alpha\mathbf{z}^\perp\cdot\boldsymbol{\omega} + \frac{L}{2}\partial_\alpha\varphi\right| \quad \text{or} \quad \frac{L\partial_\alpha\varphi}{\partial_\alpha\mathbf{z}^\perp\cdot\boldsymbol{\omega} + (L/2)\partial_\alpha\varphi} = -1.$$

Expanding the first condition, one has

$$-\partial_\alpha\mathbf{z}^\perp\cdot\boldsymbol{\omega} - \frac{3L}{2}\partial_\alpha\varphi < 0 < \partial_\alpha\mathbf{z}^\perp\cdot\boldsymbol{\omega} - \frac{L}{2}\partial_\alpha\varphi.$$

However, the parametrization of the curve by α (increasing from left to right) tells us that

$$\left|\partial_\alpha\mathbf{z}^\perp\cdot\boldsymbol{\omega} - L\left(s+\frac{1}{2}\right)\partial_\alpha\varphi\right| = \partial_\alpha\mathbf{z}^\perp\cdot\boldsymbol{\omega} - L\left(s+\frac{1}{2}\right)\partial_\alpha\varphi > 0, \quad \text{for } s \in [-1, 0].$$

Therefore, we only require that

$$\partial_\alpha\mathbf{z}^\perp\cdot\boldsymbol{\omega} + \frac{3L}{2}\partial_\alpha\varphi \geq 0. \tag{V.3.3}$$

Now, let us expand P_0 under the assumption (V.3.3). The series expansion for the natural logarithm renders the calculation

$$\ln\left(1-\frac{L\partial_\alpha\varphi}{\partial_\alpha\mathbf{z}^\perp\cdot\boldsymbol{\omega}+(L/2)\partial_\alpha\varphi}\right)=-L\widetilde{\varrho}(s=-1)\partial_\alpha\varphi-\frac{L^2}{2}(\widetilde{\varrho}(s=-1)\partial_\alpha\varphi)^2- \\ -\frac{L^3}{3}(\widetilde{\varrho}(s=-1)\partial_\alpha\varphi)^3-\cdots. \tag{V.3.4}$$

We express $\widetilde{\varrho}(s=-1)$ in terms of $\varrho:=\widetilde{\varrho}(s=-1/2)=(\partial_\alpha\mathbf{z}^\perp\cdot\boldsymbol{\omega})^{-1}$. Indeed,

$$\widetilde{\varrho}(s=-1)=\varrho-\frac{L}{2}\varrho^2\partial_\alpha\varphi+\frac{L^2}{4}\varrho^3(\partial_\alpha\varphi)^2-\frac{L^3}{8}\varrho^4(\partial_\alpha\varphi)^3+\cdots.$$

Inserting this to (V.3.4) yields

$$\ln\left(1-\frac{L\partial_\alpha\varphi}{\partial_\alpha\mathbf{z}^\perp\cdot\boldsymbol{\omega}+(L/2)\partial_\alpha\varphi}\right)=-L\varrho\partial_\alpha\varphi-\frac{L^3}{12}\varrho^3(\partial_\alpha\varphi)^3-\cdots.$$

We truncate the expansion at the second term and arrive at the approximations for small L:

$$P_0\approx-\frac{\mu^P}{L\partial_\alpha\varphi}\left(-L\varrho\partial_\alpha\varphi-\frac{L^3}{12}\varrho^3(\partial_\alpha\varphi)^3\right)=\mu^P\left(\varrho+\frac{L^2}{12}\varrho^3(\partial_\alpha\varphi)^2\right),$$

and

$$P_1\approx-\frac{1}{L\partial_\alpha\varphi}\left(\mu^P-\mu^P\left(\varrho+\frac{L^2}{12}\varrho^3(\partial_\alpha\varphi)^2\right)\frac{1}{\varrho}\right)=\frac{L\mu^P}{12}\varrho^2\partial_\alpha\varphi,$$

where we recall that the density is given by $\varrho:=(\partial_\alpha\mathbf{z}^\perp\cdot\boldsymbol{\omega})^{-1}$.

Short and rigid filaments with pressure. The approximations for small L above are inserted to (V.3.1)-(V.3.2). This gives rise to the nonlinear system

$$\begin{cases}\mu^A(\partial_t\mathbf{z}-v\boldsymbol{\omega})-\mu^P\partial_\alpha\left(\left(\varrho+\frac{L^2}{12}\varrho^3(\partial_\alpha\varphi)^2\right)\boldsymbol{\omega}^\perp\right)=0,\\ \frac{L^2}{12}\mu^A\partial_t\varphi-\mu^P\varrho\partial_\alpha\mathbf{z}\cdot\boldsymbol{\omega}-\frac{L^2}{12}\mu^P\partial_\alpha(\varrho^2\partial_\alpha\varphi)=0,\end{cases} \tag{V.3.5}$$

for $0<\alpha<1$ and $t>0$, subject to the boundary conditions

$$\begin{cases}-\mu^P\varrho\boldsymbol{\omega}^\perp+f_0\boldsymbol{\omega}^\perp=0, & \alpha=0,\\ \mu^P\varrho\boldsymbol{\omega}^\perp-f_1\boldsymbol{\omega}^\perp=0, & \alpha=1,\\ \mu^P\varrho^2\partial_\alpha\varphi=0, & \alpha=0,1.\end{cases} \tag{V.3.6}$$

In the next section System (V.3.5)-(V.3.6) is linearized around the trivial steady state.

V.3.1 Linearization around a steady state

Let us determine the equilibria of System (V.3.5)-(V.3.6) when the external forces f_0 and f_1 are independent of time t. Setting the time derivatives of (V.3.5) to zero, we obtain the steady state problem

$$\begin{cases} \mu^P \partial_\alpha \left(\varrho + \frac{L^2}{12} \varrho^3 (\partial_\alpha \varphi)^2 \right) \boldsymbol{\omega}^\perp + \left(\mu^A v - \mu^P \left(\varrho + \frac{L^2}{12} \varrho^3 (\partial_\alpha \varphi)^2 \right) \partial_\alpha \varphi \right) \boldsymbol{\omega} = 0, \\ \varrho \partial_\alpha \mathbf{z} \cdot \boldsymbol{\omega} - \frac{L^2}{12} \partial_\alpha (\varrho^2 \partial_\alpha \varphi) = 0, \end{cases} \tag{V.3.7}$$

for $0 < \alpha < 1$, with the boundary conditions

$$\begin{cases} -\mu^P \varrho \boldsymbol{\omega}^\perp + f_0 \boldsymbol{\omega}^\perp = 0, & \alpha = 0, \\ \mu^P \varrho \boldsymbol{\omega}^\perp - f_1 \boldsymbol{\omega}^\perp = 0, & \alpha = 1, \\ \mu^P \varrho^2 \partial_\alpha \varphi = 0, & \alpha = 0, 1. \end{cases} \tag{V.3.8}$$

The first equation in (V.3.7) is a linear combination of orthogonal vectors, hence, both coefficients must vanish:

$$\partial_\alpha \left(\varrho + \frac{L^2}{12} \varrho^3 (\partial_\alpha \varphi)^2 \right) = 0, \quad \text{and} \quad \mu^A v = \mu^P \left(\varrho + \frac{L^2}{12} \varrho^3 (\partial_\alpha \varphi)^2 \right) \partial_\alpha \varphi.$$

The first one implies that $\varrho + (L^2/12)\varrho^3 (\partial_\alpha \varphi)^2$ must be constant with respect to α. The second one tells us that without polymerization ($v = 0$), the angle φ must be constant. We shall denote by $\varrho_e > 0$, φ_e and $v_e = 0$ the equilibrium density, angle and velocity, respectively. With these, the last term in the second equation of (V.3.7) vanishes. We are then left with $\partial_\alpha \mathbf{z} \cdot \boldsymbol{\omega} = 0$, i.e. that the tangent vector $\partial_\alpha \mathbf{z}$ is orthogonal to the filament direction $\boldsymbol{\omega}$. This allows us to write $\partial_\alpha \mathbf{z} = -c\boldsymbol{\omega}^\perp$ for some constant $c > 0$, where the negative sign appears for convenience. Of course $\partial_\alpha \mathbf{z}^\perp \cdot \boldsymbol{\omega} = c$, and consequently, $c = (1/\varrho_e) > 0$. Therefore, $\partial_\alpha \mathbf{z} = -(1/\varrho_e)\boldsymbol{\omega}^\perp$. Integration with respect to α yields $\mathbf{z}(\alpha) = -(1/\varrho_e)\alpha \boldsymbol{\omega}(\varphi_e)^\perp$, where we have chosen $\mathbf{z}(0) = 0$.

Finally, the first and second boundary conditions in (V.3.8) yield $\mu^P \varrho_e = f_0 = f_1$. This means that the forces on the sides are both constants and are of the same magnitude. The last boundary condition in (V.3.8) is automatically satisfied since $\varphi = \varphi_e =$ constant. The equilibrium state $(\mathbf{z}_e, \varphi_e)$ is therefore

$$\mathbf{z}_e(\alpha) = -\frac{1}{\varrho_e} \alpha \boldsymbol{\omega}_e^\perp, \quad \text{and} \quad \varphi_e = \text{ constant}, \quad \text{with } v_e = 0, \tag{V.3.9}$$

where $\varrho_e > 0$ and $\boldsymbol{\omega}_e := \boldsymbol{\omega}(\varphi_e)$. This corresponds to the case when the lamellipodium strip is rectangular, with parallel filaments next to each other, differing only by equally spaced shifts in the α-direction, and without polymerization at their barbed ends.

Taylor series expansions. Linearization of system (V.3.5)-(V.3.6) around $(\mathbf{z}_e, \varphi_e)$ in (V.3.9) is executed by Taylor series expansions about the steady state, neglecting terms of order higher than one. For a sufficiently small $\delta > 0$, small deviations from the equilibrium are $\widetilde{\mathbf{z}} = \mathbf{z}_e + \delta \mathbf{z}$, $\widetilde{\varphi} = \varphi_e + \delta\varphi$, and $\widetilde{v} = \delta v$. Expanding $\boldsymbol{\omega}(\widetilde{\varphi})$ around φ_e results to

$$\boldsymbol{\omega}(\widetilde{\varphi}) = \boldsymbol{\omega}_e + \delta\varphi \boldsymbol{\omega}_e^\perp + O(\delta^2). \tag{V.3.10}$$

Multiplication of(V.3.10) with $\partial_\alpha \widetilde{\mathbf{z}}^\perp$ yields

$$\begin{aligned}\partial_\alpha \widetilde{\mathbf{z}}^\perp \cdot \boldsymbol{\omega}(\widetilde{\varphi}) &= (\partial_\alpha \mathbf{z}_e^\perp + \delta \partial_\alpha \mathbf{z}^\perp) \cdot \left(\boldsymbol{\omega}_e + \delta\varphi \boldsymbol{\omega}_e^\perp + O(\delta^2)\right) \\ &= \partial_\alpha \mathbf{z}_e^\perp \cdot \boldsymbol{\omega}_e + \delta \left(\partial_\alpha \mathbf{z}^\perp \cdot \boldsymbol{\omega}_e + \varphi \partial_\alpha \mathbf{z}_e^\perp \cdot \boldsymbol{\omega}_e^\perp\right) + O(\delta^2) \\ &= (1/\varrho_e) + \delta \left(\partial_\alpha \mathbf{z}^\perp \cdot \boldsymbol{\omega}_e + \varphi \partial_\alpha \mathbf{z}_e \cdot \boldsymbol{\omega}_e\right) + O(\delta^2).\end{aligned}$$

Because $\partial_\alpha \mathbf{z}_e \cdot \boldsymbol{\omega}_e = 0$, we have $\partial_\alpha \widetilde{\mathbf{z}}^\perp \cdot \boldsymbol{\omega}(\widetilde{\varphi}) = (1/\varrho_e) + \delta \partial_\alpha \mathbf{z}^\perp \cdot \boldsymbol{\omega}_e + O(\delta^2)$. Next, let us denote by $\widetilde{\varrho} := (\partial_\alpha \widetilde{\mathbf{z}}^\perp \cdot \boldsymbol{\omega}(\widetilde{\varphi}))^{-1}$ and expand it around $(\mathbf{z}_e, \varphi_e)$. The computations above yield

$$\widetilde{\varrho} = \varrho_e - \delta \varrho_e^2 (\partial_\alpha \mathbf{z}^\perp \cdot \boldsymbol{\omega}_e) + O(\delta^2), \tag{V.3.11}$$

From (V.3.10), we also have $\boldsymbol{\omega}(\widetilde{\varphi})^\perp = \boldsymbol{\omega}_e^\perp - \delta\varphi \boldsymbol{\omega}_e + O(\delta^2)$. Consequently,

$$\widetilde{\varrho}\boldsymbol{\omega}(\widetilde{\varphi})^\perp = \varrho_e \boldsymbol{\omega}_e^\perp - \delta \varrho_e^2 (\partial_\alpha \mathbf{z}^\perp \cdot \boldsymbol{\omega}_e)\boldsymbol{\omega}_e^\perp - \delta \varrho_e \varphi \boldsymbol{\omega}_e + O(\delta^2),$$

with α-derivative

$$\partial_\alpha(\widetilde{\varrho}\boldsymbol{\omega}(\widetilde{\varphi})^\perp) = -\delta(\varrho_e^2(\partial_\alpha^2 \mathbf{z}^\perp \cdot \boldsymbol{\omega}_e)\boldsymbol{\omega}_e^\perp + \varrho_e(\partial_\alpha\varphi)\boldsymbol{\omega}_e) + O(\delta^2).$$

Here, we used $\partial_\alpha(\varrho_e \boldsymbol{\omega}_e^\perp) = 0$. Combining the computations above and tending $\delta \to 0$ allow us to write the linearization of the first equation in (V.3.5) around $(\mathbf{z}_e, \varphi_e)$:

$$\mu^A(\partial_t \mathbf{z} - v\boldsymbol{\omega}_e) + \mu^P \varrho_e^2 (\partial_\alpha^2 \mathbf{z}^\perp \cdot \boldsymbol{\omega}_e)\boldsymbol{\omega}_e^\perp + \mu^P \varrho_e (\partial_\alpha \varphi)\boldsymbol{\omega}_e = 0.$$

For the second equation in (V.3.5), we employ the computations

$$\begin{aligned}\partial_\alpha \widetilde{\mathbf{z}} \cdot \boldsymbol{\omega}(\widetilde{\varphi}) &= (\partial_\alpha \mathbf{z}_e + \delta \partial_\alpha \mathbf{z}) \cdot \left(\boldsymbol{\omega}_e + \delta\varphi\boldsymbol{\omega}_e^\perp + O(\delta^2)\right) = \partial_\alpha \mathbf{z}_e \cdot \boldsymbol{\omega}_e + \delta\left(\partial_\alpha \mathbf{z} \cdot \boldsymbol{\omega}_e + \varphi \partial_\alpha \mathbf{z}_e \cdot \boldsymbol{\omega}_e^\perp\right) + O(\delta^2) \\ &= \delta\left(\partial_\alpha \mathbf{z} \cdot \boldsymbol{\omega}_e - \varphi \partial_\alpha \mathbf{z}_e^\perp \cdot \boldsymbol{\omega}_e\right) + O(\delta^2) = \delta\left(\partial_\alpha \mathbf{z} \cdot \boldsymbol{\omega}_e - \frac{1}{\varrho_e}\varphi\right) + O(\delta^2),\end{aligned}$$

where we used $\partial_\alpha \mathbf{z}_e \cdot \boldsymbol{\omega}_e = 0$ and $(1/\varrho_e) = \partial_\alpha \mathbf{z}_e^\perp \cdot \boldsymbol{\omega}_e$. From (V.3.11), it follows that

$$\widetilde{\varrho}\partial_\alpha \widetilde{\mathbf{z}} \cdot \boldsymbol{\omega}(\widetilde{\varphi}) = \delta\varrho_e\left(\partial_\alpha \mathbf{z} \cdot \boldsymbol{\omega}_e - \frac{1}{\varrho_e}\varphi\right) + O(\delta^2) = \delta(\varrho_e \partial_\alpha \mathbf{z} \cdot \boldsymbol{\omega}_e - \varphi) + O(\delta^2).$$

We also compute from (V.3.11) that $\widetilde{\varrho}^2 = \varrho_e^2 - 2\delta\varrho_e^3(\partial_\alpha \mathbf{z}^\perp \cdot \boldsymbol{\omega}_e) + O(\delta^2)$, so that

$$\partial_\alpha(\widetilde{\varrho}^2 \partial_\alpha \widetilde{\varphi}) = \delta \varrho_e^2 \partial_\alpha^2 \varphi + O(\delta^2).$$

Then, the linearized equation for φ around $(\mathbf{z}_e, \varphi_e)$ reads

$$\frac{L^2}{12}\mu^A \partial_t \varphi - \mu^P \varrho_e\, \partial_\alpha \mathbf{z} \cdot \boldsymbol{\omega}_e + \mu^P \varphi - \frac{L^2}{12}\mu^P \varrho_e^2\, \partial_\alpha^2 \varphi = 0.$$

Finally, since $\mu^P \varrho_e = f_0 = f_1$, the boundary conditions become

$$-\mu^P \varrho_e^2 (\partial_\alpha \mathbf{z}^\perp \cdot \boldsymbol{\omega}_e)\boldsymbol{\omega}_e^\perp = 0, \quad \text{and} \quad \mu^P \varrho_e^2\, \partial_\alpha \varphi = 0.$$

Linearized equations for (V.3.5)-(V.3.6) **around** $(\mathbf{z}_e, \varphi_e)$**.** Collecting the computations above, we arrive to the linear system

$$\begin{cases} \mu^A(\partial_t \mathbf{z} - v\boldsymbol{\omega}_e) + \mu^P \varrho_e^2(\partial_\alpha^2 \mathbf{z}^\perp \cdot \boldsymbol{\omega}_e)\boldsymbol{\omega}_e^\perp + \mu^P \varrho_e(\partial_\alpha \varphi)\boldsymbol{\omega}_e = 0, \\ \frac{L^2}{12}\mu^A \partial_t \varphi - \mu^P \varrho_e\, \partial_\alpha \mathbf{z} \cdot \boldsymbol{\omega}_e + \mu^P \varphi - \frac{L^2}{12}\mu^P \varrho_e^2\, \partial_\alpha^2 \varphi = 0, \end{cases} \tag{V.3.12}$$

subject to the boundary conditions

$$\begin{cases} -\mu^P \varrho_e^2(\partial_\alpha \mathbf{z}^\perp \cdot \boldsymbol{\omega}_e)\boldsymbol{\omega}_e^\perp = 0, & \text{for } \alpha = 0, 1, \\ \mu^P \varrho_e^2\, \partial_\alpha \varphi = 0, & \text{for } \alpha = 0, 1. \end{cases} \tag{V.3.13}$$

For simplicity, we investigate the case when the filaments are vertical and are pointing upwards, i.e. $\varphi_e = \pi/2$. The directions read $\boldsymbol{\omega}_e = (0, 1)^\top$ and $\boldsymbol{\omega}_e^\perp = (-1, 0)^\top$. Writing $\mathbf{z} = (z_1, z_2)^\top$, we compute that $\partial_\alpha^2 \mathbf{z}^\perp \cdot \boldsymbol{\omega}_e = \partial_\alpha^2 z_1$ and $\partial_\alpha \mathbf{z} \cdot \boldsymbol{\omega}_e = \partial_\alpha z_2$. Substituting these to (V.3.12)-(V.3.13), we obtain a decoupled system for z_1 and (z_2, φ):

$$\begin{cases} \mu^A \partial_t z_1 - \mu^P \varrho_e^2\, \partial_\alpha^2 z_1 = 0, & 0 < \alpha < 1,\ t > 0, \\ \mu^P \varrho_e^2\, \partial_\alpha z_1 = 0, & \text{for } \alpha = 0, 1, \end{cases} \tag{V.3.14}$$

and

$$\begin{cases} \mu^A(\partial_t z_2 - v) + \mu^P \varrho_e \partial_\alpha \varphi = 0, & 0 < \alpha < 1,\ t > 0, \\ \frac{L^2}{12}(\mu^A \partial_t \varphi - \mu^P \varrho_e^2 \partial_\alpha^2 \varphi) - \mu^P \varrho_e \partial_\alpha z_2 + \mu^P \varphi = 0, & 0 < \alpha < 1,\ t > 0, \\ \mu^P \varrho_e^2 \partial_\alpha \varphi = 0, & \text{for } \alpha = 0, 1. \end{cases} \tag{V.3.15}$$

Problem for z_1**.** The problem for z_1 in (V.3.14) is a diffusion equation subject to homogeneous Neumann boundary conditions:

$$\begin{cases} \partial_t z_1(\alpha, t) = \frac{\mu^P \varrho_e^2}{\mu^A}\, \partial_\alpha^2 z_1(\alpha, t), & 0 < \alpha < 1, \quad t > 0, \\ \partial_\alpha z_1(0, t) = 0 = \partial_\alpha z_1(1, t), & t > 0, \\ z_1(\alpha, 0) = z_1^0(\alpha), & 0 < \alpha < 1, \end{cases} \tag{V.3.16}$$

with diffusivity coefficient $(\mu^P \varrho_e^2/\mu^A) > 0$ and appropriate initial data $z_1^0(\alpha)$ for $0 < \alpha < 1$. This can be solved via separation of variables,

$$z_1(\alpha, t) = \sum_{n=0}^{\infty} c_n \cos(n\pi\alpha) e^{-(n\pi)^2(\mu^P \varrho_e^2/\mu^A)t},$$

with Fourier coefficients given by

$$c_0 = \int_0^1 z_1^0(\alpha)\, \mathrm{d}\alpha, \qquad c_n = 2\int_0^1 z_1^0(\alpha) \cos(n\pi\alpha)\, \mathrm{d}\alpha, \quad n \geq 1.$$

Problem for (z_2, φ). For simplicity, we neglect polymerization ($v = 0$). System (V.3.15) becomes

$$\begin{cases} \mu^A \partial_t z_2 + \mu^P \varrho_e \partial_\alpha \varphi = 0, & 0 < \alpha < 1,\ t > 0, \\ \frac{L^2}{12}(\mu^A \partial_t \varphi - \mu^P \varrho_e^2 \partial_\alpha^2 \varphi) - \mu^P \varrho_e \partial_\alpha z_2 + \mu^P \varphi = 0, & 0 < \alpha < 1,\ t > 0, \\ \mu^P \varrho_e^2 \partial_\alpha \varphi = 0, & \text{for } \alpha = 0, 1. \end{cases} \tag{V.3.17}$$

Let us ignore the boundary conditions for the moment, and take the Fourier transforms in the α-variable:

$$\widehat{z_2}(\xi, t) = \int_{-\infty}^{\infty} e^{-i\xi\alpha} z_2(\alpha, t)\, \mathrm{d}\alpha, \quad \text{and} \quad \widehat{\varphi}(\xi, t) = \int_{-\infty}^{\infty} e^{-i\xi\alpha} \varphi(\alpha, t)\, \mathrm{d}\alpha. \tag{V.3.18}$$

This converts (V.3.17) to the system of ODEs

$$\begin{cases} \mu^A \partial_t \widehat{z_2} + \mu^P \varrho_e \xi i \widehat{\varphi} = 0, \\ \frac{L^2}{12} \mu^A \partial_t \widehat{\varphi} + \mu^P \left(\frac{L^2}{12} \varrho_e^2 \xi^2 + 1 \right) \widehat{\varphi} - \mu^P \varrho_e \xi i \widehat{z_2} = 0. \end{cases} \tag{V.3.19}$$

From the first equation, we have $\mu^P \varrho_e \xi i \widehat{\varphi} = -\mu^A \partial_t \widehat{z_2}$ with time derivative $\mu^P \varrho_e \xi i \partial_t \widehat{\varphi} = -\mu^A \partial_{tt} \widehat{z_2}$. Inserting these to the second equation results to a second order ODE for $\widehat{z_2}$,

$$\frac{L^2}{12} \mu^A \partial_{tt} \widehat{z_2} + \mu^P \left(\frac{L^2}{12} \varrho_e^2 \xi^2 + 1 \right) \partial_t \widehat{z_2} - \frac{(\mu^P \varrho_e \xi)^2}{\mu^A} \widehat{z_2} = 0.$$

The discriminant $D(\xi)$ of the corresponding characteristic equation is positive and so we have two distinct real roots r_1 and r_2. Indeed,

$$D(\xi) = (\mu^P)^2 \left[\left(\frac{L^2}{12} \varrho_e^2 \xi^2 + 1 \right)^2 + \frac{L^2}{3} \varrho_e^2 \xi^2 \right] > 0, \quad \text{for all } \xi,$$

and

$$r_{1,2}(\xi) = \frac{-\mu^P \left((L^2/12) \varrho_e^2 \xi^2 + 1 \right) \pm \sqrt{D(\xi)}}{(L^2/6)\mu^A}.$$

Notice that $r_1(\xi) > 0$ while $r_2(\xi) < 0$ for all ξ, which means that there are instabilities (corresponding to the positive root) for all frequencies ξ. Nevertheless, a silver lining is found in the following observation. For large values of ξ, we calculate

$$\frac{L^2}{6} \mu^A r_1(\xi) = \frac{(L^2/3) \varrho_e^2 \xi^2}{\mu^P \left((L^2/12) \varrho_e^2 \xi^2 + 1 \right) + \sqrt{D(\xi)}} \longrightarrow \frac{2}{\mu^P}, \quad \text{as } \xi \to \infty.$$

Therefore $r_1(\xi) \to 12/(L^2 \mu^P \mu^A)$ as $\xi \to \infty$, or in other words, r_1 remains bounded as long as $L \neq 0$.

Instability of the steady state. The main problem we have regarding stability of the steady state is the (z_2, φ)-equations. We speculate that the instability comes from the following. Setting $v = 0$ in the first equation of (V.3.5), one has

$$\mu^A \partial_t \mathbf{z} = \mu^P \partial_\alpha \left(\varrho + \frac{L^2}{12} \varrho^3 (\partial_\alpha \varphi)^2 \right) \boldsymbol{\omega}^\perp - \mu^P \varrho (\partial_\alpha \varphi) \boldsymbol{\omega}. \tag{V.3.20}$$

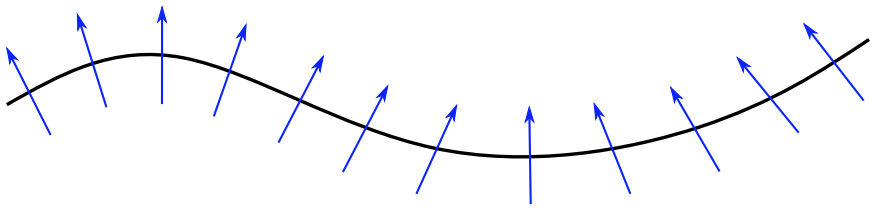

Figure V.2: Arbitrary configuration of a filament strip. The black line represents the center-of-mass curve of the filaments.

Consider the filament strip configuration in Figure V.2, and concentrate on the last term of Equation (V.3.20). On the left part of the curve, $\partial_\alpha \varphi < 0$, so the curve moves upward, while on the right part, downward. This bends the curve in opposite directions, which might be the cause for instabilities. In fact, a demonstration of the pressure term of a supplementary material to [Man+15] mentioned instabilities with respect to nonsymmetric perturbations. However, since such instabilities were not observed in the full model, they were not investigated further.

In (V.3.20), filaments communicate only through repulsion. This lack of connection in the α-direction was not an issue in the models discussed in the previous sections, since filament bending, cross-links between filaments of different families, and even forces on the filament ends (tethering and area constraint) produce α-derivatives. In the next section we introduce an effect to counteract possible pressure instabilities.

V.3.2 Adding tension of center-of-mass curve

To maintain the shape of the lamellipodium, the FBLM in [OSS08] described the cell membrane as a rubber band stretched around the barbed ends of the filaments, along with a prescribed equilibrium circumference. Inspired by this strategy, we introduce an artificial structure-preserving feature of the form

$$\mathcal{E}^K(t)[\mathbf{z}] := \mu^K \int_0^1 |\partial_\alpha \mathbf{z}| \, \mathrm{d}\alpha. \tag{V.3.21}$$

It models the resistance against stretching of the center-of-mass curve above the force-free equilibrium length, which we assume to be zero. We have chosen the force to act on the center-of-mass curve instead of the leading edge for computational simplicity. The variation of (V.3.21) is then calculated,

$$\delta\mathcal{E}^K(t)[\mathbf{z}]\boldsymbol{\delta}\mathbf{z} = \mu^K \int_0^1 \frac{\partial_\alpha \mathbf{z}}{|\partial_\alpha \mathbf{z}|} \cdot \partial_\alpha(\boldsymbol{\delta}\mathbf{z}) \, \mathrm{d}\alpha = \mu^K \frac{\partial_\alpha \mathbf{z}}{|\partial_\alpha \mathbf{z}|} \cdot \boldsymbol{\delta}\mathbf{z}\Big|_0^1 - \mu^K \int_0^1 \partial_\alpha \left(\frac{\partial_\alpha \mathbf{z}}{|\partial_\alpha \mathbf{z}|} \right) \cdot \boldsymbol{\delta}\mathbf{z} \, \mathrm{d}\alpha.$$

Euler-Lagrange equations with tension. The tension of center-of-mass curve energy (V.3.21) is added to the potential energy of System (V.3.1)-(V.3.2), resulting to

$$\begin{cases} \mu^A(\partial_t \mathbf{z} - v\boldsymbol{\omega}) - \mu^P \partial_\alpha \left(\left(\varrho + \frac{L^2}{12} \varrho^3 (\partial_\alpha \varphi)^2 \right) \boldsymbol{\omega}^\perp \right) - \mu^K \partial_\alpha \left(\dfrac{\partial_\alpha \mathbf{z}}{|\partial_\alpha \mathbf{z}|} \right) = 0, \\ \frac{L^2}{12} \mu^A \partial_t \varphi - \mu^P \varrho \partial_\alpha \mathbf{z} \cdot \boldsymbol{\omega} - \frac{L^2}{12} \mu^P \partial_\alpha (\varrho^2 \partial_\alpha \varphi) = 0, \end{cases} \tag{V.3.22}$$

for $0 < \alpha < 1$ and $t > 0$, subject to the boundary conditions

$$\begin{cases} \mu^P \varrho \boldsymbol{\omega}^\perp + \mu^K \dfrac{\partial_\alpha \mathbf{z}}{|\partial_\alpha \mathbf{z}|} = f_{0,1} \boldsymbol{\omega}^\perp, & \alpha = 0, 1, \\ \varrho^2 \partial_\alpha \varphi = 0, & \alpha = 0, 1. \end{cases} \tag{V.3.23}$$

Linearization of System (V.3.22)-(V.3.23)**.** With a constant tangent vector, i.e. $\partial_\alpha(\partial_\alpha \mathbf{z}/|\partial_\alpha \mathbf{z}|) = 0$, steady states of (V.3.22)-(V.3.23) are the same as in (V.3.9):

$$\mathbf{z}_e(\alpha) = -(1/\varrho_e)\alpha \boldsymbol{\omega}_e^\perp, \quad \text{and} \quad \varphi_e = \text{ constant},$$

where the subscript e means states in equilibrium. It follows that $(\partial_\alpha \mathbf{z}_e/|\partial_\alpha \mathbf{z}_e|) = -\boldsymbol{\omega}_e^\perp$. The first boundary condition in (V.3.23) implies that $\mu^P \varrho_e - \mu^K = f_0 = f_1$, or in other words, the external forces are constant and are of the same magnitude. The second boundary condition in (V.3.23) is automatically satisfied since $\varphi = \varphi_e =$ constant. For the linearization, we shall need the expansion

$$\frac{\partial_\alpha \widetilde{\mathbf{z}}}{|\partial_\alpha \widetilde{\mathbf{z}}|} = \frac{\partial_\alpha \mathbf{z}_e}{|\partial_\alpha \mathbf{z}_e|} + \delta \left(\frac{\partial_\alpha \mathbf{z}}{|\partial_\alpha \mathbf{z}_e|} - (\partial_\alpha \mathbf{z}_e \cdot \partial_\alpha \mathbf{z}) \frac{\partial_\alpha \mathbf{z}_e}{|\partial_\alpha \mathbf{z}_e|^3} \right) + O(\delta^2),$$

where $\widetilde{\mathbf{z}}$ is a small perturbation from equilibrium. As in the Section V.3.1, we take $\varphi_e = \pi/2$. In the end, we obtain the linear systems

$$\begin{cases} \mu^A \partial_t z_1 = \mu^P \varrho_e^2 \partial_\alpha^2 z_1, & \text{for } 0 < \alpha < 1, \\ \mu^P \varrho_e^2 \partial_\alpha z_1 = 0, & \text{for } \alpha = 0, 1, \end{cases}$$

and

$$\begin{cases} \mu^A \partial_t z_2 + \mu^P \varrho_e \partial_\alpha \varphi - \mu^K \varrho_e \partial_\alpha^2 z_2 = 0, & \text{for } 0 < \alpha < 1, \\ \frac{L^2}{12} \mu^A \partial_t \varphi - \mu^P (\varrho_e \partial_\alpha z_2 - \varphi) - \frac{L^2}{12} \mu^P \varrho_e^2 \partial_\alpha^2 \varphi = 0, & \text{for } 0 < \alpha < 1, \end{cases} \tag{V.3.24}$$

with the boundary conditions

$$\begin{cases} \mu^P (\varrho_e \partial_\alpha z_2 - \varphi) = 0, & \text{for } \alpha = 0, 1, \\ \mu^P \varrho_e \partial_\alpha \varphi = 0, & \text{for } \alpha = 0, 1. \end{cases} \tag{V.3.25}$$

Problem for (z_2, φ)**.** Let us focus on the (z_2, φ)-system in (V.3.24)-(V.3.25) since the z_1-equation is again a diffusion equation with Neumann boundary conditions and is already solved in (V.3.16). Proceeding as in the Section V.3.1, we ignore the boundary conditions and use the Fourier transforms (V.3.18) in the α-variable. Equations (V.3.24)-(V.3.25) are transformed via Fourier into a system of ODEs:

$$\begin{cases} \mu^A \partial_t \widehat{z_2} + \mu^P \varrho_e \xi i \widehat{\varphi} + \mu^K \varrho_e \xi^2 \widehat{z_2} = 0, \\ \frac{L^2}{12} \mu^A \partial_t \widehat{\varphi} + \mu^P \left(\frac{L^2}{12} \varrho_e^2 \xi^2 + 1 \right) \widehat{\varphi} - \mu^P \varrho_e \xi i \widehat{z_2} = 0. \end{cases} \tag{V.3.26}$$

Using the first equation, we have $\mu^P \varrho_e \xi i \widehat{\varphi} = -\mu^A \partial_t \widehat{z_2} - \mu^K \varrho_e \xi^2 \widehat{z_2}$ with time derivative $\mu^P \varrho_e \xi i \partial_t \widehat{\varphi} = -\mu^A \partial_{tt} \widehat{z_2} - \mu^K \varrho_e \xi^2 \partial_t \widehat{z_2}$. Inserting these to the second equation in (V.3.26) yields

$$\frac{L^2}{12}\mu^A \partial_{tt}\widehat{z_2} + \left(\frac{L^2}{12}\mu^K \varrho_e \xi^2 + \mu^P \left(\frac{L^2}{12}\varrho_e^2 \xi^2 + 1\right)\right)\partial_t \widehat{z_2}$$
$$+ (\mu^P/\mu^A)\left(\mu^K \varrho_e \left(\frac{L^2}{12}\varrho_e^2 \xi^2 + 1\right) - \mu^P \varrho_e^2\right)\xi^2 \widehat{z_2} = 0.$$

The discriminant $D(\xi)$ of the corresponding characteristic equation is

$$\begin{aligned} D(\xi) &= \left(\frac{L^2}{12}\mu^K \varrho_e \xi^2 + \mu^P \left(\frac{L^2}{12}\varrho_e^2 \xi^2 + 1\right)\right)^2 - \frac{L^2}{3}\mu^P \left(\mu^K \varrho_e \left(\frac{L^2}{12}\varrho_e^2 \xi^2 + 1\right) - \mu^P \varrho_e^2\right)\xi^2 \\ &= \left(\frac{L^2}{12}\mu^K \varrho_e \xi^2 - \mu^P \left(\frac{L^2}{12}\varrho_e^2 \xi^2 + 1\right)\right)^2 + \frac{L^2}{3}(\mu^P)^2 \varrho_e^2 \xi^2. \end{aligned} \tag{V.3.27}$$

Because $D(\xi) > 0$ for all ξ, we get two distinct real roots

$$r_{1,2}(\xi) = \frac{-\left((L^2/12)\mu^K \varrho_e \xi^2 + \mu^P \left((L^2/12)\varrho_e^2 \xi^2 + 1\right)\right) \pm \sqrt{D(\xi)}}{(L^2/6)\mu^A},$$

where $r_2(\xi) < 0$ for all ξ. To ensure that $r_1(\xi)$ is negative, the sum of the last two terms on the right hand side of the first line in (V.3.27) must be positive, in particular,

$$\mu^K > \frac{\mu^P \varrho_e}{(L^2/12)\varrho_e^2 \xi^2 + 1}, \quad \xi \neq 0.$$

For large values of ξ, one could choose μ^K to be sufficiently small, while for small ξ-values, μ^K must be large enough. Notice however that in the original problem, we do not really consider ξ on the whole real line. Instead, for a given μ^K, we could begin at a positive value of ξ (large enough) so that $r_1(\xi)$ is negative. These considerations pave the way for a more in-depth investigation of (V.3.22)-(V.3.23), where bifurcation analysis is instrumental.

V.4 Rigid filaments with pressure and tension of center-of-mass curve

In this section, stability of solutions to equations (V.3.22)-(V.3.23) for rigid filaments with pressure and center-of-mass tension are analyzed. For simplicity, the forces on the sides of the strip are assumed to be equal, i.e. $f := f_0 = f_1$ and the higher-order terms, i.e. $O(L^2)$-terms, in the first equation of (V.3.22) are dropped. The Euler-Lagrange equations now take the form

$$\begin{cases} \mu^A \partial_t \mathbf{z} - \mu^P \partial_\alpha(\varrho \boldsymbol{\omega}^\perp) - \mu^K \partial_\alpha\left(\dfrac{\partial_\alpha \mathbf{z}}{|\partial_\alpha \mathbf{z}|}\right) = 0, & \text{for } 0 < \alpha < 1, t > 0, \\ \frac{L^2}{12}\mu^A \partial_t \varphi - \mu^P \varrho \partial_\alpha \mathbf{z} \cdot \boldsymbol{\omega} - \frac{L^2}{12}\mu^P \partial_\alpha(\varrho^2 \partial_\alpha \varphi) = 0, & \text{for } 0 < \alpha < 1, t > 0, \\ (\mu^P \varrho - f)\boldsymbol{\omega}^\perp + \mu^K \dfrac{\partial_\alpha \mathbf{z}}{|\partial_\alpha \mathbf{z}|} = \partial_\alpha \varphi = 0, & \alpha = 0, 1. \end{cases} \tag{V.4.1}$$

Nondimensionalization and rescaling. A nondimensionalization is carried out where our reference density is

$$\varrho_0 := \frac{f + \mu^K}{\mu^P}.$$

We then introduce the scaling

$$t \to \frac{\mu^A}{\mu^P}\frac{1}{\varrho_0^2}\, t, \qquad \mathbf{z} \to \frac{1}{\varrho_0}\mathbf{z}, \qquad \varrho \to \varrho_0 \varrho,$$

and the dimensionless parameters

$$\beta := \frac{L}{2\sqrt{3}}\,\varrho_0, \quad \text{and} \quad \gamma := \frac{\mu^K}{\mu^P \varrho_0}. \tag{V.4.2}$$

Taking the α-derivative of the first equation in (V.4.1), and implementing the scaling above yield to the nondimensional equations

$$\begin{cases} \partial_t(\partial_\alpha \mathbf{z}) - \partial_\alpha^2(\varrho \boldsymbol{\omega}^\perp) - \gamma \partial_\alpha^2 \left(\dfrac{\partial_\alpha \mathbf{z}}{|\partial_\alpha \mathbf{z}|} \right) = 0, & \text{for } 0 < \alpha < 1,\ t > 0, \\ \beta^2 \partial_t \varphi - \varrho \partial_\alpha \mathbf{z} \cdot \boldsymbol{\omega} - \beta^2 \partial_\alpha(\varrho^2 \partial_\alpha \varphi) = 0, & \text{for } 0 < \alpha < 1,\ t > 0, \\ (\varrho - 1 + \gamma)\boldsymbol{\omega}^\perp + \gamma \dfrac{\partial_\alpha \mathbf{z}}{|\partial_\alpha \mathbf{z}|} = \partial_\alpha \varphi = 0, & \alpha = 0, 1. \end{cases} \tag{V.4.3}$$

In the following section we look at the equilibria of the dimensionless system above.

V.4.1 Existence of nontrivial steady states

The trivial steady state of System (V.4.3) satisfies $\partial_\alpha \mathbf{z} = \boldsymbol{\omega}(\vartheta_0)$, $\varphi = \vartheta_0 + (\pi/2)$, and $\varrho = 1$. Setting $\vartheta_0 = 0$ for simplicity, one has

$$\partial_\alpha \overline{\mathbf{z}} = \begin{pmatrix} 1 \\ 0 \end{pmatrix}, \quad \overline{\varphi} = \frac{\pi}{2}, \quad \text{and} \quad \overline{\varrho} = 1. \tag{V.4.4}$$

To linearize (V.4.3) around the steady state (V.4.4), we introduce the deviation (from equilibrium) variables (a_1, b_1) and φ_1, and insert

$$\partial_\alpha \mathbf{z} = \begin{pmatrix} 1 \\ 0 \end{pmatrix} + \begin{pmatrix} a_1 \\ b_1 \end{pmatrix}, \quad \text{and} \quad \varphi = \frac{\pi}{2} + \varphi_1$$

to (V.4.3). We shall need the computations

$$\varrho \approx 1 - a_1, \quad \boldsymbol{\omega}^\perp \approx \begin{pmatrix} -1 \\ 0 \end{pmatrix} + \begin{pmatrix} 0 \\ -\varphi_1 \end{pmatrix}, \quad \varrho \boldsymbol{\omega}^\perp \approx \begin{pmatrix} -1 \\ 0 \end{pmatrix} + \begin{pmatrix} a_1 \\ -\varphi_1 \end{pmatrix},$$

$$\frac{\partial_\alpha \mathbf{z}}{|\partial_\alpha \mathbf{z}|} \approx \begin{pmatrix} 1 \\ 0 \end{pmatrix} + \begin{pmatrix} 0 \\ b_1 \end{pmatrix}, \quad \varrho \partial_\alpha \mathbf{z} \cdot \boldsymbol{\omega} \approx b_1 - \varphi_1, \quad \varrho^2 \partial_\alpha \varphi = \partial_\alpha \varphi_1.$$

Linearization of (V.4.3) around (V.4.4) yields a boundary value problem for a_1 and a coupled system for (b_1, φ_1). First, we have

$$\begin{cases} \partial_t a_1 = \partial_\alpha^2 a_1, \\ a_1 = 0, \quad \alpha = 0, 1. \end{cases} \tag{V.4.5}$$

This component tends to zero exponentially. On the other hand,

$$\begin{cases} \partial_t b_1 = \partial_\alpha^2(\gamma b_1 - \varphi_1), \\ \beta^2 \partial_t \varphi_1 = \beta^2 \partial_\alpha^2 \varphi_1 + b_1 - \varphi_1, \\ b_1 - \varphi_1 = \partial_\alpha \varphi_1 = 0, \qquad \alpha = 0, 1. \end{cases} \tag{V.4.6}$$

Rotational invariance of this problem implies that we may add to any solution a constant state satisfying $b_1 - \varphi_1 = 0$. Below, we look for other nontrivial steady states.

Nontrivial equilibria. With $\mathbf{X}(\alpha) := (b_1, \varphi_1)^\top$, we write the steady state equations in the form

$$\mathbf{X}''(\alpha) = M\mathbf{X}(\alpha), \quad M := \frac{1}{\beta^2}\begin{pmatrix} -1/\gamma & 1/\gamma \\ -1 & 1 \end{pmatrix}, \tag{V.4.7}$$

where $'$ means derivative with respect to α. The eigenvalues of M are

$$\lambda_0 = 0, \quad \text{and} \quad \lambda_1 = -\frac{1}{\beta^2}\left(\frac{1-\gamma}{\gamma}\right),$$

with eigenvectors $(1, 1)$ and $(1, \gamma)$, respectively. Since $0 < \gamma < 1$, $\lambda_1 < 0$. The general solution to (V.4.7) is therefore

$$\mathbf{X} = (A\sin(\kappa\alpha) + B\cos(\kappa\alpha))\begin{pmatrix} 1 \\ \gamma \end{pmatrix} + (C\alpha + D)\begin{pmatrix} 1 \\ 1 \end{pmatrix}, \quad \kappa := \frac{1}{\beta}\sqrt{\frac{1-\gamma}{\gamma}},$$

for arbitrary constants A, B, C and D. We compute that

$$b_1 - \varphi_1 = (1-\gamma)(A\sin(\kappa\alpha) + B\cos(\kappa\alpha)).$$

With the boundary conditions in (V.4.6), this has to vanish at $\alpha = 0$, implying $B = 0$. At $\alpha = 1$, on the other hand, we require $A\sin(\kappa) = 0$. Finally,

$$\partial_\alpha \varphi_1 = \kappa\gamma A\cos(\kappa\alpha) + C = 0, \quad \alpha = 0, 1,$$

only if $C = -\kappa\gamma A$ and $A(\cos(\kappa) - 1) = 0$. A nontrivial steady state therefore exists only if $\sin\kappa = 0$ and $\cos\kappa = 1$. With the smallest choice $\kappa_0 = 2\pi$, the space of nontrivial solutions is spanned by

$$\mathbf{X} = A(t)\left(\sin(2\pi\alpha)\begin{pmatrix} 1 \\ \gamma \end{pmatrix} - 2\pi\gamma\alpha\begin{pmatrix} 1 \\ 1 \end{pmatrix}\right). \tag{V.4.8}$$

The nontrivial solution produces a nonvanishing (constant, vertical) velocity. With our choice $\kappa_0 = 2\pi$, we compute the bifurcation point

$$\beta_0 := \frac{1}{2\pi}\sqrt{\frac{1-\gamma}{\gamma}}. \tag{V.4.9}$$

Note that the value of $A(t)$ in (V.4.8) is still unknown. In the following section, we find that A satisfies a nonlinear ODE with nontrivial equilibria giving rise to the bifurcating steady states of System (V.4.3).

V.4.2 Normal form reduction close to the bifurcation point

The normal form reduction of System (V.4.3) close to the bifurcation point is derived by choosing values of β close to β_0 defined in (V.4.9). With the notations

$$\varepsilon := \sqrt{\left|\beta_0^2 - \beta^2\right|}, \quad \sigma\varepsilon^2 = \beta_0^2 - \beta^2, \quad \text{and} \quad \sigma := \operatorname{sign}(\beta_0^2 - \beta^2),$$

the derivation is carried out by looking at ε-values near zero. The ansatz

$$\begin{cases} \partial_\alpha \mathbf{z} = \begin{pmatrix} 1 \\ 0 \end{pmatrix} + \varepsilon\boldsymbol{\tau}_1 + \varepsilon^2\boldsymbol{\tau}_2 + \varepsilon^3\boldsymbol{\tau}_3 + O(\varepsilon^4), \quad \boldsymbol{\tau}_j = (a_j, b_j), \\ \varphi = \frac{\pi}{2} + \varepsilon\varphi_1 + \varepsilon^2\varphi_2 + \varepsilon^3\varphi_3 + O(\varepsilon^4), \end{cases} \tag{V.4.10}$$

expresses the fact that we expand the trivial solution for ε close to zero.

Time rescaling and expansions in ε. The expectation that the first two terms in the perturbation are in the direction of the steady states of the linearized problem motivates us to rescale the time variable $t \mapsto t/(\varepsilon^2)$. System (V.4.3) becomes

$$\begin{cases} \varepsilon^2\partial_t(\partial_\alpha \mathbf{z}) = \partial_\alpha^2(\varrho\boldsymbol{\omega}^\perp) + \gamma\partial_\alpha^2\left(\dfrac{\partial_\alpha \mathbf{z}}{|\partial_\alpha \mathbf{z}|}\right), & 0 < \alpha < 1,\ t > 0, \\ \varepsilon^2\beta^2\partial_t\varphi = \varrho\partial_\alpha \mathbf{z}\cdot\boldsymbol{\omega} + \beta^2\partial_\alpha(\varrho^2\partial_\alpha\varphi), & 0 < \alpha < 1,\ t > 0, \\ (\varrho - 1 + \gamma)\boldsymbol{\omega}^\perp + \gamma\dfrac{\partial_\alpha \mathbf{z}}{|\partial_\alpha \mathbf{z}|} = \partial_\alpha\varphi = 0, & \alpha = 0, 1. \end{cases} \tag{V.4.11}$$

Terms in the system above are expanded around ε through the ansatz (V.4.10). Then, at each order of ε, we extract a system of equations which shall be utilized to write the normal form reduction of the original system in (V.4.3). Notice that at $O(1)$, we just go back to the steady state equations of (V.4.3).

Now we expand the relevant terms,

$$\begin{aligned} \boldsymbol{\omega}^\perp &\approx \begin{pmatrix} -1 \\ 0 \end{pmatrix} - \varepsilon\begin{pmatrix} 0 \\ \varphi_1 \end{pmatrix} + \varepsilon^2\begin{pmatrix} \frac{1}{2}\varphi_1^2 \\ -\varphi_2 \end{pmatrix} + \varepsilon^3\begin{pmatrix} \varphi_1\varphi_2 \\ \frac{1}{6}\varphi_1^3 - \varphi_3 \end{pmatrix}, \\ \varrho &\approx 1 - \varepsilon a_1 + \varepsilon^2\left(-a_2 + a_1^2 - b_1\varphi_1 + \frac{1}{2}\varphi_1^2\right) \\ &\quad - \varepsilon^3\left(a_3 - 2a_1a_2 + b_1\varphi_2 + b_2\varphi_1 + \varphi_1\varphi_2 - 2a_1b_1\varphi_1 + \frac{1}{2}a_1\varphi_1^2 + a_1^3\right), \end{aligned}$$

so that

$$\begin{aligned} \varrho\boldsymbol{\omega}^\perp \approx \begin{pmatrix} -1 \\ 0 \end{pmatrix} + \varepsilon\begin{pmatrix} a_1 \\ -\varphi_1 \end{pmatrix} + \varepsilon^2\begin{pmatrix} a_2 - a_1^2 + b_1\varphi_1 \\ -\varphi_2 + a_1\varphi_1 \end{pmatrix} \\ + \varepsilon^3\begin{pmatrix} a_3 - 2a_1a_2 + b_1\varphi_2 + b_2\varphi_1 - 2a_1b_1\varphi_1 - a_1^3 \\ -\varphi_3 + a_1\varphi_2 + a_2\varphi_1 - a_1^2\varphi_1 + b_1\varphi_1^2 - \frac{1}{3}\varphi_1^3 \end{pmatrix}. \end{aligned}$$

In addition, we shall need the expansions

$$
\begin{aligned}
&|\partial_\alpha \mathbf{z}|^{-1} \approx 1 - \varepsilon a_1 + \varepsilon^2\left(-a_2 + a_1^2 - \frac{1}{2}b_1^2\right) + \varepsilon^3\left(-a_3 + 2a_1a_2 - b_1b_2 + \frac{3}{2}a_1b_1^2 - a_1^3\right),\\
&\frac{\partial_\alpha \mathbf{z}}{|\partial_\alpha \mathbf{z}|} \approx \begin{pmatrix}1\\0\end{pmatrix} + \varepsilon\begin{pmatrix}0\\b_1\end{pmatrix} + \varepsilon^2\begin{pmatrix}-\frac{1}{2}b_1^2\\ b_2 - a_1b_1\end{pmatrix} + \varepsilon^3\begin{pmatrix}-b_1b_2 + a_1b_1^2\\ b_3 - a_1b_2 - a_2b_1 + a_1^2b_1 - \frac{1}{2}b_1^3\end{pmatrix},\\
&\varrho\partial_\alpha \mathbf{z}\cdot\boldsymbol{\omega} \approx \varepsilon(b_1 - \varphi_1) + \varepsilon^2(b_2 - \varphi_2 - a_1b_1)\\
&\qquad + \varepsilon^3\left(b_3 - \varphi_3 - a_1b_2 - a_2b_1 + a_1^2b_1 + b_1\varphi_1^2 - b_1^2\varphi_1 - \frac{1}{3}\varphi_1^3\right),\\
&\varrho^2 \approx 1 - 2\varepsilon a_1 + \varepsilon^2(-2a_2 + 3a_1^2 - 2b_1\varphi_1 + \varphi_1^2),\\
&\varrho^2\partial_\alpha\varphi \approx \varepsilon\partial_\alpha\varphi_1 + \varepsilon^2(\partial_\alpha\varphi_2 - 2a_1\partial_\alpha\varphi_1)\\
&\qquad + \varepsilon^3(\partial_\alpha\varphi_3 - 2a_1\partial_\alpha\varphi_2 + (-2a_2 + 3a_1^2 - 2b_1\varphi_1 + \varphi_1^2)\partial_\alpha\varphi_1).
\end{aligned}
$$

Because $\beta^2 = \beta_0^2 - \sigma\varepsilon^2$, then $\beta^2\partial_t\varphi \approx \varepsilon\beta_0^2\partial_t\varphi_1 + \varepsilon^2\beta_0^2\partial_t\varphi_2 + \varepsilon^3\left(\beta_0^2\partial_t\varphi_3 - \sigma\partial_t\varphi_1\right)$, and

$$
\begin{aligned}
\beta^2\varrho^2\partial_\alpha\varphi \approx{}& \varepsilon\beta_0^2\partial_\alpha\varphi_1 + \varepsilon^2\beta_0^2(\partial_\alpha\varphi_2 - 2a_1\partial_\alpha\varphi_1)\\
&+ \varepsilon^3\left(\beta_0^2(\partial_\alpha\varphi_3 - 2a_1\partial_\alpha\varphi_2 + (-2a_2 + 2a_1^2 - 2b_1\varphi_1 + \varphi_1^2)\partial_\alpha\varphi_1) - \sigma\partial_\alpha\varphi_1\right).
\end{aligned}
$$

In the following paragraphs, we discuss up to the third ε-order equations of System (V.4.11).

$O(\varepsilon)$-equations of System (V.4.11)**.** We find that the lowest ε-order equations of System (V.4.11) are just the steady state equations for System (V.4.5)-(V.4.6):

$$
\begin{cases}
\partial_\alpha^2 a_1 = 0,\\
a_1 = 0, \quad \alpha = 0, 1,
\end{cases}
$$

and

$$
\begin{cases}
\partial_\alpha^2(\gamma b_1 - \varphi_1) = 0,\\
\beta_0^2\partial_\alpha^2\varphi_1 + b_1 - \varphi_1 = 0,\\
b_1 - \varphi_1 = \partial_\alpha\varphi_1 = 0, \qquad \alpha = 0, 1.
\end{cases}
$$

Again $a_1 = 0$ in the former, and the nontrivial solution of the latter is already computed in (V.4.8).

Adjoint equations for (b_1, φ_1). We consider the scalar product in $L^2(0,1)$,

$$
\left\langle (b_1, \varphi_1), (\hat{b}, \hat{\varphi})\right\rangle = \int_0^1 (b_1\hat{b} + \varphi_1\hat{\varphi})\,\mathrm{d}\alpha,
$$

and define a linear operator $\mathcal{L}_1$ by

$$
\mathcal{L}_1(b_1, \varphi_1) := \begin{pmatrix}\partial_\alpha^2(\gamma b_1 - \varphi_1)\\ \beta_0^2\partial_\alpha^2\varphi_1 + b_1 - \varphi_1\end{pmatrix}, \tag{V.4.12}
$$

with domain $\mathcal{D}(\mathcal{L}_1) := \{(b_1, \varphi_1) : b_1 - \varphi_1 = \partial_\alpha \varphi_1 = 0 \text{ for } \alpha = 0, 1\}$. Integration by parts yield

$$\begin{aligned}\left\langle \mathcal{L}_1(b_1, \varphi_1), (\hat{b}, \hat{\varphi}) \right\rangle &= \int_0^1 \left(\partial_\alpha^2(\gamma b_1 - \varphi_1)\right) \hat{b} + \left(\beta_0^2 \partial_\alpha^2 \varphi_1 + b_1 - \varphi_1\right) \hat{\varphi} \, \mathrm{d}\alpha \\ &= \left(\hat{b}\partial_\alpha(\gamma b_1 - \varphi_1) - \partial_\alpha \hat{b}(\gamma b_1 - \varphi_1) + \hat{\varphi}\beta_0^2 \partial_\alpha \varphi_1 - (\partial_\alpha \hat{\varphi})\beta_0^2 \varphi_1\right) \Big|_0^1 \\ &\quad + \int_0^1 \left((\gamma b_1 - \varphi_1)\partial_\alpha^2 \hat{b} + \beta_0^2 \varphi_1 \partial_\alpha^2 \hat{\varphi} + (b_1 - \varphi_1)\hat{\varphi}\right) \mathrm{d}\alpha.\end{aligned}$$

Rearranging and using the boundary conditions for (b_1, φ_1), we obtain

$$\begin{aligned}\left\langle \mathcal{L}_1(b_1, \varphi_1), (\hat{b}, \hat{\varphi}) \right\rangle &= \left(\hat{b}\partial_\alpha b_1 + \left((1-\gamma)\partial_\alpha \hat{b} - \beta_0^2 \partial_\alpha \hat{\varphi}\right) b_1\right) \Big|_0^1 \\ &\quad + \int_0^1 \left(\left(\gamma \partial_\alpha^2 \hat{b} + \hat{\varphi}\right) b_1 + \left(\beta_0^2 \partial_\alpha^2 \hat{\varphi} - \hat{\varphi} - \partial_\alpha^2 \hat{b}\right) \varphi_1\right) \mathrm{d}\alpha.\end{aligned}$$

From the computations above, we define the formal adjoint of $\mathcal{L}_1$ by

$$\mathcal{L}_1^*(\hat{b}, \hat{\varphi}) := \begin{pmatrix} \gamma \partial_\alpha^2 \hat{b} + \hat{\varphi} \\ \beta_0^2 \partial_\alpha^2 \hat{\varphi} - \hat{\varphi} - \partial_\alpha^2 \hat{b}, \end{pmatrix}$$

with domain $\mathcal{D}(\mathcal{L}_1^*) := \left\{\hat{b} = (1-\gamma)\partial_\alpha \hat{b} - \beta_0^2 \partial_\alpha \hat{\varphi} = 0, \text{ for } \alpha = 0, 1\right\}$. In particular, $(\hat{b}, \hat{\varphi})$ satisfies

$$\begin{cases} \gamma \partial_\alpha^2 \hat{b} + \hat{\varphi} = 0, & 0 < \alpha < 1, \\ \beta_0^2 \partial_\alpha^2 \hat{\varphi} - \hat{\varphi} - \partial_\alpha^2 \hat{b} = 0, & 0 < \alpha < 1, \\ \hat{b} = (1-\gamma)\partial_\alpha \hat{b} - \beta_0^2 \partial_\alpha \hat{\varphi} = 0, & \alpha = 0, 1. \end{cases} \tag{V.4.13}$$

Substituting the first equation to the second gives

$$\partial_\alpha^2 \hat{\varphi} = -\frac{(1-\gamma)}{\gamma \beta_0^2} \, \hat{\varphi} = -4\pi^2 \hat{\varphi}.$$

Solutions to the adjoint system (V.4.13)**.** With $\hat{\mathbf{X}} := (\hat{b}, \hat{\varphi})^\top$, we write (V.4.13) in a compact form:

$$\hat{\mathbf{X}}''(\alpha) = \hat{M}\hat{\mathbf{X}}(\alpha), \qquad \hat{M} := \begin{pmatrix} 0 & -1/\gamma \\ 0 & -4\pi^2 \end{pmatrix}. \tag{V.4.14}$$

The eigenvalues and corresponding eigenvectors of $\hat{M}$ are $\lambda_0 = 0$, $v_0 = (1, 0)^\top$, and $\lambda_1 = -4\pi^2$, $v_1 = (1, 4\pi^2\gamma)^\top$. Therefore, the solutions must be of the form

$$\hat{\mathbf{X}} = (\hat{A}\sin(2\pi\alpha) + \hat{B}\cos(2\pi\alpha)) \begin{pmatrix} 1 \\ 4\pi^2\gamma \end{pmatrix} + (\hat{C}\alpha + \hat{D}) \begin{pmatrix} 1 \\ 0 \end{pmatrix},$$

where $\hat{A}$, $\hat{B}$, $\hat{C}$, and $\hat{D}$ are arbitrary constants. With the boundary condition $\hat{b} = 0$ at $\alpha = 0, 1$, we find that $\hat{C} = 0$ and $\hat{D} = -\hat{B}$. The other boundary condition is always satisfied since $\beta_0^2 = (1-\gamma)/(4\pi^2\gamma)$. Hence $\hat{A}$ and $\hat{B}$ can be chosen arbitrarily. The space of nontrivial solutions is spanned by

$$\hat{\mathbf{X}} = (\hat{A}\sin(2\pi\alpha) + \hat{B}\cos(2\pi\alpha)) \begin{pmatrix} 1 \\ 4\pi^2\gamma \end{pmatrix} - \hat{B} \begin{pmatrix} 1 \\ 0 \end{pmatrix}.$$

Notice that inserting a different value $\beta \neq \beta_0$ yields $\hat{A} = 0$. These solutions correspond to those obtained from the rotational symmetry of the problem. Removing these states means that we take $\hat{B} = 0$. Moreover, we choose $\hat{A} = 1$ for simplicity, so that

$$\hat{\mathbf{X}} = \sin(2\pi\alpha) \begin{pmatrix} 1 \\ 4\pi^2\gamma \end{pmatrix}. \tag{V.4.15}$$

$O(\varepsilon^2)$-equations of System (V.4.11)**.** Now, let us look at the $O(\varepsilon^2)$-terms of (V.4.11). We have the system of equations

$$\begin{cases} \partial_\alpha^2 \left(a_2 + b_1\varphi_1 - a_1^2 - \frac{1}{2}\gamma b_1^2 \right) = 0, \\ a_2 + b_1\varphi_1 - a_1^2 - \frac{1}{2}\gamma b_1^2 = (1-\gamma)\varphi_1^2/2, \qquad \alpha = 0, 1, \end{cases}$$

and

$$\begin{cases} \partial_\alpha^2(\gamma b_2 - \varphi_2 - a_1(\gamma b_1 - \varphi_1)) = 0, \\ \beta_0^2\partial_\alpha^2\varphi_2 + b_2 - \varphi_2 - a_1 b_1 - 2\beta_0^2\partial_\alpha(a_1\partial_\alpha\varphi_1) = 0, \\ \gamma(b_2 - \varphi_2) - a_1(\gamma b_1 - \varphi_1) = \partial_\alpha\varphi_2 = 0, \qquad \alpha = 0, 1. \end{cases}$$

Since $a_1 = 0$, these reduce to

$$\begin{cases} \partial_\alpha^2 \left(a_2 + b_1\varphi_1 - \frac{1}{2}\gamma b_1^2 \right) = 0, \\ a_2 + b_1\varphi_1 - \frac{1}{2}\gamma b_1^2 = \frac{1}{2}(1-\gamma)\varphi_1^2, \qquad \alpha = 0, 1, \end{cases} \tag{V.4.16}$$

and

$$\begin{cases} \partial_\alpha^2(\gamma b_2 - \varphi_2) = 0, \\ \beta_0^2\partial_\alpha^2\varphi_2 + b_2 - \varphi_2 = 0, \\ b_2 - \varphi_2 = \partial_\alpha\varphi_2 = 0, \qquad \alpha = 0, 1. \end{cases}$$

The second system has already been solved. Moreover, it tells us that $\mathcal{L}_1(b_2, \varphi_2) = 0$, with $\mathcal{L}_1$ defined in (V.4.12). On the other hand, solving for a_2 in (V.4.16), one has

$$a_2 = -b_1\varphi_1 + \frac{\gamma}{2}b_1^2 + \frac{1-\gamma}{2}\left(\varphi_1^2(1) - \varphi_1^2(0)\right)\alpha + \frac{1-\gamma}{2}\,\varphi_1^2(0).$$

Note that $\varphi_1(0) = 0$ and $\varphi_1(1) = -2\pi A$. Hence

$$a_2 = -b_1\varphi_1 + \frac{\gamma}{2}b_1^2 + 2\pi^2(1-\gamma)A^2\alpha. \tag{V.4.17}$$

$O(\varepsilon^3)$-equations of System (V.4.11)**.** Finally, we look at the $O(\varepsilon^3)$-terms of (V.4.11), namely,

$$\begin{cases} \partial_t a_1 = \partial_\alpha^2 \left(a_3 - 2a_1a_2 + b_1\varphi_2 + b_2\varphi_1 - 2a_1b_1\varphi_1 + a_1^3 - \gamma b_1 b_2 + \gamma a_1 b_1^2 \right), \\ a_3 - 2a_1a_2 + b_1\varphi_2 + b_2\varphi_1 - 2a_1b_1\varphi_1 + a_1^3 - \gamma b_1 b_2 + \gamma a_1 b_1^2 = (1-\gamma)\varphi_1\varphi_2, \qquad \alpha = 0, 1, \end{cases}$$

and

$$\begin{cases} \partial_t b_1 = \partial_\alpha^2 \left(\gamma b_3 - \varphi_3 - a_1(\gamma b_2 - \varphi_2) + (a_1^2 - a_2)(\gamma b_1 - \varphi_1) + b_1\varphi_1^2 - \frac{1}{3}\varphi_1^3 - \frac{1}{2}\gamma b_1^3 \right), \\ \beta_0^2 \partial_t \varphi_1 = \beta_0^2 \partial_\alpha^2 \varphi_3 + b_3 - \varphi_3 - a_1 b_2 - a_2 b_1 + a_1^2 b_1 + b_1\varphi_1^2 - b_1^2\varphi_1 - \frac{1}{3}\varphi_1^3 - \sigma\partial_\alpha^2\varphi_1 \\ \qquad\qquad + \beta_0^2 \left(-2\partial_\alpha(a_1\partial_\alpha\varphi_2) + \partial_\alpha((-2a_2 + 3a_1^2 - 2b_1\varphi_1 + \varphi_1^2)\partial_\alpha\varphi_1) \right) \\ \gamma(b_3 - \varphi_3) - a_1(\gamma b_2 - \varphi_2) + (a_1^2 - a_2)(\gamma b_1 - \varphi_1) + b_1\varphi_1^2 - \frac{1}{3}\varphi_1^3 - \frac{1}{2}\gamma b_1^3 = \frac{1}{6}(1-\gamma)\varphi_1^3, \\ \partial_\alpha \varphi_3 = 0, \qquad \alpha = 0, 1. \end{cases} \tag{V.4.18}$$

Since $a_1 = 0$, we have

$$\begin{cases} \partial_\alpha^2 \left(a_3 + b_1\varphi_2 + b_2\varphi_1 - \gamma b_1 b_2 \right) = 0, \\ a_3 + b_1\varphi_2 + b_2\varphi_1 - \gamma b_1 b_2 = (1-\gamma)\varphi_1\varphi_2, \qquad \alpha = 0, 1. \end{cases}$$

Therefore, we find

$$a_3(\alpha) = -b_1\varphi_2 - b_2\varphi_1 + \gamma b_1 b_2 + (1-\gamma)\left[(\varphi_1(1)\varphi_2(1) - \varphi_1(0)\varphi_2(0))\,\alpha + \varphi_1(0)\varphi_2(0) \right].$$

Again setting $a_1 = 0$ in (V.4.18), one has

$$\begin{cases} \partial_t b_1 = \partial_\alpha^2 \left(\gamma b_3 - \varphi_3 - a_2(\gamma b_1 - \varphi_1) + b_1\varphi_1^2 - \frac{1}{3}\varphi_1^3 - \frac{1}{2}\gamma b_1^3 \right), \\ \beta_0^2 \partial_t \varphi_1 = \beta_0^2 \partial_\alpha^2 \varphi_3 + b_3 - \varphi_3 - a_2 b_1 + b_1\varphi_1^2 - b_1^2\varphi_1 - \frac{1}{3}\varphi_1^3 - \sigma\partial_\alpha^2\varphi_1 \\ \qquad\qquad + \beta_0^2 \partial_\alpha((-2a_2 - 2b_1\varphi_1 + \varphi_1^2)\partial_\alpha\varphi_1) \\ \gamma(b_3 - \varphi_3) - a_2(\gamma b_1 - \varphi_1) + b_1\varphi_1^2 - \frac{1}{3}\varphi_1^3 - \frac{\gamma}{2} b_1^3 = \frac{1}{6}(1-\gamma)\varphi_1^3, \\ \partial_\alpha \varphi_3 = 0, \qquad \alpha = 0, 1. \end{cases} \tag{V.4.19}$$

Derivation of an equation for $A(t)$. With the goal of finding A, we take the scalar product of $(\partial_t b_1, \beta_0^2 \partial_t \varphi_1)$ in (V.4.19) with $(\hat{b}, \hat{\varphi})$. We arrive to the equation

$$\left\langle (\partial_t b_1, \beta_0^2 \partial_t \varphi_1), (\hat{b}, \hat{\varphi}) \right\rangle = \left\langle \mathcal{L}_3(b_3, \varphi_3), (\hat{b}, \hat{\varphi}) \right\rangle, \tag{V.4.20}$$

where

$$\mathcal{L}_3(b_3, \varphi_3) := \left(\partial_\alpha^2 \left(\gamma b_3 - \varphi_3 - a_2(\gamma b_1 - \varphi_1) + b_1\varphi_1^2 - \frac{1}{3}\varphi_1^3 - \frac{1}{2}\gamma b_1^3 \right), \right.$$

$$\left. \beta_0^2 \partial_\alpha^2 \varphi_3 + b_3 - \varphi_3 - a_2 b_1 + b_1\varphi_1^2 - b_1^2\varphi_1 - \frac{1}{3}\varphi_1^3 - \sigma\partial_\alpha^2\varphi_1 + \beta_0^2 \partial_\alpha((-2a_2 - 2b_1\varphi_1 + \varphi_1^2)\partial_\alpha\varphi_1) \right),$$

with domain

$$\mathcal{D}(\mathcal{L}_3) := \Big\{(b_3,\varphi_3) : \gamma(b_3-\varphi_3) - a_2(\gamma b_1-\varphi_1) + b_1\varphi_1^2 - \frac{1}{3}\varphi_1^3 - \frac{1}{2}\gamma b_1^3 - \frac{1}{6}(1-\gamma)\varphi_1^3 = 0 \\ \text{and } \partial_\alpha\varphi_3 = 0, \text{ for } \alpha = 0,1\Big\}.$$

We remember that the values of (b_1,φ_1) and $(\hat{b},\hat{\varphi})$ are already computed in (V.4.8) and (V.4.15), respectively. These are used to expand the left-hand side of (V.4.20):

$$\begin{aligned}
&\int_0^1 \Big((\partial_t b_1)\hat{b} + \beta_0^2(\partial_t\varphi_1)\hat{\varphi}\Big)\,\mathrm{d}\alpha \\
&= \dot{A}(t)\int_0^1 \Big((\sin(2\pi\alpha) - 2\pi\gamma\alpha) + 4\pi^2\gamma^2\beta_0^2\,(\sin(2\pi\alpha) - 2\pi\alpha)\Big)\sin(2\pi\alpha)\,\mathrm{d}\alpha \\
&= \dot{A}(t)\int_0^1 \Big(\Big(1+4\pi^2\gamma^2\beta_0^2\Big)\sin^2(2\pi\alpha) - 2\pi\gamma\Big(1+4\pi^2\gamma\beta_0^2\Big)\,\alpha\sin(2\pi\alpha)\Big)\,\mathrm{d}\alpha.
\end{aligned}$$

From the relations $1+4\pi^2\gamma^2\beta_0^2 = 1+\gamma-\gamma^2$ and $1+4\pi^2\gamma\beta_0^2 = 2-\gamma$, and the integrals

$$\int_0^1 \sin^2(2\pi\alpha)\,\mathrm{d}\alpha = \frac{1}{2} \quad \text{and} \quad \int_0^1 \alpha\sin(2\pi\alpha)\,\mathrm{d}\alpha = -\frac{1}{2\pi},$$

the left-hand side of Equation (V.4.20) becomes

$$\Big\langle(\partial_t b_1, \beta_0^2\partial_t\varphi_1), (\hat{b},\hat{\varphi})\Big\rangle = \frac{1}{2}\dot{A}(t)(1+5\gamma-3\gamma^2). \tag{V.4.21}$$

Now let us focus on the right-hand side of Equation (V.4.20) which requires a longer computation. It reads

$$\begin{aligned}
\Big\langle\mathcal{L}_3(b_3,\varphi_3), (\hat{b},\hat{\varphi})\Big\rangle = \int_0^1 \Bigg(&\partial_\alpha^2\left(\gamma b_3 - \varphi_3 - a_2(\gamma b_1-\varphi_1) + b_1\varphi_1^2 - \frac{1}{3}\varphi_1^3 - \frac{1}{2}\gamma b_1^3\right)\hat{b} \\
&+ \Big(\beta_0^2\partial_\alpha^2\varphi_3 + b_3 - \varphi_3 - a_2 b_1 + b_1\varphi_1^2 - b_1^2\varphi_1 - \frac{1}{3}\varphi_1^3 - \sigma\partial_\alpha^2\varphi_1 \\
&- \beta_0^2\partial_\alpha((2a_2 + 2b_1\varphi_1 - \varphi_1^2)\partial_\alpha\varphi_1)\Big)\hat{\varphi}\Bigg)\,\mathrm{d}\alpha,
\end{aligned} \tag{V.4.22}$$

which, after integration by parts, becomes

$$\begin{aligned}
&\Big(\hat{b}\,\partial_\alpha\Big(\gamma b_3-\varphi_3-a_2(\gamma b_1-\varphi_1)+b_1\varphi_1^2-\frac{1}{3}\varphi_1^3-\frac{1}{2}\gamma b_1^3\Big)\\
&-\partial_\alpha\hat{b}\Big(\gamma b_3-\varphi_3-a_2(\gamma b_1-\varphi_1)+b_1\varphi_1^2-\frac{1}{3}\varphi_1^3-\frac{1}{2}\gamma b_1^3\Big)+\beta_0^2\hat{\varphi}\,\partial_\alpha\varphi_3-\beta_0^2(\partial_\alpha\hat{\varphi})\varphi_3\\
&-\sigma\hat{\varphi}\,\partial_\alpha\varphi_1+\sigma(\partial_\alpha\hat{\varphi})\varphi_1-\beta_0^2\hat{\varphi}\,(2a_2+2b_1\varphi_1-\varphi_1^2)\partial_\alpha\varphi_1\Big)\Big|_0^1\\
&+\int_0^1\Big(\Big(\gamma b_3-\varphi_3-a_2(\gamma b_1-\varphi_1)+b_1\varphi_1^2-\frac{1}{3}\varphi_1^3-\frac{1}{2}\gamma b_1^3\Big)\partial_\alpha^2\hat{b}+(\beta_0^2\varphi_3-\sigma\varphi_1)\partial_\alpha^2\hat{\varphi}\\
&\quad+\Big(b_3-\varphi_3-a_2b_1+b_1\varphi_1^2-b_1^2\varphi_1-\frac{1}{3}\varphi_1^3\Big)\hat{\varphi}+\beta_0^2(2a_2+2b_1\varphi_1-\varphi_1^2)(\partial_\alpha\varphi_1)\partial_\alpha\hat{\varphi}\Big)\,\mathrm{d}\alpha. \qquad \text{(V.4.23)}
\end{aligned}$$

From (V.4.13), we know that $\hat{b}=0$ at $\alpha=0,1$, so the first line above vanishes. The boundary conditions for (b_3,φ_3) in (V.4.19) allows us to write the second line as

$$\begin{aligned}
\Big((1-\gamma)\partial_\alpha\hat{b}\Big(\varphi_3-\frac{1}{6}\varphi_1^3\Big)-\beta_0^2(\partial_\alpha\hat{\varphi})\varphi_3\Big)\Big|_0^1&=\Big(\Big((1-\gamma)\partial_\alpha\hat{b}-\beta_0^2\partial_\alpha\hat{\varphi}\Big)\varphi_3-\frac{1}{6}(1-\gamma)(\partial_\alpha\hat{b})\varphi_1^3\Big)\Big|_0^1\\
&=-\frac{1}{6}(1-\gamma)(\partial_\alpha\hat{b})\varphi_1^3\Big|_0^1=-\frac{1}{6}\beta_0^2(\partial_\alpha\hat{\varphi})\varphi_1^3\Big|_0^1, \qquad \text{(V.4.24)}
\end{aligned}$$

where the last line follows from the boundary condition $(1-\gamma)\partial_\alpha\hat{b}-\beta_0^2\partial_\alpha\hat{\varphi}=0$ at $\alpha=0,1$, for the adjoint system (V.4.13). Since $\partial_\alpha\varphi_1=0$ at $\alpha=0,1$, then the third line in (V.4.23) reduces to

$$\sigma(\partial_\alpha\hat{\varphi})\varphi_1\Big|_0^1. \qquad \text{(V.4.25)}$$

This ends the computations for the boundary terms in (V.4.23).

We now focus on the integral in (V.4.23). Rearranging the terms in the integrand, one has

$$\begin{aligned}
&\int_0^1\Big((b_3-a_2b_1)(\gamma\partial_\alpha^2\hat{b}+\hat{\varphi})+\varphi_3(-\partial_\alpha^2\hat{b}+\beta_0^2\partial_\alpha^2\hat{\varphi}-\hat{\varphi})+\Big(b_1\varphi_1^2-\frac{1}{3}\varphi_1^3\Big)(\partial_\alpha^2\hat{b}+\hat{\varphi})\\
&\quad+\Big(a_2\varphi_1-\frac{1}{2}\gamma b_1^3\Big)\partial_\alpha^2\hat{b}-\sigma\varphi_1\partial_\alpha^2\hat{\varphi}-b_1^2\varphi_1\hat{\varphi}+\beta_0^2(2a_2+2b_1\varphi_1-\varphi_1^2)(\partial_\alpha\varphi_1)\partial_\alpha\hat{\varphi}\Big)\,\mathrm{d}\alpha. \qquad \text{(V.4.26)}
\end{aligned}$$

The first two terms inside the integral vanish from the $(\hat{b},\hat{\varphi})$-equation. We integrate the last term by parts and rearrange the terms to write (V.4.26) into

$$\begin{aligned}
&\beta_0^2\varphi_1(2a_2+2b_1\varphi_1-\varphi_1^2)\partial_\alpha\hat{\varphi}\Big|_0^1+\int_0^1\Big(\Big(b_1\varphi_1^2-\frac{1}{3}\varphi_1^3\Big)(\partial_\alpha^2\hat{b}+\hat{\varphi}-\beta_0^2\partial_\alpha^2\hat{\varphi})\\
&-\beta_0^2\Big(b_1\varphi_1^2-\frac{2}{3}\varphi_1^3+\sigma\varphi_1+2a_2\varphi_1\Big)\partial_\alpha^2\hat{\varphi}+\Big(a_2\varphi_1-\frac{1}{2}\gamma b_1^3\Big)\partial_\alpha^2\hat{b}-b_1^2\varphi_1\hat{\varphi}\\
&-\beta_0^2\varphi_1\partial_\alpha(2a_2+2b_1\varphi_1-\varphi_1^2)\partial_\alpha\hat{\varphi}\Big)\,\mathrm{d}\alpha.
\end{aligned}$$

The first term inside the integral above is zero from $(\hat{b},\hat{\varphi})$-equation. Another integration by parts gets rid of the boundary terms and gives us

$$\int_0^1 \Big(-\beta_0^2(b_1\varphi_1^2 - 2\varphi_1^3/3 + \sigma\varphi_1 + 2a_2\varphi_1)\partial_\alpha^2\hat{\varphi} + (a_2\varphi_1 - \gamma b_1^3/2)\partial_\alpha^2\hat{b} - b_1^2\varphi_1\hat{\varphi} \\ + \beta_0^2(2a_2 + 2b_1\varphi_1 - \varphi_1^2)(\partial_\alpha\varphi_1)\partial_\alpha\hat{\varphi} + \beta_0^2(2a_2 + 2b_1\varphi_1 - \varphi_1^2)\varphi_1\partial_\alpha^2\hat{\varphi}\Big)\,\mathrm{d}\alpha.$$

Combining like terms and using $\partial_\alpha^2\hat{b} = -(1/\gamma)\hat{\varphi}$, we have

$$\int_0^1 \Big((\beta_0^2 b_1\varphi_1^2 - \beta_0^2\varphi_1^3/3 - \sigma\varphi_1)\partial_\alpha^2\hat{\varphi} + \beta_0^2(2a_2 + 2b_1\varphi_1 - \varphi_1^2)(\partial_\alpha\varphi_1)\partial_\alpha\hat{\varphi} \\ + ((b_1^3/2) - (1/\gamma)a_2\varphi_1 - b_1^2\varphi_1)\hat{\varphi}\Big)\,\mathrm{d}\alpha.$$

This is now added to (V.4.24) and (V.4.25), so that the right-hand side of (V.4.20) becomes

$$\Big\langle \mathcal{L}_3(b_3,\varphi_3),(\hat{b},\hat{\varphi})\Big\rangle = \left(\sigma\varphi_1 - \frac{\beta_0^2}{6}\varphi_1^3\right)\partial_\alpha\hat{\varphi}\Big|_0^1 + \int_0^1 \left(\left(\beta_0^2 b_1\varphi_1^2 - \frac{1}{3}\beta_0^2\varphi_1^3 - \sigma\varphi_1\right)\partial_\alpha^2\hat{\varphi} \right. \\ \left. + \beta_0^2(2a_2 + 2b_1\varphi_1 - \varphi_1^2)(\partial_\alpha\varphi_1)\partial_\alpha\hat{\varphi} + \left(\frac{1}{2}b_1^3 - \frac{1}{\gamma}a_2\varphi_1 - b_1^2\varphi_1\right)\hat{\varphi}\right)\mathrm{d}\alpha. \tag{V.4.27}$$

Again we recall the values of (b_1,φ_1) and the bifurcation point β_0 in (V.4.8) and (V.4.9), respectively, and insert them in the equation above. First, the boundary terms are expanded:

$$\left(\sigma\varphi_1 - \frac{1}{6}\beta_0^2\varphi_1^3\right)\partial_\alpha\hat{\varphi}\Big|_0^1 = 8\pi^3\gamma\left(\sigma\gamma A(\sin(2\pi\alpha) - 2\pi\alpha) - \frac{1}{6}\beta_0^2\gamma^3A^3(\sin(2\pi\alpha) - 2\pi\gamma\alpha)^3\right)\cos(2\pi\alpha)\Big|_0^1$$

$$= -16\pi^4\gamma^2\left(\sigma A - \frac{2}{3}\pi^2\gamma^2\beta_0^2A^3\right) = -16\pi^4\gamma^2\sigma A + \frac{8}{3}\pi^4\gamma^3(1-\gamma)A^3. \tag{V.4.28}$$

Second, the terms inside the integral in (V.4.27) are considered one-by-one. The first term is computed as

$$\int_0^1 \left(\beta_0^2 b_1\varphi_1^2 - \beta_0^2\frac{1}{3}\varphi_1^3 - \sigma\varphi_1\right)\partial_\alpha^2\hat{\varphi}\,\mathrm{d}\alpha = -16\pi^4\gamma\int_0^1\left(\beta_0^2\left(b_1 - \frac{1}{3}\varphi_1\right)\varphi_1^2 - \sigma\varphi_1\right)\sin(2\pi\alpha)\,\mathrm{d}\alpha. \tag{V.4.29}$$

The computations

$$\beta_0^2\int_0^1\left(b_1 - \frac{1}{3}\varphi_1\right)\varphi_1^2\sin(2\pi\alpha)\,\mathrm{d}\alpha \\ = \beta_0^2\gamma^2A^3\int_0^1\left(\left(1 - \frac{1}{3}\gamma\right)\sin^2(2\pi\alpha) - \frac{4}{3}\pi\gamma\alpha\sin(2\pi\alpha)\right)(\sin(2\pi\alpha) - 2\pi\alpha)^2\,\mathrm{d}\alpha \\ = \beta_0^2\gamma^2A^3\int_0^1\left(\left(1 - \frac{1}{3}\gamma\right)\sin^4(2\pi\alpha) - 4\pi\alpha\sin^3(2\pi\alpha) + 4\pi^2(1+\gamma)\alpha^2\sin^2(2\pi\alpha)\right. \\ \left. - \frac{16}{3}\pi^3\gamma\alpha^3\sin(2\pi\alpha)\right)\mathrm{d}\alpha = \beta_0^2\gamma^2A^3\left(\frac{2}{3}\pi^2 + \frac{35}{24} + \left(\frac{10}{3}\pi^2 - \frac{35}{8}\right)\gamma\right),$$

and

$$\sigma \int_0^1 \varphi_1 \sin(2\pi\alpha)\,\mathrm{d}\alpha = \sigma\gamma A \int_0^1 \Big(\sin^2(2\pi\alpha) - 2\pi\alpha\sin(2\pi\alpha)\Big)\,\mathrm{d}\alpha = \frac{3}{2}\gamma\sigma A,$$

allow us to write (V.4.29) into

$$-16\pi^4\gamma^3\beta_0^2\left(\frac{2}{3}\pi^2 + \frac{35}{24} + \left(\frac{10}{3}\pi^2 - \frac{35}{8}\right)\gamma\right)A^3 + 24\pi^4\gamma^2\sigma A. \tag{V.4.30}$$

For the second term inside the integral in (V.4.27), we recall (V.4.17). In particular, one has $2a_2 = -2b_1\varphi_1 + \gamma b_1^2 + 4\pi^2(1-\gamma)A^2\alpha$, and so

$$\begin{aligned}
&\int_0^1 \beta_0^2(2a_2 + 2b_1\varphi_1 - \varphi_1^2)(\partial_\alpha\varphi_1)\partial_\alpha\hat{\varphi}\,\mathrm{d}\alpha \\
&= 16\pi^4\gamma^2\beta_0^2 A\int_0^1 \Big(\gamma b_1^2 + 4\pi^2(1-\gamma)A^2\alpha - \varphi_1^2\Big)\Big(\cos^2(2\pi\alpha) - \cos(2\pi\alpha)\Big)\,\mathrm{d}\alpha \\
&= 16\pi^4\gamma^2(1-\gamma)\beta_0^2 A^3\int_0^1 \Big(\gamma\sin^2(2\pi\alpha) - 4\pi^2\gamma^2\alpha^2 + 4\pi^2\alpha\Big)\Big(\cos^2(2\pi\alpha) - \cos(2\pi\alpha)\Big)\,\mathrm{d}\alpha \\
&= 16\pi^4\gamma^2(1-\gamma)\beta_0^2\left(\pi^2 + \frac{1}{8}\gamma + \left(-\frac{2}{3}\pi^2 + \frac{9}{4}\right)\gamma^2\right)A^3.
\end{aligned} \tag{V.4.31}$$

Finally, the last term inside the integral in (V.4.27) is computed:

$$\begin{aligned}
&\int_0^1 \left(\frac{1}{2}b_1^3 - \frac{1}{\gamma}a_2\varphi_1 - b_1^2\varphi_1\right)\hat{\varphi}\,\mathrm{d}\alpha \\
&= 4\pi^2\gamma\int_0^1 \left(\frac{b_1^3}{2} + \frac{1}{\gamma}b_1\varphi_1^2 - \frac{3}{2}b_1^2\varphi_1 - \frac{2}{\gamma}\pi^2(1-\gamma)A^2\varphi_1\alpha\right)\sin(2\pi\alpha)\,\mathrm{d}\alpha,
\end{aligned}$$

which follows from $-(1/\gamma)a_2\varphi_1 = (1/\gamma)b_1\varphi_1^2 - (1/2)b_1^2\varphi_1 - (2\pi^2/\gamma)(1-\gamma)A^2\varphi_1\alpha$. We shall need the computations

$$\begin{aligned}
-\frac{2}{\gamma}\pi^2(1-\gamma)A^2\int_0^1 \varphi_1\alpha\sin(2\pi\alpha)\,\mathrm{d}\alpha &= -2\pi^2(1-\gamma)A^3\int_0^1 \Big(\alpha\sin^2(2\pi\alpha) - 2\pi\alpha^2\sin(2\pi\alpha)\Big)\,\mathrm{d}\alpha \\
&= -\frac{5}{2}\pi^2(1-\gamma)A^3
\end{aligned}$$

and

$$\begin{aligned}
&\int_0^1 \left(\frac{b_1^2}{2} + \frac{1}{\gamma}\varphi_1^2 - \frac{3}{2}b_1\varphi_1\right)b_1\sin(2\pi\alpha)\,\mathrm{d}\alpha \\
&= (1-\gamma)A^3\int_0^1 \left(\frac{1}{2}\sin^2(2\pi\alpha) - 3\pi\gamma\alpha\sin(2\pi\alpha) + 4\pi^2\gamma\alpha^2\right)(\sin(2\pi\alpha) - 2\pi\gamma\alpha)\sin(2\pi\alpha)\,\mathrm{d}\alpha \\
&= (1-\gamma)A^3\left(\frac{3}{16} + \left(\frac{2}{3}\pi^2 + \frac{13}{12}\right)\gamma + \left(5\pi^2 - \frac{51}{8}\right)\gamma^2\right),
\end{aligned}$$

to arrive at the relation

$$\int_0^1 \left(\frac{b_1^3}{2} - \frac{a_2\varphi_1}{\gamma} - b_1^2\varphi_1\right)\hat{\varphi}\,\mathrm{d}\alpha = 4\pi^2\gamma(1-\gamma)\left(-\frac{5}{2}\pi^2 + \frac{3}{16} + \left(\frac{2}{3}\pi^2 + \frac{13}{12}\right)\gamma + \left(5\pi^2 - \frac{51}{8}\right)\gamma^2\right)A^3. \tag{V.4.32}$$

In summary, the right-hand side of (V.4.27) can be written more explicitly with the help of computations (V.4.28), (V.4.30), (V.4.31) and (V.4.32). The following paragraphs use the resulting explicit equations to solve for $A(t)$.

Dynamic normal form reduction. The expansion of Equation (V.4.20) from the preceding computations yields an ODE for $A(t)$. Indeed, equating (V.4.21) to the sum of (V.4.28), (V.4.30), (V.4.31) and (V.4.32), one obtains

$$\frac{\mathrm{d}A}{\mathrm{d}t} = A\left(\kappa_1\sigma - \kappa_2 A^2\right), \tag{V.4.33}$$

with the positive constants $(0 < \gamma < 1)$

$$\kappa_1 := \frac{16\pi^4\gamma^2}{1+5\gamma-3\gamma^2}, \quad \kappa_2 := \frac{8\pi^2\gamma(1-\gamma)}{1+5\gamma-3\gamma^2}\,\kappa_3,$$
$$\kappa_3 := \frac{3}{2}\pi^2 - \frac{3}{16} + \left(\pi^2 - \frac{1}{4}\right)\gamma - \left(\frac{5}{3}\pi^2 + \frac{1}{8}\right)\gamma^2 - \left(\frac{2}{3}\pi^2 - \frac{9}{4}\right)\gamma^3.$$

Equation (V.4.33) is the normal form of the pitchfork bifurcation. In particular, it is an indication that for $\sigma := \operatorname{sign}(\beta_0^2 - \beta^2) < 0$ the trivial steady state is stable, whereas for $\sigma > 0$, stability is transferred to the bifurcating steady states

$$\partial_\alpha \mathbf{z} = \begin{pmatrix}1\\0\end{pmatrix} \pm \sqrt{\frac{\kappa_1}{\kappa_2}}\,\varepsilon\begin{pmatrix}0\\ \sin(2\pi\alpha) - 2\pi\gamma\alpha\end{pmatrix}, \tag{V.4.34}$$

$$\varphi = \frac{\pi}{2} \pm \sqrt{\frac{\kappa_1}{\kappa_2}}\,\varepsilon\gamma(\sin(2\pi\alpha) - 2\pi\alpha), \tag{V.4.35}$$

where we recall that $\varepsilon := \sqrt{\left|\beta_0^2 - \beta^2\right|}$.

Illustration of trivial and nontrivial equilibria. We close this section with a plot of filament configurations in trivial side-by-side with the nontrivial equilibrium. Figure V.3 depicts two strips, each with 50 short filaments. The trivial steady state (V.4.4) is portrayed as a strip with red filaments (on the left), while the nontrivial one (V.4.34) is the strip with blue filaments (on the right). In the figure however, the filaments are scaled $(0.1 \times L)$ to get a better view of the shape of the center-of-mass curve and direction angles of the nontrivial equilibrium.

An inset plot of the nontrivial filament directions is also included to emphasize that filaments are not parallel. The parameter values we used are summarized in Table V.1. As a result of our choice for values, the dimensionless parameters in (V.4.2) become $\beta = 0.0693$ and $\gamma = 0.2500$. The bifurcation point is then $\beta_0 = 0.2757$.

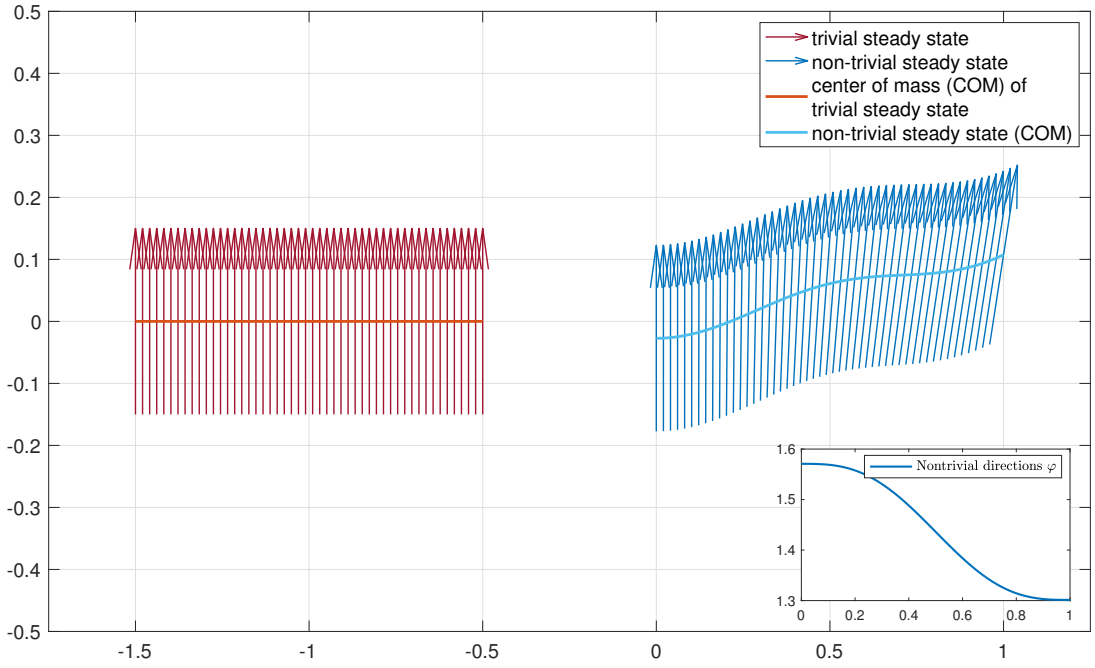

Figure V.3: Equilibrium configurations for filament strip. The trivial equilibrium corresponds to the red filament strip and the nontrivial to the blue filament strip. Filaments are scaled to $0.1L$ for a better view of the nontrivial shape and directions. The onset figure on the lower right depicts the nontrivial equilibrium directions, where filaments are almost parallel.

Var.	Meaning	Value	Reference/Comment
μ^A	macroscopic friction caused by adhesions	0.41 pN min μm^{-2}	[Man+17], estimations and calculations in [OSS08], [OS10a], [OS10b]
L	filament length	3 μm	half of length considered in [OSS08]
μ^K	center-of-mass curve tension	0.1 pN / μm	
f	magnitude of external force	0.3 pN / μm	
μ^P	pressure constant	5.0 pN	

Table V.1: Parameter values for Figure V.3

Chapter VI

Evolution equations for filament density

Contents

This short chapter supplements the results of Chapter V. In the first section, a system of equations for the interaction of the filament density

$$\varrho := \varrho[\partial_\alpha \mathbf{z}, \varphi] = \frac{1}{\partial_\alpha \mathbf{z}^\perp \cdot \boldsymbol{\omega}(\varphi)} \tag{VI.1}$$

and filament direction φ is derived from the model for rigid filaments with pressure. In Section VI.2, a coordinate change is carried out, which is similar to the transformation performed in the 1D model in Section V.1. We conclude this chapter with a numerical implementation in Section VI.3 of special solutions to the density model.

VI.1 Model derivation

Starting from System (V.3.5)-(V.3.6), we derive equations for the filament density ϱ in (VI.1) and direction φ. For simplicity, the polymerization speed v is set to zero. To motivate the computations below, let us consider the Fourier expansion of the curve $\partial_\alpha \mathbf{z}$ (c.f. (II.1.1));

$$\partial_\alpha \mathbf{z} = \Pi_{\boldsymbol{\omega}} \partial_\alpha \mathbf{z} + \Pi_{\boldsymbol{\omega}^\perp} \partial_\alpha \mathbf{z} = (\partial_\alpha \mathbf{z} \cdot \boldsymbol{\omega})\boldsymbol{\omega} - (\partial_\alpha \mathbf{z}^\perp \cdot \boldsymbol{\omega})\boldsymbol{\omega}^\perp, \tag{VI.1.1}$$

which decomposes $\partial_\alpha \mathbf{z}$ into its components in the directions $\boldsymbol{\omega}$ and $\boldsymbol{\omega}^\perp$. Introducing the notation

$$r := r(\partial_\alpha \mathbf{z}, \varphi) = \partial_\alpha \mathbf{z} \cdot \boldsymbol{\omega}(\varphi)$$

and using ϱ in (VI.1), Equation (VI.1.1) becomes

$$\partial_\alpha \mathbf{z} = r\boldsymbol{\omega} - \frac{1}{\varrho}\boldsymbol{\omega}^\perp. \tag{VI.1.2}$$

Evolution equations for the curve $\partial_\alpha \mathbf{z}$ shall therefore help us find equations for r, ϱ, and φ. In fact, we have already seen the decomposition (VI.1.2) in the previous chapter, but with $r = 0$, constant ϱ and constant φ. The latter are equilibrium states for rigid filaments with pressure in Equation (V.3.9) and rigid filaments with pressure and tension in Equation (V.4.4).

Derivation of equations for ϱ and r. Our goal is to derive the evolution of ϱ and r from System (V.3.5)-(V.3.6). The derivative of its first equation with respect to α is

$$\mu^A \partial_t(\partial_\alpha \mathbf{z}) = \mu^P \left((\partial_\alpha^2 \varrho)\boldsymbol{\omega}^\perp - 2(\partial_\alpha \varrho)(\partial_\alpha \varphi)\boldsymbol{\omega} - \varrho(\partial_\alpha^2 \varphi)\boldsymbol{\omega} - \varrho(\partial_\alpha \varphi)^2 \boldsymbol{\omega}^\perp \right),$$

where sufficient smoothness for $\mathbf{z}$ is assumed so that $\partial_\alpha(\partial_t \mathbf{z}) = \partial_t(\partial_\alpha \mathbf{z})$. Taking the orthogonal complements of both sides of the equation above, one has

$$\mu^A \partial_t(\partial_\alpha \mathbf{z}^\perp) = \mu^P \left(-(\partial_\alpha^2 \varrho)\boldsymbol{\omega} - 2(\partial_\alpha \varrho)(\partial_\alpha \varphi)\boldsymbol{\omega}^\perp - \varrho(\partial_\alpha^2 \varphi)\boldsymbol{\omega}^\perp + \varrho(\partial_\alpha \varphi)^2 \boldsymbol{\omega} \right). \tag{VI.1.3}$$

Then, scalar multiplication of (VI.1.3) with $\boldsymbol{\omega}$ and the relation $\partial_t(\partial_\alpha \mathbf{z}^\perp \cdot \boldsymbol{\omega}) = \partial_t(\partial_\alpha \mathbf{z}^\perp) \cdot \boldsymbol{\omega} + \partial_\alpha \mathbf{z} \cdot \boldsymbol{\omega}\, \partial_t \varphi$ imply

$$\mu^A \left(\partial_t(\partial_\alpha \mathbf{z}^\perp \cdot \boldsymbol{\omega}) - \partial_\alpha \mathbf{z} \cdot \boldsymbol{\omega} \partial_t \varphi \right) = \mu^P \left(-\partial_\alpha^2 \varrho + \varrho(\partial_\alpha \varphi)^2 \right).$$

Notice that $\partial_t(\partial_\alpha \mathbf{z}^\perp \cdot \boldsymbol{\omega}) = \partial_t(1/\varrho) = -(1/\varrho^2)\partial_t \varrho$, hence, the equation above becomes

$$\mu^A \left(\partial_t \varrho + \varrho^2 r \partial_t \varphi \right) = \mu^P \varrho^2 \left(\partial_\alpha^2 \varrho - \varrho(\partial_\alpha \varphi)^2 \right). \tag{VI.1.4}$$

On the other hand, scalar multiplication of (VI.1.3) with $\boldsymbol{\omega}^\perp$ and the computation

$$\partial_t(\partial_\alpha \mathbf{z}^\perp) \cdot \boldsymbol{\omega}^\perp = \partial_t(\partial_\alpha \mathbf{z}) \cdot \boldsymbol{\omega} = \partial_t(\partial_\alpha \mathbf{z} \cdot \boldsymbol{\omega}) + \partial_\alpha \mathbf{z}^\perp \cdot \boldsymbol{\omega} \partial_t \varphi = \partial_t r + \frac{1}{\varrho} \partial_t \varphi$$

together give

$$\mu^A \left(\partial_t r + \left(\frac{1}{\varrho} \right) \partial_t \varphi \right) = -\mu^P \left(2(\partial_\alpha \varrho)\partial_\alpha \varphi + \varrho \partial_\alpha^2 \varphi \right), \tag{VI.1.5}$$

Collecting (VI.1.4) and (VI.1.5) with the last equation in (V.3.5) give rise to the nonlinear system

$$\begin{cases} \mu^A \left(\partial_t \varrho + \varrho^2 r \partial_t \varphi \right) = \mu^P \varrho^2 \left(\partial_\alpha^2 \varrho - \varrho(\partial_\alpha \varphi)^2 \right), \\ \mu^A \left(\partial_t r + \frac{1}{\varrho} \partial_t \varphi \right) = -\mu^P \left(2(\partial_\alpha \varrho)\partial_\alpha \varphi + \varrho \partial_\alpha^2 \varphi \right), \\ \mu^A \partial_t \varphi = \mu^P \varrho \left(\frac{12}{L^2} r + 2(\partial_\alpha \varrho)\partial_\alpha \varphi + \varrho \partial_\alpha^2 \varphi \right), \end{cases} \tag{VI.1.6}$$

subject to the boundary conditions (scalar multiplication of (V.3.6) with $\boldsymbol{\omega}^\perp$)

$$\begin{cases} \mu^P \varrho = f_{0,1}, & \alpha = 0, 1, \\ \mu^P \varrho^2 \partial_\alpha \varphi = 0, & \alpha = 0, 1. \end{cases} \tag{VI.1.7}$$

Equations (VI.1.6)-(VI.1.7) form a closed system for the unknowns ϱ, r, and φ. Notice that boundary conditions ($\alpha = 0, 1$) are only necessary for ϱ and φ since there are no α-derivatives of r.

Evolution equations for (ϱ, r, φ). The mixing of time derivatives of the unknowns in the first two equations of System (VI.1.6) is removed by inserting its third equation to the first and second ones. Rearranging the terms, explicit evolution equations for ϱ, r and φ are obtained:

$$\begin{cases} \mu^A \partial_t \varrho = \mu^P \varrho^2 \partial_\alpha^2 \varrho - \mu^P \varrho^3 \left((\partial_\alpha \varphi)^2 + r \left(\varrho \partial_\alpha^2 \varphi + \frac{12}{L^2} r + 2(\partial_\alpha \varrho) \partial_\alpha \varphi \right) \right), & 0 < \alpha < 1, \\ \mu^A \partial_t r = -\mu^P \left(\frac{12}{L^2} r + 4(\partial_\alpha \varrho) \partial_\alpha \varphi + 2\varrho \partial_\alpha^2 \varphi \right), & 0 < \alpha < 1, \\ \mu^A \partial_t \varphi = \mu^P \varrho^2 \partial_\alpha^2 \varphi + \mu^P \varrho \left(\frac{12}{L^2} r + 2(\partial_\alpha \varrho) \partial_\alpha \varphi \right), & 0 < \alpha < 1, \\ \mu^P \varrho = f_{0,1}, & \alpha = 0, 1, \\ \mu^P \varrho^2 \partial_\alpha \varphi = 0, & \alpha = 0, 1, \end{cases} \tag{VI.1.8}$$

with Dirichlet boundary conditions for ϱ and Neumann for φ. In the next section, we try to understand the dynamics of System (VI.1.8) in terms of specific locations in space through a change of coordinates. This is similar to the transformation implemented in Section V.1.

VI.2 Transformation to Eulerian coordinates

System (VI.1.6)-(VI.1.7) is observed in the context of its surrounding space by implementing a transformation to Eulerian coordinates. This has the advantage that heat operators appear linearly. In particular, the coordinate change

$$\tau = t, \quad x = \int_0^\alpha \frac{\mathrm{d}\beta}{\varrho(\beta, t)}, \tag{VI.2.1}$$

transforms the nonlinear heat equation $\mu^A \partial_t \varrho = \mu^P \varrho^2 \partial_\alpha^2 \varrho$ to the linear heat equation $\mu^A \partial_\tau \varrho = \mu^P \partial_x^2 \varrho$, since

$$\partial_t \mapsto \partial_\tau - \frac{\mu^P}{\mu^A} \frac{1}{\varrho} (\partial_x \varrho) \partial_x \quad \text{and} \quad \partial_\alpha \mapsto \frac{1}{\varrho} \partial_x.$$

In the following, we replace τ by t for simplicity. We shall also need the following transformations due to the coordinate change (VI.2.1):

$$\partial_t \varrho \mapsto \partial_t \varrho - \frac{\mu^P}{\mu^A} \frac{1}{\varrho} (\partial_x \varrho)^2, \quad \partial_\alpha \varrho \mapsto \frac{1}{\varrho} \partial_x \varrho, \quad \partial_\alpha^2 \varrho \mapsto -\frac{1}{\varrho^3} (\partial_x \varrho)^2 + \frac{1}{\varrho^2} \partial_x^2 \varrho.$$

System (VI.1.8) **in Eulerian coordinates.** The change of coordinates (VI.2.1) transforms System (VI.1.8) to

$$\begin{cases} \mu^A \partial_t \varrho = \mu^P \partial_x^2 \varrho - \mu^P \varrho \left((\partial_x \varphi)^2 + r \left((\partial_x \varrho) \partial_x \varphi + \varrho \partial_x^2 \varphi + \frac{12}{L^2} \varrho^2 r \right) \right), \\ \mu^A \partial_t r = -\mu^P \left(\frac{12}{L^2} r + \frac{1}{\varrho} \partial_x \varrho \left(\frac{2}{\varrho} \partial_x \varphi - \partial_x r \right) + \frac{2}{\varrho} \partial_x^2 \varphi \right), \\ \mu^A \partial_t \varphi = \mu^P \partial_x^2 \varphi + \mu^P \left(\frac{12}{L^2} \varrho r + \frac{2}{\varrho} (\partial_x \varrho) \partial_x \varphi \right), \end{cases} \tag{VI.2.2}$$

subject to the transformed boundary conditions

$$\begin{cases} \mu^P \varrho = f_{0,1}, & x = x_{\mathrm{left}}(t), x_{\mathrm{right}}(t), \\ \mu^P \partial_x \varphi = 0, & x = x_{\mathrm{left}}(t), x_{\mathrm{right}}(t). \end{cases} \tag{VI.2.3}$$

Here, the boundary points $x_{\text{left}}(t)$ and $x_{\text{right}}(t)$ correspond to the x-coordinates of the filaments with label $\alpha = 0$ and $\alpha = 1$, respectively, at time t. Special solutions of System (VI.2.2)-(VI.2.3) along with their interpretations are discussed in the following paragraphs.

Solution 1. (Constant ϱ, r and φ in x) When ϱ, r and φ are all constant in x, the equations in (VI.2.2) form a system of ODEs:

$$\begin{cases} \mu^A \dot{\varrho} = -\frac{12}{L^2}\mu^P \varrho^3 r^2, \\ \mu^A \dot{r} = -\frac{12}{L^2}\mu^P r, \\ \mu^A \dot{\varphi} = \frac{12}{L^2}\mu^P \varrho r, \end{cases} \tag{VI.2.4}$$

which should also satisfy the boundary conditions for a special time-dependent choice of $f_0 = f_1$ due to (VI.2.3). In this situation, filaments are parallel and are equally spaced in a quadrilateral strip. The second equation in System (VI.2.4) has the solution

$$r(t) = r_0 \exp\left(-\frac{12}{L^2}\,\frac{\mu^P}{\mu^A}\,t\right), \tag{VI.2.5}$$

for an initial data $r_0 := r(t = 0)$. As t tends to infinity, r converges to zero exponentially. Inserting $r(t)$ to the equation for ϱ in (VI.2.4), one has

$$\frac{\dot{\varrho}}{\varrho^3} = -\frac{\mathrm{d}}{\mathrm{d}t}\left(\frac{1}{\varrho^2}\right) = -\frac{12}{L^2}\frac{\mu^P}{\mu^A} r_0^2 \exp\left(-\frac{24}{L^2}\,\frac{\mu^P}{\mu^A}\,t\right),$$

and integration with respect to time yields

$$\frac{1}{\varrho^2} = -\frac{1}{2} r_0^2 \exp\left(-\frac{24}{L^2}\,\frac{\mu^P}{\mu^A}\,t\right) + \frac{1}{2} r_0^2 + \frac{1}{\varrho_0^2},$$

for an initial density $\varrho_0 := \varrho(t = 0)$. As $t \to \infty$, we find that

$$\varrho^2 \to \frac{\varrho_0^2}{(1/2)\varrho_0^2 r_0^2 + 1},$$

which means that the density ϱ stays bounded above by its initial value ϱ_0 for large times. This is consistent with the fact that pressure caused by filament repulsion produces spreading in the α-direction, consequently, in the x-direction.

Solution 2. (Constant φ in x and $r = 0$) Problem (VI.2.2) reduces to a linear heat equation for ϱ,

$$\mu^A \partial_t \varrho = \mu^P \partial_x^2 \varrho \tag{VI.2.6}$$

and the direction φ does not change in time. With a constant φ and $r = 0$, the filaments of the same length are parallel to each other in a rectangular strip. Therefore, the dynamics is governed only by the evolution of density (VI.2.6), which is in fact the 1D free-boundary problem (V.1.13) considered in Section V.1. This should come as no surprise since in this situation, the filaments can be seen as just points on the line, possibly unequally spaced from each other. However, this family of solutions to System (V.3.5)-(V.3.6) is typically unstable, as we have seen in the analysis in Section V.3.1.

VI.3 Numerical experiment of a rectangular strip with parallel filaments

In this section, we decide to work with Lagrangian coordinates, i.e. (α, t), instead of the Eulerian variables (VI.2.1) since the free-boundary problem (VI.2.2)-(VI.2.3) requires one to solve also for the unknown boundaries x_{left} and x_{right}. In the end, we recover the traveling wave solutions computed in Section V.1.

System (VI.1.8) with $r = 0$ and $\partial_\alpha \varphi = 0$ corresponds to a rectangular strip with parallel filaments, with dynamics governed by an evolution equation for ϱ,

$$\begin{cases} \partial_t \varrho = \frac{\mu^P}{\mu^A} \varrho^2 \partial_\alpha^2 \varrho & 0 < \alpha < 1, \\ \mu^P \varrho = f_{0,1} & \alpha = 0, 1. \end{cases} \tag{VI.3.1}$$

This has solutions that can be expressed via solutions of the linear heat equation (VI.2.6), obtained by using the transformation (VI.2.1). Introducing the variable $q := (1/\varrho)$, System (VI.3.1) transforms to

$$\begin{cases} \partial_t q = -\frac{\mu^P}{\mu^A} \partial_\alpha^2 \left(\frac{1}{q}\right) & 0 < \alpha < 1, \\ \mu^P \frac{1}{q} = f_{0,1} & \alpha = 0, 1, \end{cases}$$

which can be rewritten in the form of the *Fujita-Storm equation* [PZ03, Equation 5.1.10.3],

$$\begin{cases} \partial_t q(\alpha, t) = \partial_\alpha (D(q) \partial_\alpha q(\alpha, t)) & 0 < \alpha < 1, \quad t > 0, \\ \dfrac{\mu^P}{q(0, t)} = f_0(t) & t > 0, \\ \dfrac{\mu^P}{q(1, t)} = f_1(t) & t > 0, \end{cases} \tag{VI.3.2}$$

with the nonlinear diffusivity $D(q) := (\mu^P/\mu^A)(1/q^2) > 0$. System (VI.3.2) is solved together with an appropriate initial condition

$$q(\alpha, 0) = q_0(\alpha), \quad 0 < \alpha < 1. \tag{VI.3.3}$$

Space-time discretization. We discretize the (α, t)-plane by choosing a uniform mesh width $h \equiv \Delta\alpha$ and a uniform time step size $k \equiv \Delta t$. The mesh points (α_j, t_n) are defined as

$$\begin{cases} \alpha_j = (j-1)h, & j = 1, \ldots, J, J+1, \quad h = 1/J, \\ t_n = nk, & n = 0, 1, \ldots, N, \quad k = T/N, \end{cases}$$

where J is the number of space grid points and T denotes the final time. We would like to produce discrete approximations $Q_j^n \in \mathbb{R}$ to the point values $q(\alpha_j, t_n)$ (or to *cell averages* $\bar{q}(\alpha_j, t_n)$) of the true solution at the discrete grid points.

Semi-implicit conservative scheme. A semi-implicit Euler scheme is employed for the temporal discretization of the PDE in (VI.3.2). In particular, the nonlinear diffusivity is evaluated at the previous time step:

$$Q^{n+1} = Q^n + k\frac{\mathrm{d}}{\mathrm{d}\alpha}\left[D(Q^n)\frac{\mathrm{d}}{\mathrm{d}\alpha}(Q^{n+1})\right], \quad \text{for } n = 0, 1, \ldots, N,$$

where $Q^i := Q^i(\alpha) \approx u(t_i, \alpha)$, for $i = n, n+1$, denotes discrete approximations. This yields to a linear system at each time step, which is robust for computations.

For the spatial discretization, we use a method in conservation form to take advantage of the structure of System (VI.3.2)-(VI.3.3),

$$Q_j^{n+1} = Q_j^n + \frac{k}{h}\left[F(Q^n, Q^{n+1}; j) - F(Q^n, Q^{n+1}; j-1)\right]. \tag{VI.3.4}$$

where the flux function *centered* about the jth point is given by

$$F(Q^n, Q^{n+1}; j) := D(Q^n_{j+1/2})(Q^{n+1}_{j+1} - Q^{n+1}_j)/h, \quad \text{with } Q^n_{j+1/2} = (Q^n_j + Q^n_{j+1})/2.$$

At the end points where $j = 1$ and $j = J+1$, we impose the boundary values

$$f_0^n := f_0(t_n), \quad f_1^n := f_1(t_n), \quad \text{for each } n = 0, 1, \ldots, N. \tag{VI.3.5}$$

Finally, we need the discrete values from the initial condition:

$$\begin{cases} Q_j^0 := q_0(\alpha_j), & j = 2, \ldots, J-1, \\ Q_1^0 = f_0^0, \quad Q_{J+1}^0 = f_1^0. \end{cases} \tag{VI.3.6}$$

Taking the sum of (VI.3.4) over all $j = 1, \ldots, J+1$, the fluxes cancel out except those at the boundaries, and we are left with

$$h\sum_{j=1}^{J+1}(Q_j^{n+1} - Q_j^n) = k\left(D(Q^n_{J+1/2})\,(Q^{n+1}_{J+1} - Q^{n+1}_J)/h - D(Q^n_{1/2})\,(Q^{n+1}_1 - Q^{n+1}_0)/h\right),$$

which is the discrete form of the conservation law (integral form).

In compact form, the discrete system (VI.3.4)-(VI.3.6) can be written as

$$\mathbf{A}^{n+1}\mathbf{Q}^{n+1} = \mathbf{b}^{n+1}.$$

where $\mathbf{A}^{n+1} = [A_{ij}]_{i,j=1}^{J+1}$ is a $(J+1)\times(J+1)$ tridiagonal (positive definite) matrix with non-zero entries given by

$$\begin{cases} A_{1,1} = 1, \quad A_{J+1,J+1} = 1, \\ \text{for } j = 2, \ldots, J: \\ A_{j,j-1} = -D(Q^n_{j-1/2}), \\ A_{j,j} = h^2/k + D(Q^n_{j+1/2}) + D(Q^n_{j-1/2}), \\ A_{j,j+1} = -D(Q^n_{j+1/2}), \end{cases}$$

The solution vector at each time step is denoted by $\mathbf{Q}^{n+1} = [Q_1^{n+1}, Q_1^{n+1}, \ldots, Q_{J+1}^{n+1}]^\top$. Finally, the right hand side $(J+1)$-vector $\mathbf{b}^{n+1} = [b_j]_{j=1}^{J+1}$ has the entries

$$\begin{cases} b_1 = f_0^{n+1}, \quad b_{J+1} = f_1^{n+1}, \\ \text{for } j = 2, \ldots, J: \\ b_j = (h^2/k) Q_j^n. \end{cases}$$

Numerical example. Consider a quadratic (in α) initial data (see Figure VI.1) given by

$$q_0(\alpha) = (\alpha + 0.5)(\alpha - 1.5) - \frac{\alpha + 0.5}{2} + 2, \quad q_0(0) = 1, \quad q_0(1) = 0.5. \tag{VI.3.7}$$

The constant boundary values $f_0 = 1$ and $f_1 = 0.5$ are prescribed for $t \geq 0$. We used $N = 10$ temporal degrees of freedom (dofs) for $0 \leq t \leq T = 1$, so that the time step size $k = T/N = 0.1$. We also take $J = 50$ spatial dofs, so that the mesh width $h = 1/J = 0.02$. [1]

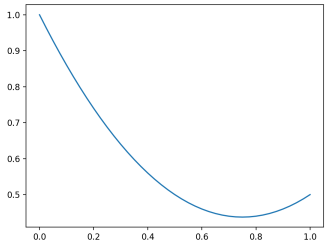

Figure VI.1: Initial data q_0

Figure VI.2 shows the numerical solution to System (VI.3.2)-(VI.3.3) with q_0 in (VI.3.7) implemented with the proposed semi-implicit scheme above. The picture on the left plots the solution q against the (α, t)-axis. On the right is a side view of the 3D-plot on the left, to better see the evolution of the curve q at each time step. We observe that the shape of the quadratic function almost becomes linear as it comes to a steady shape. This is to be expected because of the effects of diffusion. Going back to the original variable ϱ, one can take the reciprocal of the numerical solution above, and in the same way the curve ϱ becomes almost linear.

[1] The algorithm is implemented in Python 3.8.10 (Python Software Foundation, `https://www.python.org/`) on a 2.7 GHz Intel Core i5 with 8 GB RAM.

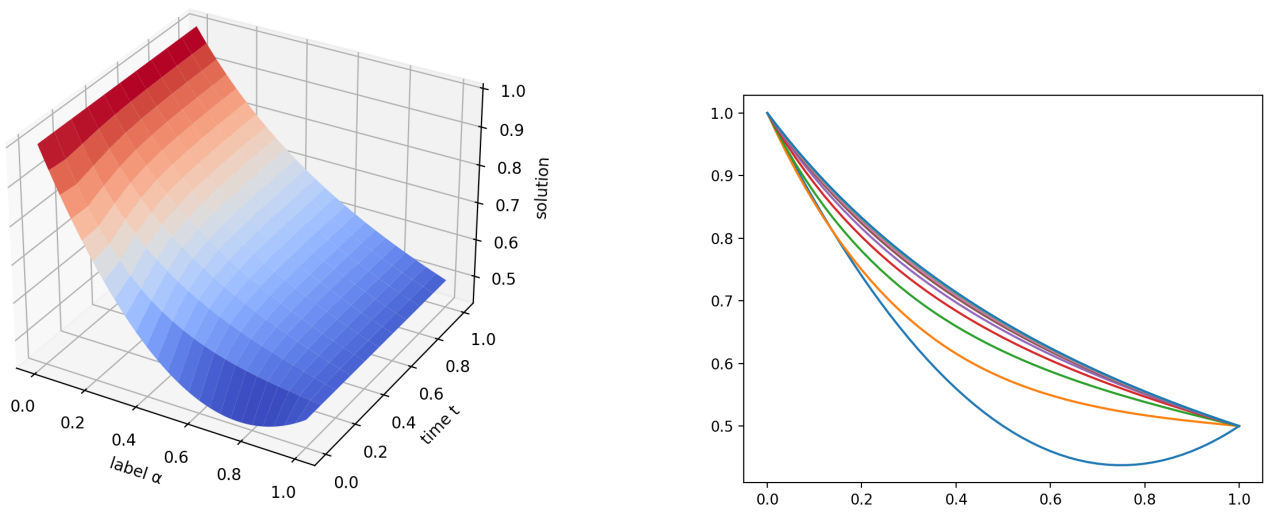

Figure VI.2: Plots of the evolution of solution $q := (1/\varrho)$ using a semi-implicit scheme.

Summary and Outlook

In this thesis, we proposed simplified versions of the Filament Based Lamellipodium (FBLM). The underlying assumption of the simplified model versions is that the lamellipodium width around the cell periphery is much smaller than the cell circumference. Passing to a zero-width limit for the lamellipodium, we were able to reproduce the results from the previous FBLM papers, including the degenerate cases mentioned in [OSS08] and the desired circular-shaped cell in equilibrium [OSS08; HMS17]. The resulting zero-width model is significantly simpler than the full FBLM, yet not too restrictive that it allows (possibly) shapes other than the circle as the initial configuration.

In the second part of this work, we focused on the effects of the pressure term on the FBLM. Although the pressure term has a stabilizing effect on the full FBLM, we discovered that it could cause instabilities with respect to non-symmetric perturbations. To counteract the instabilities caused by pressure, we introduced an artificial tension energy of the center-of-mass curve of a lamellipodial strip. A pitchfork bifurcation away from the trivial, non-moving, equilibrium emerged as a consequence of the competing effects of pressure and tension. The nontrivial steady state produced a constant and nonvanishing velocity that translocates the filament network structure.

In the last chapter, we performed a numerical experiment for special solutions to the evolution of filament density. We were compelled to implement a semi-implicit conservative scheme to preserve the system structure. This scheme proved to be robust for numerical computations.

In summary, the models we derived in this study may be utilized in future works, on one hand, for existence results and, on the other, for numerical simulations. Below, we mention possible extensions of this thesis.

Analysis. The derivation of the FBLM is based on a potential energy functional and dominating friction effects, suggesting an interpretation as a *generalized gradient flow*. This view will guide the approach for existence analysis, based on time discretization and the solution of a variational problem for each time step. Because of the complexity of the FBLM, simplified situations will be studied, concentrating on the mechanical part of the model and simplifying its biochemical ingredients. Possible extensions of the analytical theory involve the study of the long-time behavior of model problems as well as an analysis of the regularity of solutions. Preliminary heuristic considerations indicate that the solution operator is of a quasi-elliptic nature and smooth solutions can be expected.

Zero-width limit for the lamellipodium. We have identified an appropriate scaling such that a nontrivial zero-width limit exists. Based on the analysis approach described above, a next step is to provide a rigorous justification of the vanishing lamellipodium limit.

Adding the nucleus. It is known that lamellar fragments of fish epidermal keratocytes, which lack nuclei, possess the ability for locomotion [VSB99]. Because of this, the influence of the nucleus on the lamellipodium was paid little attention. However, studies that emphasized on the importance of the nucleus in cell motility, in particular, in three-dimensional environments, have surfaced recently [Kha+12]. A detailed discussion of the interplay between the coupling of the nucleus and cytoskeleton (and indirectly to the extracellular matrix) is also reported in [FH16]. Cell polarization yielding changes in migration direction sometimes involve nuclear positioning and rotations. Moreover, a prerequisite for cells to migrate through constrictions smaller than the size of the nucleus is nucleus deformation. This must be given attention since the nucleus, compared to the rest of the cell, is less deformable, and hence, may hinder passage of cells through constrictions and inhibit migration. Finally, because metastatic cancer cells possess nuclei with abnormal shapes and stiffness, it will be crucial to understand the role of nucleus in cell motility. Motivated by these results, we shall incorporate the influence of the nucleus, in particular for crawling in confined geometries. The nucleus will be modelled as an elastic body with spherical equilibrium shape located in the cytoplasmic region away from the lamellipodium. The coupling to the lamellipodium will be provided by a simple model for the action of *microtubules*, emanating from a *centrosome* tied to the nucleus and acting as a *Microtubule Organisation Center*.

Simulations. A finite element implementation of the FBLM has been carried out [Man+17], and a running code exists in the group of C. Schmeiser. Therefore it will be possible to integrate the nucleus model without a very big effort. Numerical experiments will include the chemotaxis-driven crawling of cells through narrow channels. The zero-width model requires a new implementation. This task will be much simpler than the implementation of the full FBLM, and it will also lead to much shorter run times. A goal is the simulation of ensembles of hundreds or thousands of cells.

Bibliography

[Abe80] M. Abercrombie. "The Croonian Lecture, 1978 – The crawling movement of metazoan cells". *Proceedings of the Royal Society of London. Series B. Biological Sciences* 207 (1980), pp. 129–147. DOI: 10.1098/rspb.1980.0017.

[Alb+02] B. Alberts et al. *Molecular Biology of the Cell*. 6th. Garland Science, 2002. DOI: 10.1201/9781315735368.

[AD99] W. Alt and M. Dembo. "Cytoplasm dynamics and cell motion: two-phase flow models". *Mathematical Biosciences* 156.1-2 (1999). DOI: 10.1016/S0025-5564(98)10067-6.

[AE07] R. Ananthakrishnan and A. Ehrlicher. "The forces behind cell movement". *International journal of biological sciences* 3.5 (2007), p. 303. DOI: 10.7150/ijbs.3.303.

[Ara16] I.S. Aranson. *Physical Models of Cell Motility*. Springer, 2016. DOI: 10.1007/978-3-319-24448-8.

[CPV10] A. Chauvière, L. Preziosi, and C. Verdier. *Cell mechanics: from single scale-based models to multiscale modeling*. Chapman and Hall/CRC, 2010. DOI: 10.1201/9781420094558.

[FH16] A. Fruleux and R.J. Hawkins. "Physical role for the nucleus in cell migration". *Journal of Physics: Condensed Matter* 28.36 (2016), p. 363002. DOI: 10.1088/0953-8984/28/36/363002.

[GO04] M.E. Gracheva and H.G. Othmer. "A continuum model of motility in ameboid cells". *Bulletin of Mathematical Biology* 66.1 (2004), pp. 163–193. DOI: 10.1016/j.bulm.2003.08.007.

[Hen17] S. Henze. "The Filament Based Lamellipodium Model in the Limit of Short Filaments". Master's Thesis, University of Vienna. 2017.

[HMS17] S. Hirsch, A. Manhart, and C. Schmeiser. "Mathematical modeling of Myosin induced bistability of Lamellipodial fragments". *Journal of Mathematical Biology* 74.1 (2017), pp. 1–22. DOI: 10.1007/s00285-016-1008-2.

[Kha+12] S.B. Khatau et al. "The distinct roles of the nucleus and nucleus-cytoskeleton connections in three-dimensional cell migration". *Scientific reports* 2.1 (2012), pp. 1–11. DOI: 10.1038/srep00488.

[Kno+11] M. Knorr et al. "Stochastic actin dynamics in lamellipodia reveal parameter space for cell type classification". *Soft Matter* 7.7 (2011), pp. 3192–3203. DOI: 10.1039/C0SM01028F.

[Koe+08] S.A. Koestler et al. "Differentially oriented populations of actin filaments generated in lamellipodia collaborate in pushing and pausing at the cell front". *Nature cell biology* 10.3 (2008), pp. 306–313. DOI: 10.1038/ncb1692.

[Kre91] E. Kreyszig. *Introductory functional analysis with applications*. Vol. 17. John Wiley & Sons, 1991.

[Kue15] C. Kuehn. *Multiple time scale dynamics*. Vol. 191. Springer, 2015.

[Lac+07] C.I. Lacayo et al. "Emergence of large-scale cell morphology and movement from local actin filament growth dynamics". *PLoS biology* 5.9 (2007), e233. DOI: 10.1371/journal.pbio.0050233.

[Lei15] L. Leingang. "Stability Analysis of an Actin-driven Lamellipodium Model with Pressure". Master's Thesis, University of Vienna. 2015.

[Lod+08] H. Lodish et al. *Molecular cell biology*. 5th. Macmillan, 2008.

[MB01] I.V. Maly and G.G. Borisy. "Self-organization of a propulsive actin network as an evolutionary process". *Proceedings of the National Academy of Sciences* 98.20 (2001), pp. 11324–11329. DOI: 10.1073/pnas.181338798.

[MS17] A. Manhart and C. Schmeiser. "Existence of and decay to equilibrium of the filament end density along the leading edge of the lamellipodium". *Journal of mathematical biology* 74 (2017), pp. 169–193. DOI: 10.1007/s00285-016-1027-z.

[Man+15] A. Manhart et al. "An extended Filament Based Lamellipodium Model produces various moving cell shapes in the presence of chemotactic signals". *Journal of theoretical biology* 382 (2015), pp. 244–258. DOI: 10.1016/j.jtbi.2015.06.044.

[Man+17] A. Manhart et al. "Numerical treatment of the Filament Based Lamellipodium Model". *Modeling Cellular Systems, Springer* (2017). Ed. by F. Matthäus F. Graw and J. Pahle. DOI: 10.1007/978-3-319-45833-5_7.

[Mar+06] A.F.M. Marée et al. "Polarization and movement of keratocytes: a multiscale modelling approach". *Bulletin of mathematical biology* 68.5 (2006), pp. 1169–1211. DOI: 10.1007/s11538-006-9131-7.

[MO11] V. Milišić and D. Oelz. "On the asymptotic regime of a model for friction mediated by transient elastic linkages". *Journal de mathématiques pures et appliquées* 96.5 (2011), pp. 484–501. DOI: 10.1016/j.matpur.2011.03.005.

[Mog09] A. Mogilner. "Mathematics of cell motility: have we got its number?" *Journal of mathematical biology* 58.1-2 (2009), pp. 105–134. DOI: 10.1007/s00285-008-0182-2.

[MMB01] A. Mogilner, E. Marland, and D. Bottino. "A minimal model of locomotion applied to the steady gliding movement of fish keratocyte cells". *Mathematical Models for Biological Pattern Formation* 121 (2001), pp. 269–293. DOI: 10.1007/978-1-4613-0133-2_12.

[MO96] A. Mogilner and G. Oster. "Cell motility driven by actin polymerization". *Biophysical journal* 71.6 (1996), pp. 3030–3045. DOI: 10.1016/S0006-3495(96)79496-1.

[Oel11] D. Oelz. "On the curve straightening flow of inextensible, open, planar curves". *SeMA Journal* 54.1 (2011), pp. 5–24. DOI: 10.1007/BF03322585.

[OS10a] D. Oelz and C. Schmeiser. "Derivation of a model for symmetric lamellipodia with instantaneous cross-link turnover". *Archive for Rational Mechanics and Analysis* 198.3 (2010), pp. 963–980. DOI: 10.1007/s00205-010-0304-z.

[OS10b] D. Oelz and C. Schmeiser. "How do cells move? Mathematical modelling of cytoskeleton dynamics and cell migration". *Cell mechanics: from single scale-based models to multi-scale modelling*. Ed. by A. Chauviere, L. Preziosi, and C. Verdier. Chapman and Hall / CRC Press, 2010. Chap. 5, pp. 133–157.

[OSS08] D. Oelz, C. Schmeiser, and J.V. Small. "Modeling of the actin-cytoskeleton in symmetric lamellipodial fragments". *Cell adhesion & migration* 2.2 (2008), pp. 117–126. DOI: 10.4161/cam.2.2.6373.

[Pol07] T.D. Pollard. "Regulation of actin filament assembly by Arp2/3 complex and formins". *Annu. Rev. Biophys. Biomol. Struct.* 36 (2007), pp. 451–477. DOI: 10.1146/annurev.biophys.35.040405.101936.

[PZ03] A.D. Polyanin and V.F. Zaitsev. *Handbook of Nonlinear Partial Differential Equations: Exact Solutions, Methods, and Problems*. Chapman and Hall/CRC, 2003. DOI: 10.1201/9780203489659.

[Ram11] J. Ramic. "On a model for a lamellipodial actin filament layer including pressure". Diploma Thesis, University of Vienna. 2011.

[RJM05] B. Rubinstein, K. Jacobson, and A. Mogilner. "Multiscale two-dimensional modeling of a motile simple-shaped cell". *Multiscale modeling & simulation* 3.2 (2005), pp. 413–439. DOI: 10.1137/04060370X.

[STB07] T.E. Schaus, E.W. Taylor, and G.G. Borisy. "Self-organization of actin filament orientation in the dendritic-nucleation/array-treadmilling model". *Proceedings of the National Academy of Sciences* 104.17 (2007), pp. 7086–7091. DOI: 10.1073/pnas.0701943104.

[Sch20] C. Schmeiser. "Lecture notes for Mathematical Cell Biology". Faculty for Mathematics, University of Vienna. 2020.

[SW15] C. Schmeiser and C. Winkler. "The flatness of Lamellipodia explained by the interaction between actin dynamics and membrane deformation". *Journal of Theoretical Biology* 380 (2015), pp. 144–155. DOI: 10.1016/j.jtbi.2015.05.010.

[Sfa+18] N. Sfakianakis et al. "Modelling cell-cell collision and adhesion with the Filament Based Lamellipodium Model". *Biomath* 7.2 (2018). DOI: 10.11145/j.biomath.2018.11.097.

[SSM14] E. Shchepakina, V. Sobolev, and M.P. Mortell. *Singular Perturbations: Introduction to system order reduction methods with applications*. Vol. 2114. Springer, 2014.

[SIC78] J.V. Small, G. Isenberg, and J.E. Celis. "Polarity of actin at the leading edge of cultured cells". *Nature* 272.5654 (1978), pp. 638–639. DOI: 10.1038/272638a0.

[VSB99] A.B. Verkhovsky, T.M. Svitkina, and G.G. Borisy. "Self-polarization and directional motility of cytoplasm". *Current Biology* 9.1 (1999), 11–S1. ISSN: 0960-9822. DOI: 10.1016/S0960-9822(99)80042-6.

[Vin+12] M. Vinzenz et al. "Actin branching in the initiation and maintenance of lamellipodia". *Journal of cell science* 125.11 (2012), pp. 2775–2785. DOI: 10.1242/jcs.107623.